

Ultrasound to Assess Lipid Content in Salmon Muscle

by

Russell A. Shannon



Robotics Research Group
Department of Engineering Science
University of Oxford

Trinity Term 2002

Declaration

This thesis is submitted to the Department of Engineering Science, University of Oxford, in partial fulfilment of the requirements for the degree of Doctor of Philosophy. The thesis is entirely my own work and, except where otherwise stated, describes my own research.

Russell A. Shannon, Hertford College, Oxford
Copyright ©2002 Russell A. Shannon
All Rights Reserved

Russell A. Shannon
Hertford College

Doctor of Philosophy
Trinity Term 2002

Ultrasound to Assess Lipid Content in Salmon Muscle

Abstract

In this thesis, ultrasound pulse transit time measurement techniques are applied to aquaculture, specifically to measure the intramuscular fat in salmon muscle tissue. The main advantages of this technique are that it is noninvasive and that it uses low-cost components.

Fat in salmon muscle exists as oil dispersed throughout the tissue. Therefore, a phantom was built to empirically model a dispersed fat system. The phantom was a mixture of low-fat milk and high-fat double cream. By varying the quantities of each component, the fat level of the phantom could be controlled. A trend of increasing speed of sound and attenuation with fat content was observed. From velocity measurements at a single temperature, it was possible to predict the fat content of the mixture to within $\pm 1.5\%$ fat.

A measurement system was created to measure the sample thickness and the speed of sound through a sample at the same time. Velocity and attenuation measurements were made on fifty samples of salmon muscle tissue containing two distinct fat ranges. A trend of decreasing speed of sound with fat content was observed. Further measurements were taken on twelve more samples and compared to the results of chemical fat analysis to determine the strength of the correlation between fat content and speed of sound through the samples. Again, a trend of decreasing speed of sound with increasing fat content was observed ($r=0.73$, $n=12$). This trend was not as strong as that observed for the phantom due to natural variation in the structure of the tissue. A conclusion drawn from this part of the research is that it may be possible to group the data into “high fat”, “medium fat” and “low fat” categories. Attenuation measurements proved too dependent on muscle structure to yield a correlation between attenuation and fat content.

Ray-tracing techniques were used to model the propagation velocity of a wavefront travelling through a single salmon sample. The model provided an insight into how variations in temperature, fat content, myoseptum thickness and myosepta configuration affect measured velocity.

This thesis provides an insight into how ultrasound velocity measurement may be used to assess the fat content of salmon white muscle tissue. It also

provides a starting point for future work in which these techniques may be combined with a vision system to enable similar measurements on live fish.

Acknowledgements

I dedicate this tome to my father, who taught me the valuable basic arithmetic which was used every day during this project. My only regret is that he did not live to see his son graduate from Oxford University.

I thank the John G. Martin Trust for sending me to Oxford as their 12th Martin Scholar and supporting me for the first two years. Their selection has changed the direction and experiences of my life beyond description. For that, I will always be grateful.

To paraphrase Woody Allen, a D.Phil. project is like a shark. It has to keep moving forward or it will die. There were several times when we thought what we had on our hands was a dead shark. I thank my main supervisor Dr. Penny Probert-Smith for always keeping the faith and giving me invaluable advice and direction throughout the project. I must also thank Dr. Fares Mayia for being not only an outstanding supervisor, but for becoming a friend and mentor as well. Thanks, too, to Dr. Jeff Lines of Silsoe Research Institute for acting as our “fish guy” and for ensuring that the experimental rig which finally yielded the desired results was built at all.

I am truly grateful for the support of my family throughout the project. When 14 years ago, my mother suggested that I would be studying at Oxford one day, I just scoffed and changed the subject. I could not predict that her dream would become a reality. Without the love and generosity of both she and my stepfather, this thesis would not have happened. I will always be indebted to you both.

Finally, I will always be grateful to my friends and work colleagues for helping me keep my sanity, and have a good time doing it, over four tremendous years. My life would be much emptier if I had never come here and met all you wonderful - if slightly weird - people.

Contents

Declaration	i
Abstract	ii
Acknowledgements	iv
Table of Contents	v
List of Figures	ix
1 Introduction	1
1.1 Fat Content Determination Methods	2
1.1.1 Destructive Fat Determination Methods	3
1.1.2 Nondestructive Fat Determination Methods	6
1.2 Contributions of the Thesis	10
1.3 Organisation of the Thesis	12
2 Methods and Materials	14
2.1 Ultrasound for Tissue Characterisation	15
2.1.1 Speed of Sound	17
2.1.2 Attenuation	20
2.2 Measurement System	22
2.2.1 Pulser-receiver	24
2.2.2 Transducers	25
2.2.3 Oscilloscope	30
2.3 Signal Processing	33
2.4 Summary	36
3 Phantoms	37
3.1 Acoustic Properties of Liquids	39
3.2 Methods and Materials	43
3.3 Calibration	49
3.3.1 Medical Phantom	49
3.3.2 Distilled Degassed Water	52
3.3.3 Salt Water	56
3.4 Milk/Cream Mixtures	60

3.4.1	Measurement Temperature	61
3.4.2	Measurements at 10°C	64
3.4.3	Repeatability	68
3.5	Foam Phantom	69
3.5.1	Calibration	69
3.5.2	Milk/Cream Mixtures	71
3.6	Conclusion	73
4	Salmon Tissue	74
4.1	Acoustic Properties of Tissue	77
4.2	Target Area for Sample Extraction	79
4.3	Muscle Tissue Structure	83
4.3.1	Types of Muscle Tissue	83
4.3.2	Myosepta	85
4.3.3	Tissue Constituents	88
4.4	Methods and Materials	88
4.5	Measurement Temperature	97
4.6	Tissue Measurements	100
4.6.1	Sample Orientation	100
4.6.2	Repeatability	101
4.6.3	Salmon Samples	103
4.6.4	Comparison to Chemical Analysis	106
4.7	Conclusion	110
5	Salmon Tissue Model	111
5.1	Model Geometry and Methods	113
5.1.1	Using Snell's Law	117
5.1.2	Speed of Sound Through Salmon Tissue	120
5.2	Results	127
5.2.1	Temperature and Fat Profiles	128
5.2.2	Changing Myosepta Configuration	132
5.2.3	Changing Myoseptum Thickness and Myosepta Con- figuration	135
5.2.4	Contribution of Individual Myosepta	137
5.2.5	Additive Contribution of Individual Myosepta	142
5.3	Validity of Model with Respect to Wavelength	146
5.4	Conclusion	147
6	Discussion	149
6.1	Overview and Analysis of Results	149
6.2	Conclusions	154

6.3	Future Work	156
A	Velocity and Attenuation Calculation Code	159
B	One-dimensional derivation of the equation for longitudinal wave velocity in an elastic medium	161
C	Fatty Acids	166
D	Salmon Tissue Model Code	168
D.1	Temperature and Fat Profiles	168
D.1.1	allmuscle.m	168
D.1.2	muscleworks.m	169
D.1.3	TopHalf.m	170
D.1.4	BottomHalf.m	173
D.2	Changing Transducer Position	175
D.2.1	change_position.m	175
D.2.2	muscleworks.m	175
D.2.3	TopHalf.m	177
D.2.4	BottomHalf.m	177
D.2.5	TransducerDown.m	177
D.3	Changing Myoseptum Thickness and Transducer Position . . .	178
D.3.1	allmuscle_myo.m	178
D.3.2	muscleworks_myo.m	179
D.3.3	TopHalf.m	179
D.3.4	BottomHalf.m	179
D.3.5	TransducerDown.m	179
D.4	Contribution of Individual Myosepta	179
D.4.1	single_myo.m	179
D.4.2	myo_zero.m to myo_eight.m	180
D.4.3	TopHalf_zero.m to TopHalf_eight.m	182
D.4.4	BottomHalf_zero.m to BottomHalf_eight.m	182
D.4.5	TransducerDown.m	182
D.5	Additive Contribution of Individual Myosepta	182
D.5.1	additive_myo.m	182
D.5.2	add_myo_zero.m to add_myo_all.m	183
D.5.3	add_TopHalf_zero.m to all_TopHalf_all.m	185
D.5.4	add_BottomHalf_zero.m to add_BottomHalf_all.m	185
D.5.5	TransducerDown.m	185
D.6	Utility Functions	186
D.6.1	reverse.m	186

D.6.2	sind.m	186
D.6.3	cosd.m	186
D.6.4	asind.m	186
D.6.5	acosd.m	186
Bibliography		187

List of Figures

1.1	A typical longitudinal image of the <i>Longissimus dorsi</i> muscle of a beef cow.	9
1.2	B-mode image of a salmon fillet.	10
2.1	The measurement system. “A” is the ultrasonic probes, “B” is the pulser-receiver and “C” is the oscilloscope.	22
2.2	Schematic view of the measurement system.	23
2.3	The pulser-receiver.	24
2.4	Diagram of a typical single-element probe.	25
2.5	Two ultrasonic probes.	26
2.6	Axial view of the acoustic field from a plane circular single-element source.	27
2.7	Typical intensity versus distance plot for an unfocused single-element transducer.	28
2.8	The ultrasonic field of a 2.25MHz transducer in distilled water at 20°C.	29
2.9	Expected beam spreading in the Fraunhofer region.	30
2.10	HP Infinium Oscilloscope 54820A.	31
2.11	Typical waveforms. The pulse on the very left of the image is the transmitted signal. The other waveform is the received signal.	32
2.12	Typical transmitted pulse (left) and received waveform (right).	33
3.1	Perspex measurement cell. “A” and “B” are the ultrasonic probes. “C” is the Perspex measurement cell.	45
3.2	Temperature-controlled water bath with Perspex cell inside it.	46
3.3	Phantom containing a block of reticulated foam.	48
3.4	Water bottle containing distilled water inside the ultrasonic cleaning bath.	54
3.5	Speed of sound in distilled degassed water versus temperature. The dots represent measured values. The solid line is the solution to Equation 3.10.	55

3.6	The velocity gap between pure water, bottom, and water of various salinities. Shapes represent experimental data. The bottom line is the solution to Equation 3.10 for pure water. The other solid lines are the solutions to Equation 3.11 for the three salinities.	58
3.7	Speed of sound versus temperature profiles for cream-in-milk concentrations of 0% (dots), 10% (circles), 20% (diamonds), 30% (squares), 40% (triangles), and 50% (hexagrams). The solid curves are best-fits.	63
3.8	Speed of sound versus concentration of 48% fat double cream in 0.1% fat milk at 10°C.	64
3.9	Attenuation versus concentration of cream. Dots are experimental data. The solid curve is a best-fit.	67
3.10	Speed of sound versus concentration of 48% fat cream in 0.1% fat milk inside a reticulated foam structure.	71
3.11	Attenuation versus concentration of cream. Dots are experimental data. The curve is a best-fit.	72
4.1	General anatomy of a teleost.	80
4.2	Skeletal structure of a teleost.	81
4.3	Anatomical cross-section of a fish.	82
4.4	Red and white muscle as distributed in teleosts. The fish's spine (centre of the fish) is not labelled.	84
4.5	Myosepta structure in teleosts.	86
4.6	View of a single myoseptum (right) and muscle tissue without myosepta (left). Both pictures were taken using a scanning optical microscope. The scale in the top right of each image shows that 200 pixels is equivalent to 280 microns, or 1 pixel is equivalent to 1.4 microns.	87
4.7	Linear micropositioning stage. Units are millimetres.	89
4.8	The tissue measurement rig.	90
4.9	Speed of sound versus distance between transducers.	93
4.10	Speed of sound versus distance between transducers. This data has been corrected for distance measurement errors.	94
4.11	Tissue measurement rig holding a tissue sample submerged in the plastic tub of distilled degassed water.	95
4.12	Speed of sound versus time for eight tissue samples. The dots represent data for samples containing approximately 11% fat. The circles represent data for samples containing approximately 8% fat.	96

4.13	Mean velocity versus time results for 50 samples. Mean velocity of Unilever samples is represented by circles. Mean velocity of Tesco samples is represented by dots.	97
4.14	Speed of sound through cod liver oil and pure water versus temperature. The diamonds represent cod liver oil data. The dots represent data for pure water.	99
4.15	System of axes applied to fish samples.	101
4.16	Speed of sound versus sample thickness. The circles represent data from Unilever samples. The dots represent data from Tesco samples.	103
4.17	Speed of sound versus fat content at 10°C. The line is a best-fit.	107
4.18	Attenuation versus fat content at 10°C.	109
5.1	Model salmon sample cross-section. This figure is not to scale.	114
5.2	A single ray refracting as it enters a medium with a different speed of sound.	117
5.3	Rays encountering a single myoseptum.	118
5.4	Geometry for the calculation of a ray's path length within a myoseptum.	119
5.5	Speeds of sound versus temperature for 13 fat levels.	129
5.6	Speed of sound versus fat content at 10°C.	130
5.7	A Bland-Altman plot of fish and model data.	131
5.8	Three transducer positions and resultant beams. Parts of the beam outside of the sample are not shown.	133
5.9	Speed of sound versus transducer position for fat contents of 1% (crosses, top), 9% (circles), 17% (triangles), and 25% (hexagrams, bottom).	134
5.10	Speed of sound versus transducer position for myoseptum thicknesses of 0.1mm (crosses, bottom), 0.9mm (circles), 1.7mm (triangles), and 2.5mm (hexagrams, top).	136
5.11	Numbering scheme applied to the myosepta.	138
5.12	Speed of sound versus transducer position for fat contents of 1% (crosses, top), 9% (circles), 17% (triangles) and 25% (hexagrams, bottom). The results for zero myosepta are shown in the graph at the top left. The results for myoseptum number 3 are shown in the graph at the bottom right.	140
5.13	Speed of sound versus transducer position for fat contents of 1% (crosses, top), 9% (circles), 17% (triangles) and 25% (hexagrams, bottom). The results for myoseptum number 4 are shown in the graph on the top left. The results for myoseptum number 8 are shown in the graph at the bottom.	141

5.14	Speed of sound versus transducer position for fat contents of 1% (crosses, top), 9% (circles), 17% (triangles) and 25% (hexagrams, bottom). The results for zero myosepta are shown in the graph at the top left. The results for three myosepta are shown in the graph at the bottom right.	144
5.15	Speed of sound versus transducer position for fat contents of 1% (crosses, top), 9% (circles), 17% (triangles) and 25% (hexagrams, bottom). The results for four myosepta are shown in the graph on the top left. The results for eight myosepta are shown in the graph at the bottom.	145
B.1	Particle displacement due to a one-dimensional longitudinal wave passing through a cylinder.	163

Chapter 1

Introduction

“I know the human being and fish can coexist peacefully.”
-President George W. Bush, September 29, 2000

Agricultural meat production is becoming increasingly subject to quality control. One area in which few techniques are currently available to provide this is fish husbandry. The salmon industry has struggled for years to find a reliable nondestructive method for evaluating fish quality.

The fat content is a particularly important indicator of the condition of the fish because of the overwhelming importance of fat as an energy reserve for reproduction [1, 2, 3]. Many fish naturally accumulate very large body reserves of energy by generating intramuscular fat in the form of oil in relation to their breeding cycle. Molecular genetic breeding programmes are being developed to produce salmon with more uniform and more controlled flesh oil levels. Such programmes depend on a rapid, accurate and above all noninvasive method of determining fat levels in fish.

There exists a variety of different methods for determining levels of intramuscular fat in fish, but the only standardised methods involve destruction of the fish so that chemical testing may be performed. A percentage of the fish stock must be sacrificed for such measurements. There is currently no reliable nondestructive system on the market that can perform such measurements. It was hoped that ultrasound pulse transit time techniques could be applied to aquaculture to provide a low-cost noninvasive way to measure quantitatively levels of intramuscular fat in salmon. Ultimately the technique could be part of a system to monitor fish to improve the efficiency and quality of fish husbandry as part of a more automated fish farming industry.

1.1 Fat Content Determination Methods

One definition of a “lipid” is a hydrocarbon compound in which the hydrogen and carbon atoms are linked in a long chain [4]. Lipids can also be defined in terms of their solubility in a solvent [5]. Fatty acids are derived from lipids. They are classified as either “polar” lipids or “nonpolar” lipids. This means that the lipids are either soluble or insoluble in water depending on the ionic groups present.

The most abundant nonpolar lipids in salmonids are triacylglycerides, which constitute more than 90% of the total lipids. Phospholipids are the

most abundant polar lipid group in salmonids. They constitute approximately 6% of the total lipids [5].

Several methods exist to measure the total fat content within fish muscle. All of these methods can be classified as “destructive” or “nondestructive.” Destructive methods mainly involve lipid extraction and measurement. Non-destructive methods attempt to measure the quantities of lipids *in situ*.

1.1.1 Destructive Fat Determination Methods

Destructive fat determination methods involve solvent extraction of lipids from a homogenized sample. Solvent properties play a role in determining how much fat is extracted from a sample. The types of lipid extracted are dependent on the dielectric constant of the solvent used. For example, methods using diethylether, whose dielectric constant is 4.3, extract only nonpolar lipids. However, methods using methanol, whose dielectric constant is 32.6, extract both nonpolar and polar lipids [5]. Total lipid content of a sample is determined by weight after removal of the solvent.

The Soxhlet method is the most widely used nonpolar lipid extraction method. This method involves drying the sample for a period of approximately seventeen hours in an air oven, or approximately four hours in a vacuum oven, at 100°C. Then, nonpolar lipids are extracted from the sam-

ple for eight hours using petroleum spirit or diethyl ether. This is followed by evaporation of the solvent and finally weighing of the extracted lipids [6]. The exact procedure for this extraction method has been standardised by the Association of the Official Analytical Chemists [7] and the British Standards Institution [8]. Because nonpolar lipids constitute approximately 90% of the total lipid content in fish, this method is often used to make an approximation of the overall lipid content of a fish sample [9].

Polar lipids are only extractable by the use of polar solvent mixtures. These mixtures are capable of extracting all the lipids within a sample [10]. The Bligh and Dyer method [11] uses a mixture of chloroform and methanol to extract both polar lipids and nonpolar lipids. It has been used previously to evaluate the total lipid content of fish muscle [5]. In this method, the homogenised sample is diluted with chloroform, methanol and water. This separates the mixture into two layers; the chloroform layer containing all the lipids and the methanolic layer containing the nonlipids. The lipids are then extracted by isolating the chloroform layer [11].

The Werner-Schmid method (also known as the Schmid-Bondzynski-Ratzlaff method) is similar to the Bligh and Dyer method and has been used to measure the fat content of fish muscle. It involves first dissolving the protein in a sample in concentrated hydrochloric acid. The lipids are then extracted using diethyl ether and petroleum ether. Again, the total quantity of lipids

in the sample is ascertained by weighing the fat residue after evaporation of the solvents [12]. This method extracts both polar and nonpolar lipids.

Other methods exist which extract all the nonpolar lipids but only some of the polar lipids within a sample. The ethylacetate method is the Norwegian reference method for the determination of the fat content in fish. This method has been shown to yield a total lipid measurement between that expected from the Bligh and Dyer method and from the Soxhlet method. This is because ethylacetate does not extract all the polar lipids present in a sample [5].

All of the methods mentioned above require skilled operators in order to obtain accurate results. They are also time-consuming [9]. Numerous machines have been developed to reduce the time required for the Soxhlet method. However, the Soxhlet method is still considered to take too long [6]. Therefore more rapid methods have been developed. Rapid destructive methods commonly make use of automatic analysers capable of simultaneously determining the quantities of more than one component. A widely used system is the CEM Meat Analysis System. The CEM analyser is designed to perform rapid moisture and fat determination on a wide range of meats. It consists of two instruments. One is the “automatic volatility computer”. This is a moisture and solids analyser with a microwave drying system linked to an electronic scale and a computer. The other instrument is the fat ex-

traction unit, consisting of an automatic extraction system and a solvent recovery system. It uses dichloromethane for lipid determination [6]. The performance of the CEM analyser in comparison to the Soxhlet method has been studied for meats. Crossland and Bratchell [6] concluded that the CEM consistently underestimated the lipid content in both raw meat and sausages when compared to the Soxhlet method. The unit has not been tested on fish.

1.1.2 Nondestructive Fat Determination Methods

Nondestructive methods aim to minimize damage to the sample exterior, while maintaining accuracy of measurement. Near-infrared reflectance (NIR) is a rapid nondestructive method for determining fat and moisture contents of whole fish. A good correlation ($r^2=0.97$) has been found between fat measurements on Atlantic salmon using NIR and fat measurements using the Soxhlet method [5]. The principle behind NIR is that chemical bonds are able to absorb light of specific wavelengths. A sample is illuminated by monochromatic light from a lamp that scans through wavelengths in a range from 1100nm to 2500nm [13]. The light is partially reflected by the sample. The amount of reflected light depends on which chemical bonds are present in the sample. It is possible to calibrate the amount of reflected light to the lipid content present in the sample. Destruction of the sample and the

performance of chemical testing is required for calibration.

The procedure requires little preparation of the samples. This is because there are no chemical reactions which must take place, as with the destructive methods. The fiberoptic probes must be placed on both sides of the fish under examination [14]. Lee [15] used fiberoptic NIR probes placed at three different positions on a rainbow trout to measure lipid content. A major disadvantage of using NIR analysis for fish tissue is interference from water bands within the fish. These bands can interfere with important spectral features [15]. To overcome this, most NIR techniques require that the fish first be freeze dried. This means that this technique cannot be used on live fish.

The Torry Fish Fatmeter is a hand-held device that was developed by the Torry Research Station of the UK Ministry of Agriculture. Its operation is based on the fact that the fat content of a fish is inversely proportional to its water content [16]. The Fatmeter uses a microstrip microwave sensor that is sensitive to the water content of the fish. The instrument converts the response of the sensor into a displayed percentage of fat. This is achieved using stored calibration data to internally measure against the sensor input.

Some of its advantages include the ability to operate equally well on live, dead and defrosted fish. It can potentially be used to determine quickly the fat content of large numbers of fish. Its developers claim an accuracy rate of

near 95% if calibration is done correctly [16]. However, users report a general lack of accuracy in measurements taken using the device [17]. Skin thickness, scale thickness and residual moisture on the fish surface are known to affect results [5].

Ultrasound provides a suitable approach to fat content estimation as it is one of the few methods that can currently be used on live animals with little damage. Texture analysis of B-mode ultrasound images has been reported to be effective in detecting intramuscular fat levels in beef cattle [18]. Nine hundred real-time ultrasound images from ribeye muscles across the eleventh and thirteenth ribs of live beef cattle were collected over a period of four years. It was found that fat deposits within the muscle cause an effect known as “speckle” in which fat appears as bright spots against the dark of the muscle in a B-mode image. Because speckle alters the texture of the image, the percentage of intramuscular fat can be estimated using texture analysis [18].

A computerized system has been developed to detect intramuscular fat through B-mode texture analysis. The success of this system is highly dependent on the nature of fat within beef. Figure 1.1 illustrates this.

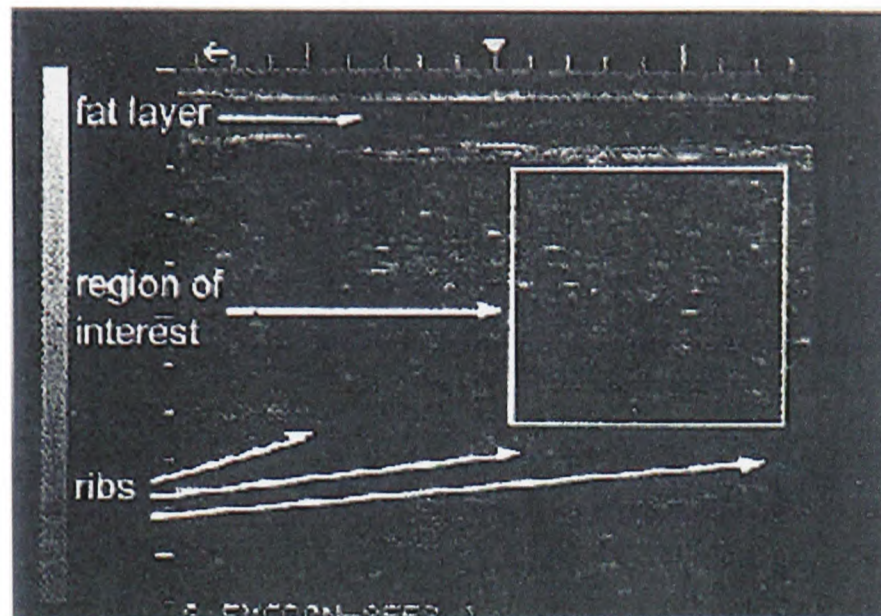


Figure 1.1: A typical longitudinal image of the *Longissimus dorsi* muscle of a beef cow.

In the centre of Figure 1.1, one can see that globules of fat in the muscle appear as white spots in the centre of the image [19]. However, the intramuscular fat in fish is quite different. In fish, intramuscular fat exists as oil dispersed throughout the muscle. There does not exist the same globules of fat which can be seen in Figure 1.1. Increases in fat content of fish muscle have not been shown to produce noticeable increases in the speckle content of a B-mode image.

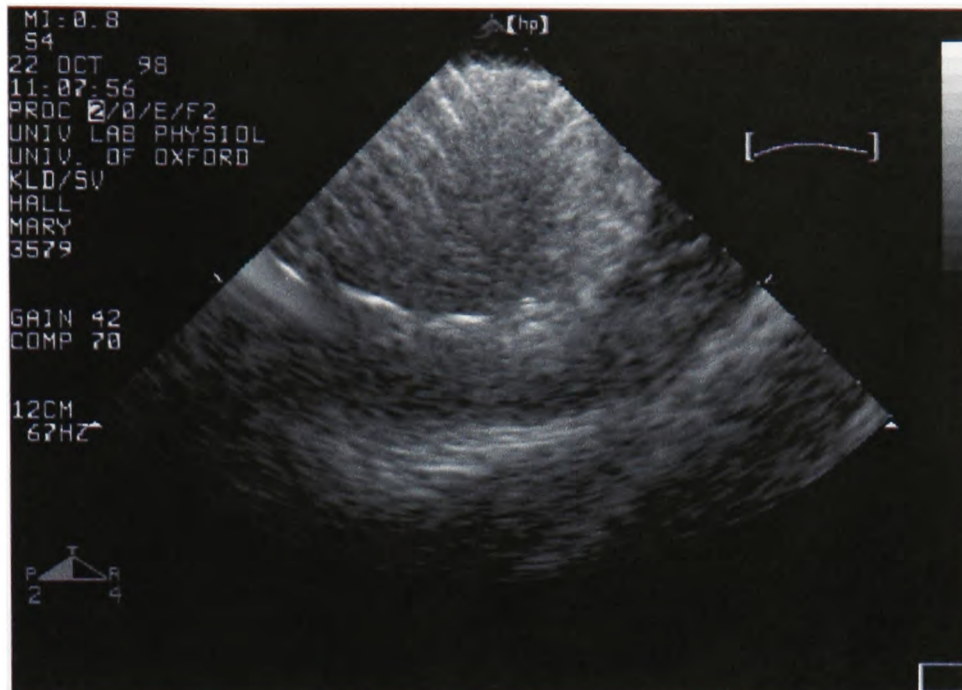


Figure 1.2: B-mode image of a salmon fillet.

Figure 1.2 was taken using a HP Sonos 5500 ultrasound scanner manufactured by Agilent Technologies, which is now a part of Philips Medical Systems. It shows that the tendons within salmon muscles show up as thin white lines in the image. These features will further inhibit texture analysis on B-mode images from salmon muscle. Thus, image analysis does not seem like a viable method for detecting intramuscular fat in fish.

1.2 Contributions of the Thesis

This section describes the principal contributions made by this thesis. Other studies have looked at predicting the fat content of salmonid muscle tissue using ultrasound velocity measurements [20, 21]. However, as far as the

author is aware, this is the first study to look solely at salmon and salmon muscle structure. This thesis will show that:

- Pulse transit time measurements can be used to predict fat levels in dispersed fat liquid mixtures.
- Pulse transit time measurements can be used to highlight a trend of changing speed of sound with fat content in salmon muscle tissue.
- Attenuation measurements may be used to detect changes in fat content in dispersed fat liquid mixtures, but not salmon muscle tissue.
- Such measurements need only be made at a single temperature. An appropriate temperature is 10°C. Most previous studies have used temperatures well above 25°C, or have advocated the use of measurements at multiple temperatures.
- It is possible to create a two-dimensional ray tracing model to investigate the effects that the internal structure of the tissue has on velocity measurements.
- It is perhaps unwise to model salmon tissue as an aqueous mixture of tissue components.

1.3 Organisation of the Thesis

Chapter 2 describes the reasons for using the speed of sound and attenuation as parameters for salmon tissue characterisation. It describes the selection of transducers and states the expected system resolution with these transducers. The anticipated ultrasound field using circular single-element transducers is described. The hardware which comprised the measurement system is described in detail as well as the signal processing necessary to extract time of flight and intensity information from the raw data.

In Chapter 3, the measurement system described in Chapter 2 is calibrated using a medical phantom, distilled degassed water and salt water at three salinities. After calibration, a phantom made of mixtures of milk and cream is used to experimentally model a dispersed fat system of several different fat levels. 10°C is shown to be an appropriate temperature at which to take measurements. The phantom is used to find an empirical equation relating fat content to the measured speed of sound. Finally, a block of reticulated foam is inserted into the mixture to simulate tissue-like attenuation.

Chapter 4 explains why muscle samples from certain parts of a salmon will give a better idea of overall fat content than will samples from other parts. It shows the area of a salmon from which samples were cut. Orientation and repeatability experiments are conducted on several salmon samples.

Again, 10°C is shown to be an appropriate temperature at which to take measurements. Ultrasound results from salmon samples are compared to chemical analysis to find a trend relating ultrasound velocity to the quantity of intramuscular fat in a sample.

In Chapter 5, a ray-tracing model of ultrasound travelling through a salmon sample is described. The model output is compared to empirical results from Chapter 4. The model is used to investigate the effects on measured velocity of changing temperature, fat content, myoseptum thickness and myosepta configuration. It also models the effects that individual myosepta have on overall velocity.

Finally, Chapter 6 provides an overview and analysis of the results in this thesis. Conclusions are derived from both the experimental work and the mathematical model. Future work which could improve the reported results is discussed.

Chapter 2

Methods and Materials

Information about the physical composition of a medium may be obtained by propagating low-intensity ultrasound through it and measuring the influence of the medium on the properties of the wave. Two parameters which have been used widely for fat assessment of muscle tissue are the speed of sound and the attenuation. These parameters have been used to provide information about the concentration, anatomical structure and physical state of components of muscle tissue [22].

The equipment needed to measure the speed of sound and the attenuation is generally inexpensive and provides a rapid means of characterising a medium. The measurement system used here was comprised of two transducers, one pulser-receiver and a digital oscilloscope for displaying and storing data. Matlab was used to extract pulse transit time and pulse intensity

information from saved data.

This chapter relates the reasons for choosing the speed of sound and attenuation as parameters for detection of fat in salmon muscle. It also details the measurement system and signal processing algorithms used to collect the time of flight and intensity information from which the two parameters were calculated.

2.1 Ultrasound for Tissue Characterisation

The spatial resolution of an ultrasound system is approximately equal to the wavelength of the ultrasound beam in the medium under examination.

Frequency is related to wavelength such that

$$c = f\lambda \quad (2.1)$$

where f is frequency, λ is wavelength and c is the speed of sound. In a nondispersive medium, sound waves of different frequencies travel at approximately the same speed; i.e., in such a medium wave velocity is independent of frequency [23]. Greater spatial resolution may be achieved by decreasing wavelength and thus increasing frequency. However, attenuation also increases with frequency [24]. Therefore, the distance over which useful amounts of energy can be propagated decreases as frequency increases.

Most studies investigating the acoustic properties of tissues or tissue components have used frequencies between 1MHz and 15MHz [25, 26]. Those specifically involving the properties of beef or fish muscle other than salmon have used frequencies of 1MHz [27], 1-6MHz [28], 1-5MHz [29], 1.25MHz [30], 2.5MHz [31, 32], 3MHz [33], 3.5MHz [22, 34, 20], 5MHz [35] or 10MHz [36].

In choosing a working frequency, it was important to take into consideration the size of the samples under examination. All of the fish samples varied in thickness, but none was thicker than 25mm. Therefore, it was necessary to choose a frequency which would guarantee that several wavelengths would propagate through a sample. A frequency in the MHz range would guarantee this, as the expected wavelength at 1MHz, assuming an average tissue speed of sound of approximately 1540ms^{-1} is 1.54mm. The myosepta in salmon muscle are approximately 2mm in thickness. Therefore, a frequency greater than 1MHz should provide better resolution of these features. As mentioned above, increasing frequency will also increase attenuation. Therefore, more energy will need to be put into the system to overcome this. Increasing input amplitude to too great a level could lead to nonlinear effects occurring in the tissue. A frequency of 2.25MHz was chosen because this frequency was seen to provide sufficient spatial resolution while keeping attenuation relatively low.

Table 2.1 shows the expected wavelengths and speeds of sound through

salmon muscle and salmon muscle components at 20°C.

	approximate c	λ ($f=2.25\text{MHz}$)
Distilled Water	1482ms^{-1}	0.66mm
Salmon Oil	1486ms^{-1}	0.66mm
Salmon Muscle	1556ms^{-1}	0.69mm
Connective Tissue	1729ms^{-1}	0.77mm

Table 2.1: Approximate velocities and wavelengths in salmon muscle tissue and tissue components [37, 38, 39].

The data in Table 2.1 is temperature dependent. The speeds of sound through distilled water and salmonid muscle have been shown to increase with temperature [38, 20]. The speeds of sound through edible oils have been shown to decrease with temperature [37, 39]. It is expected that the speed of sound through connective tissue will also decrease with temperature. This is because the speeds of sound through most of the amino acids in the proteins that make up salmon connective tissue have been shown to decrease with temperature [40]. However, Table 2.1 gives an approximate idea of the expected spatial resolution of the system.

2.1.1 Speed of Sound

Measuring the speed of sound has been shown to be a rapid nondestructive method for the characterisation of muscle tissue and tissue components. Specifically, the speed of sound has been used to assess the fat content of beef [31, 29], lamb [41], chicken [42], Atlantic mackerel [43], cod [22], North

Atlantic albacore [28] and whitefish [21]. The speed of sound has also been used to characterise the fats and edible oils which exist in muscle tissue [25]. Moreover, the speed of sound has been measured through combinations of fats, proteins and distilled water in an attempt to predict measured velocities when various fish tissues are insonified [34, 20].

There are various techniques for measuring the speed of sound. Some well-known methods include the sing-around technique, the velocity difference method, the pulse transit time measurement and the multiple echo technique [44, 26].

The sing-around technique involves measuring the number of times a pulse travels backwards and forwards through a medium over a known period of time. If n pulses are counted per second, then

$$c = \frac{d}{\left(\frac{1}{n} - \Delta_t\right)} \quad (2.2)$$

where d is the distance between transducers and Δ_t is the constant delay associated with each transit of the pulse through the electronics from the receiving transducer to the transmitting transducer [26].

In the velocity difference method, both transducers are mounted on a rig which can be translated horizontally. One transducer is in water, the other is in the medium under investigation. The separation between transducers is fixed. If the velocities in the water and the sample differ, a phase change

occurs in the received signal as the transducer is moved horizontally. With this method

$$c_s = c_w^2 \left(\frac{1}{f\Delta_z - c_w} \right) + c_w \quad (2.3)$$

where c_w and c_s are the velocities in the water and in the sample respectively and Δ_z is the distance at which a phase change of 360 degrees is measured [26].

The most straight-forward method is pulse transit time measurement. It requires uncomplicated signal processing. With this method velocity is calculated as

$$c = \frac{d}{t} \quad (2.4)$$

where t is the time of flight of the pulse once through the medium under investigation.

A similar technique to pulse transit time measurement is the multiple echo technique. It uses one transducer and measures the time between the first and third received echoes. Therefore, with this method

$$c = \frac{d}{(t_{1-3}/2)} \quad (2.5)$$

where t_{1-3} is the time between the first and third echoes. The multiple echo technique has been reported to yield better results than pulse transit

time measurement in nondestructive testing (NDT) applications [44]. This technique was investigated for use here. However, there was a degree of attenuation in the muscle tissue samples such that usable echo data beyond the first echo could not be attained. Moreover, the calibration results in Chapter 3 will show that a sufficient degree of accuracy was attained using pulse transit time measurement with two transducers. Therefore, the multiple echo technique was not used.

Pulse transit time measurement was used to measure the speed of sound because it required uncomplicated signal processing and inexpensive experimental equipment.

2.1.2 Attenuation

Reduction of a wave's intensity as the wave propagates is termed "attenuation". Attenuation can be caused by absorption, scattering or reflection of the wave at an interface between media. In complex media, such as tissue, all three of these mechanisms contribute to the overall attenuation [45].

There are three main techniques for measuring attenuation from pulse data [26]. The first involves a signal being propagated through a sample from a transmitting transducer to a receiving transducer. A pulse may also be propagated through a sample from a transmitting transducer to a reflector,

and then back along the same path to the transmitting transducer, which now acts a receiver. In both cases, the attenuation of a pulse may be measured by comparing the amplitude of the received signal to the amplitude of the original input signal. The third method involves transmitting a pulse into a sample using a transmitting transducer which then receives echoes from distributed discontinuities in characteristic impedance within the sample. This makes it possible to measure the rate of decay of echo amplitude with distance. The first of these methods is the one used in experiments described here.

Wells [26] observed that “the major difficulty with all pulse systems of attenuation measurement arises as a result of the frequency dispersive characteristics of most materials, including almost all of biological origin.” This is because short pulses contain energy over a wide frequency spectrum. However, the literature shows that changes in attenuation with fat content have been recorded using short pulses for both milk/cream mixtures and whitefish muscle tissue [21, 46]. This suggests that attenuation may be a supportive parameter in assessing the fat content of salmon muscle. Therefore, attenuation was measured as well. From a practical standpoint, it required no extra effort in terms of data acquisition to measure at the same time as the speed of sound was measured.

2.2 Measurement System

Figure 2.1 shows the complete measurement system used in all experiments described herein.

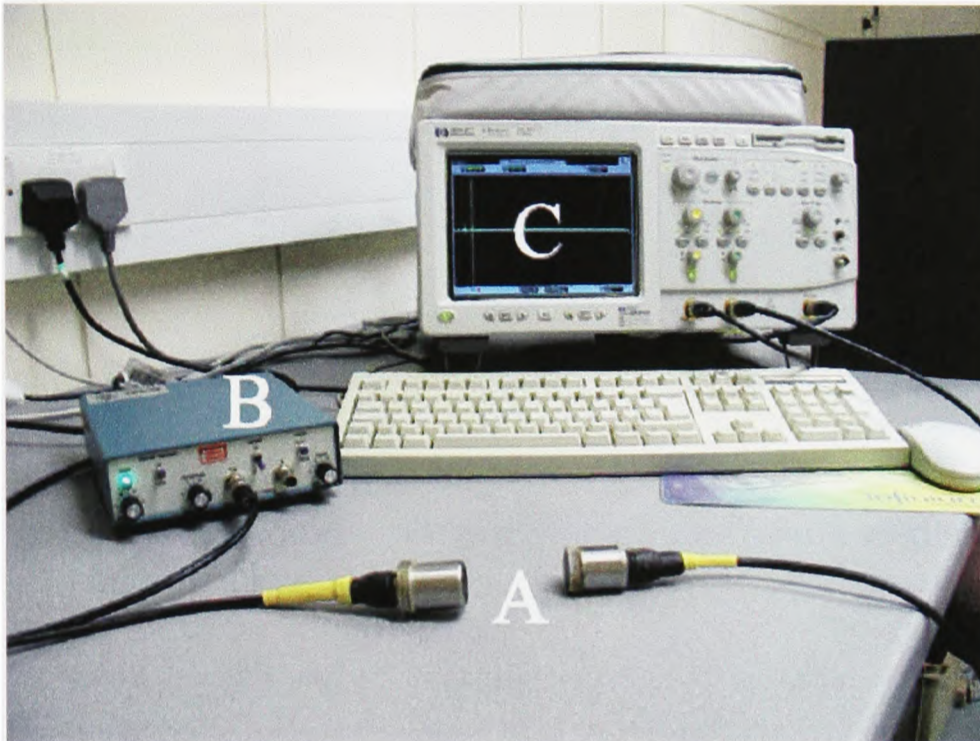


Figure 2.1: The measurement system. “A” is the ultrasonic probes, “B” is the pulser-receiver and “C” is the oscilloscope.

In Figure 2.1, “A” is the ultrasonic probes, “B” is the pulser-receiver and “C” is the oscilloscope. Some experiments required equipment to be supplied or developed specifically for that experiment. Such hardware is described in Sections 3.2 and 4.4. Figure 2.2 shows a schematic representation of the system.

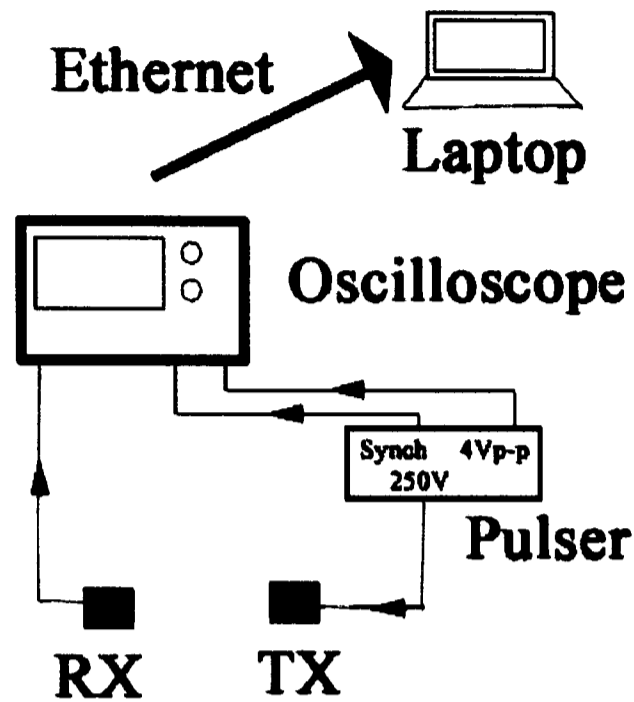


Figure 2.2: Schematic view of the measurement system.

A pulse created by the pulser-receiver was used to drive the transmitting transducer. The receiving transducer was connected directly to the oscilloscope. The receiver part of the pulser-receiver combination was not used.

Waveforms were saved to the hard drive of the oscilloscope. The saved files contained amplitude and time scale information about the signals. Data was then transferred to a laptop computer via an Ethernet network connection. Time of flight and attenuation information were extracted from the data using a programme written in Matlab.

2.2.1 Pulser-receiver

The transmitted pulse was produced by a Panametrics 500PR pulser-receiver. It was manufactured by the NDT Division of Panametrics, Inc. of Massachusetts, USA. Figure 2.3 shows the pulser-receiver.



Figure 2.3: The pulser-receiver.

The pulser is capable of generating a sharp pulse of either 250V or 125V peak amplitude. The rise time of the pulse is approximately 10ns. A 250V pulse drove the transmitting transducer. Signals output from the pulser to the oscilloscope were scaled down to a maximum amplitude of $4V_{p-p}$. Therefore, attenuation calculations assumed an input voltage of 250V.

2.2.2 Transducers

Figure 2.4 shows the typical construction of a transducer probe built for the generation and detection of short pulses [26]. The radiating face of the transducer is protected by a thin matching layer of epoxy resin. The backing material is chosen to have a similar characteristic impedance to that of the transducer and to absorb as much as possible of the energy which enters it. A typical backing material is a mixture of tungsten powder in Araldite. The ultrasonic insulator between the case of the probe and the transducer and backing block assembly minimizes coupling of ultrasonic energy into the case. Such coupling is undesirable because the case is often made of low-loss materials, such as metals, and is likely to ring for some time in response to an ultrasonic transient. Suitable backing materials include cork, rubber and polymers such as nylon [26]. Information on the construction materials of the probes used here was unavailable from the manufacturers.

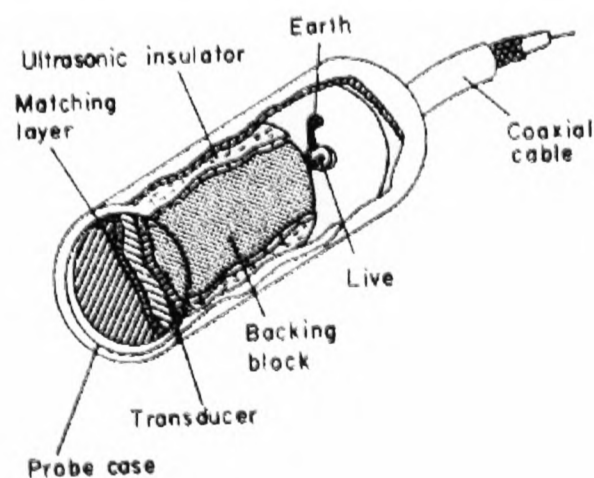


Figure 2.4: Diagram of a typical single-element probe.

The transducers used in all experiments described here were two 2.25MHz unfocused circular single-element immersion transducers. Each transducer has a bandwidth of approximately 2MHz, or ± 1 MHz from the centre frequency. They were manufactured by Advanced NDT Instruments of Worcester, England and Sonatest PLC of Milton Keynes, England. Transducers whose impedances are matched to that of water were chosen because many of the experiments described herein involved sending ultrasound through a liquid. Moreover, salmon muscle tissue is approximately 60% to 75% water. Both probes have an acoustical impedance of approximately 1.49 MRayls.



Figure 2.5: Two ultrasonic probes.

The piezoelectric transducer elements within the casings pictured in Figure 2.5 are in the form of a disc which is aligned to radiate or receive energy at its plane surfaces. The acoustic field generated by such a source can be divided into the Frésnel and Fraunhofer regions. The regions are also called the “near” and “far” fields respectively, due to each region’s proximity to the

transducer face. These regions are illustrated in Figure 2.6 [47].

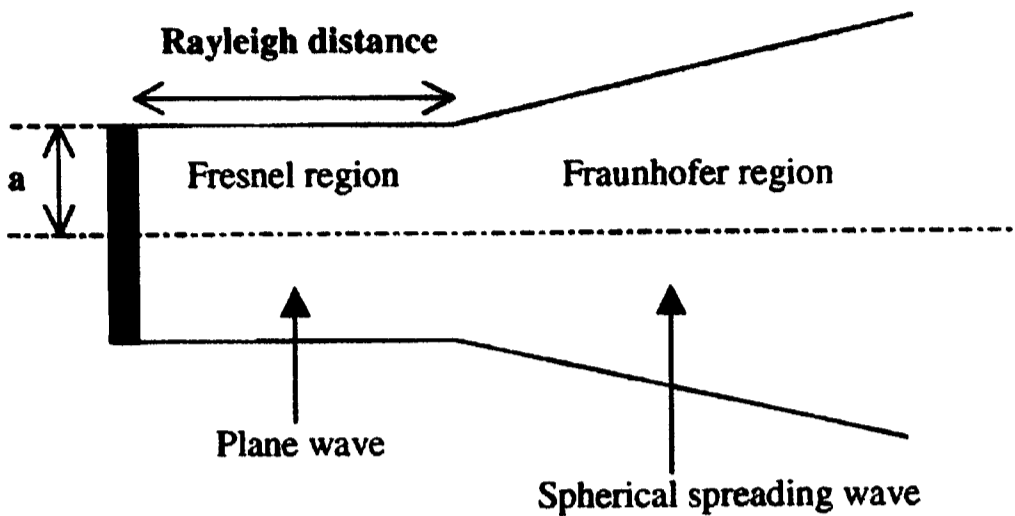


Figure 2.6: Axial view of the acoustic field from a plane circular single-element source.

Acoustic energy propagates as a plane wave in the Frésnel region. This gives the beam a roughly cylindrical shape, with a series of pressure intensity maxima and minima of decreasing complexity moving away from the transducer. Expanding spherical waves in the Fraunhofer region result in a diverging beam shape with pressure intensity varying inversely with the square of the distance from the transducer [24].

The relationship between intensity and distance from the radiating source is

$$\frac{I_x}{I_o} = \sin^2 \frac{\pi}{\lambda} \left(\sqrt{(a^2 + x^2)} - x \right) \quad (2.6)$$

where I_o is the maximum intensity, I_x is the intensity at distance x from the transducer and a is the radius of the transducer element [26]. Equation 2.6

applies only along the axis of the transducer. A typical graph of Equation 2.6 is shown in Figure 2.7 [23].

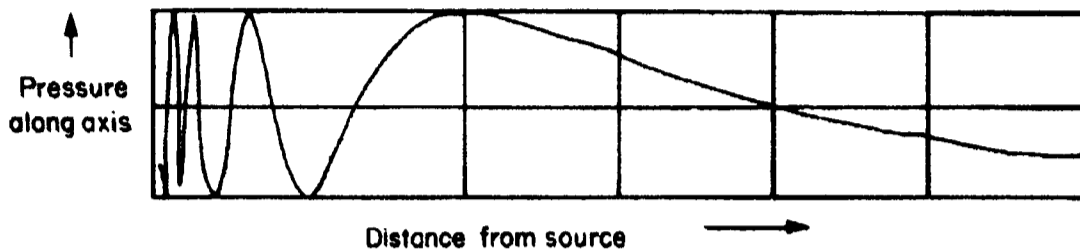


Figure 2.7: Typical intensity versus distance plot for an unfocused single-element transducer.

Solutions to Equation 2.6 give the positions of maxima and minima within the Frésnel region as

$$x_{\max} = \frac{4a^2 - \lambda^2 (2m + 1)^2}{4\lambda (2m + 1)} \quad (2.7)$$

$$x_{\min} = \frac{a^2 - \lambda^2 n^2}{2n\lambda} \quad (2.8)$$

where $m=0, 1, 2, \dots$ and $n=1, 2, 3, \dots$. The last maximum is taken to correspond to the end of the Frésnel region and the beginning of the Fraunhofer region. This maximum occurs at a distance from the transducer of

$$x_{\max_last} = \frac{4a^2 - \lambda^2}{4\lambda} \quad (2.9)$$

If a^2 is much greater than λ^2 , then the length of the Frésnel region can be calculated as

$$d = \frac{a^2}{\lambda} \quad (2.10)$$

where d is the distance from the transducer face at which the cylindrical beam begins to diverge [26, 23]. This distance is also called the Rayleigh distance.

The transducers used here had an element size of 0.5 inches, or 12.7mm. Therefore, one would expect a Frésnel region length of approximately 61.09mm in distilled water and a length of approximately 52.37mm in connective tissue, both at 20°C. Figure 2.8 shows a plot of the field in distilled water from one of the transducers used here.

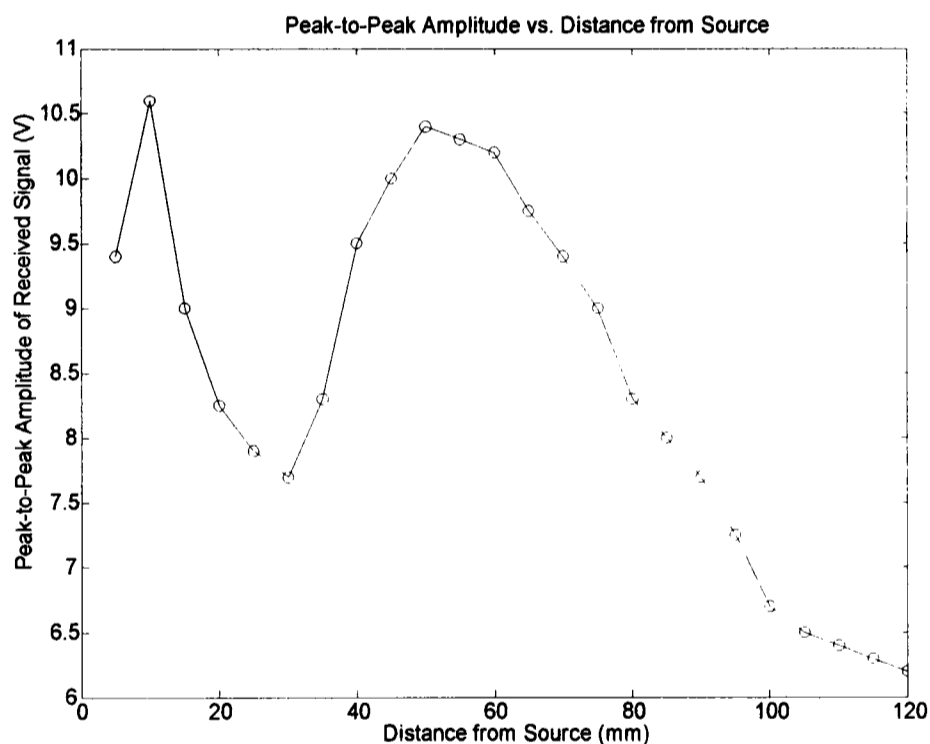


Figure 2.8: The ultrasonic field of a 2.25MHz transducer in distilled water at 20°C.

Figure 2.8 shows that for these transducers the Frésnel region ends at approximately 55mm in distilled water. This is close to the approximately 61mm which was predicted by Equation 2.10. In the Fraunhofer region,

where $x \gg x_{\max_last}$, intensity I_x is approximately inversely proportional to x^2 . The directivity of beam spreading is governed by the directivity function D_s such that

$$D_s = \frac{2J_1(ka \sin \theta)}{ka \sin \theta} \quad (2.11)$$

where J_1 is a first order Bessel function of the first kind and wave number $k=2\pi/\lambda$. Now, $J_1(ka \sin \theta)=0$ when $ka \sin \theta= 3.83, 7.02, 10.17, 13.32\dots$ In physical terms, this means that the energy is confined into lobes. The energy of the side lobes is much lower than that in the main lobe [26]. Figure 2.9 shows the expected beam pattern in the Fraunhofer region [26].

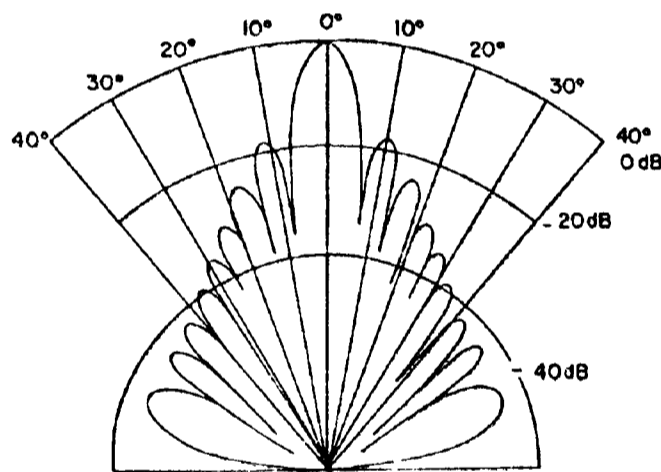


Figure 2.9: Expected beam spreading in the Fraunhofer region.

2.2.3 Oscilloscope

The oscilloscope is a two-channel Infinium 54820A digital oscilloscope manufactured by the Hewlett-Packard Company. The oscilloscope is Windows95-

driven and incorporates a PC motherboard, internal hard drive, floppy disk drive and Ethernet network port in its design. It is essentially a computer with an oscilloscope front end. Useful features include the ability to halt signal acquisition on all channels simultaneously. Each channel can then be stored as a separate data file for further processing. Random noise can be reduced through signal averaging. All waveform data presented here is an average of 128 waveforms. The input electrical impedance of the oscilloscope is 50 Ohm.



Figure 2.10: HP Infinium Oscilloscope 54820A.

The oscilloscope samples at a maximum rate of 2 gigasamples per second. The data used here was taken at a sampling rate of 250 megasamples per second. Each file contained 25041 samples which were recorded over a time-range of $100\mu\text{s}$. This degree of sampling means that the saved data has

a resolution of approximately 4ns. The number of samples saved at each sampling rate was determined by the oscilloscope. Figure 2.11 shows typical transmitted and received waveforms as they appeared on the oscilloscope screen.



Figure 2.11: Typical waveforms. The pulse on the very left of the image is the transmitted signal. The other waveform is the received signal.

Figure 2.11 shows the transmitted and received signals of an ultrasound pulse travelling through approximately 25mm of distilled water. The two signals appear on separate channels, distinguished by different coloured traces; yellow for channel 1 (extreme left), green for channel 2. The pulse on the extreme left of Figure 2.11 is the transmitted signal from the pulser-receiver. The other waveform is the received signal.

2.3 Signal Processing

Data was transferred from the oscilloscope to a Windows95 laptop computer. There, it was analysed using Matlab. A Matlab code listing of the programme used to calculate speed of sound and attenuation is in Appendix A. Figure 2.12 shows typical data.

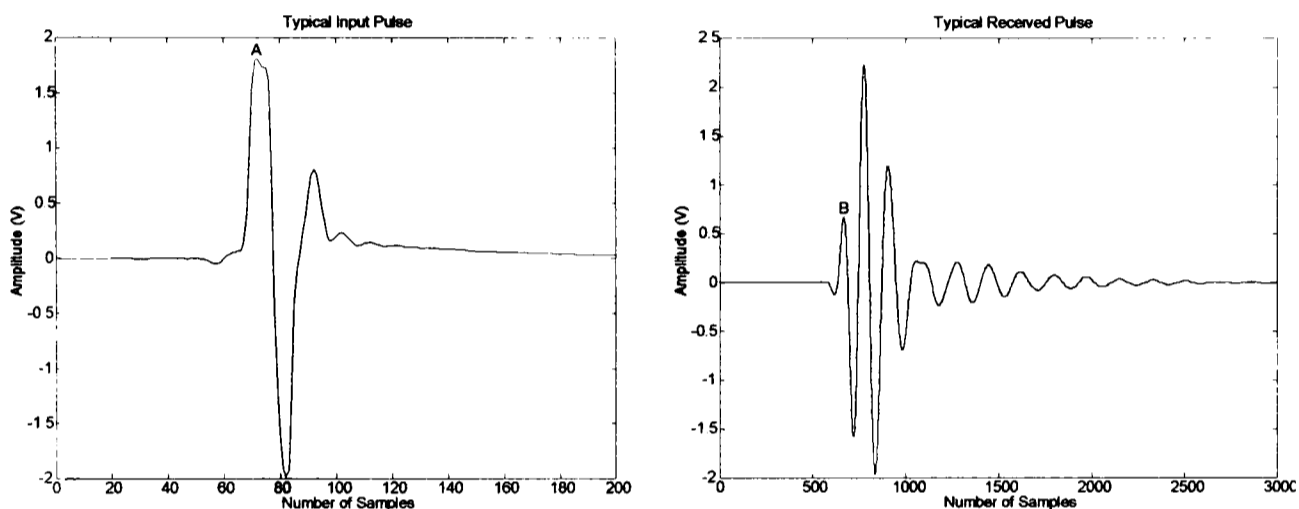


Figure 2.12: Typical transmitted pulse (left) and received waveform (right).

In Figure 2.12, the time range represented in the graph on the left is 800ns. The time range represented in the graph on the right is $12\mu\text{s}$. The resolution of both graphs is approximately 4ns per sample. The time of flight was determined by measuring the difference in time between the first peak of both signals. The peaks are labelled "A" and "B" in Figure 2.12. The amplitude of the transmitted signal shown in Figure 2.12 is the result of the scaling down of the signal as described in Section 2.2.1.

Figure 2.4 shows that the physical distance between transducer elements

cannot be readily measured due to the matching layer between the transducer element and the face of each probe. Therefore, there exists an error in distance measurement which is dependent on the thickness of the matching layers in both probes. Since this distance is difficult to measure in sealed transducer casings, a time offset was used to correct for this distance error. By placing the transducers face-to-face, a time delay of approximately 531.5ns was measured. This delay also includes the time taken for the signal to travel through the coaxial cables which connect all components. This is approximately 5ns m^{-1} [48]. The delay does not include the time taken for the oscilloscope to process the signals, as this would be the same for both signals.

Other distance measurement errors encountered as part of using an experimental rig or a particular experimental setup are discussed in their relevant chapters. Corrections were incorporated into the calculation of velocity such that Equation 2.4 became

$$c = \frac{d + d_{offset}}{t - 531.5 \cdot 10^{-9}} \quad (2.12)$$

where d is in units of metres and t is in units of seconds. Attenuation is manifested as an exponential decline of signal amplitude A with distance x travelled by the wave. This relationship is shown in Equation 2.13.

$$A = A_0 e^{-\alpha x} \quad (2.13)$$

where A_0 is the initial value of the amplitude at distance $x = 0$ and α is the attenuation coefficient [23]. The attenuation coefficient is in units of distance⁻¹. However, in practice it is measured in units of dB cm⁻¹ such that

$$\alpha(\text{dB cm}^{-1}) = -\frac{1}{x} 10 \log_{10} \left(\frac{A^2}{A_0^2} \right) \quad (2.14)$$

$$\alpha(\text{dB cm}^{-1}) = -\frac{1}{x} 20 \log_{10} \left(\frac{A}{A_0} \right) \quad (2.15)$$

The greater the value of the attenuation coefficient, the more rapid the decline of amplitude of the wave with distance travelled [49]. The attenuation values quoted in later chapters were arrived at by calculating α using Equation 2.15. In such calculations, the initial input amplitude was defined as 250V. A was defined as the peak amplitude of the received signal. All measurements were made in the near field.

Equation 2.15 does not take diffraction effects into consideration. However, Seki [50] showed that a general estimate of the attenuation due to diffraction is given by 1 dB per a^2/λ . This is thought to be accurate to within one order of magnitude

2.4 Summary

This chapter described the method which was used to characterise salmon tissue using ultrasound. Pulse transit time measurement was used to measure the speed of sound. Attenuation was calculated from pulse intensity values as a supportive parameter to the speed of sound measurements. The measurement system was described. The signal processing methods which were used to attain and analyse raw data were also explained. All experiments described in subsequent chapters used this system to acquire velocity and attenuation data.

Chapter 3

Phantoms

A “phantom” is a material, or combination of materials, that mimics the ultrasound characteristics of another material, such as soft tissue. Phantoms can be used to model how the speed of sound and the attenuation within a material will alter as the components of that material are altered. This chapter describes experiments which were conducted using phantoms to model dispersed fat concentrations within salmon muscle tissue.

Water and fat constitute roughly 80% of salmon muscle tissue. The other 20% is composed of proteins and of a very small percentage of non-flammable trace minerals collectively known as “ash.” Fat within salmon muscle exists as dispersed oil concentrations. The fat is in the form of oil due to its high quantities of polyunsaturates [51]. This type of fat is called “intramuscular” fat. There are no fat layers within salmon muscle itself. Therefore, it was

important to investigate if the ultrasound system was capable of picking out concentration differences in a dispersed fat system. Some studies [22, 34, 43, 28, 20] have treated fish tissue as a liquid because its shear modulus is much smaller than its bulk modulus.

Skimmed milk and double cream were chosen as the two components for a phantom. The skimmed milk contained 0.1% fat, while the cream contained 48% fat. The skimmed milk represented the water and protein components of the tissue, and the cream represented fat, water and protein. By mixing the two components in differing proportions, a dispersed fat system of many different fat levels could be created.

The acoustic velocities of both water and fat change with temperature. The velocity through water is known to increase with temperature. The velocity through edible fats and oils is known to decrease with temperature. The point at which they are equal has been shown to be approximately 18°C for some oils [34]. Therefore, experiments were conducted to find the temperature at which the fat and the water within the phantom components had equal velocities. Further experiments were conducted at a temperature at which one could more easily distinguish between velocity changes caused by changes in fat level. It was possible to generate an empirical equation to predict the amount of fat in the milk/cream phantom given only the measured velocity. This equation was then assessed for repeatability by a

series of blind tests.

Finally, reticulated foam was introduced into the milk/cream phantom. Lerski [52] has shown that the structure within Bulpren S20 reticulated foam was capable of producing tissue-like attenuation. The measured velocity drop due to the introduction of the foam into the phantom was approximately 0.1%. Again, velocity and attenuation measurements were taken to determine if the system was capable of detecting changes in dispersed fat level in this more tissue-like structure.

3.1 Acoustic Properties of Liquids

Sound is a mechanical vibratory form of energy which propagates through a medium by means of the motions of the particles within the medium. All liquids absorb energy because of frictional forces which act to oppose the periodic motion of the particles within the medium [23]. In addition, the density of a liquid changes with temperature. For example, liquids are less dense at 40°C than they are at 4°C. A less dense liquid can be compressed more during the high-pressure portion of the cycle.

On a larger scale, the propagation of sound waves can be understood in terms of the elastic properties of the medium. A substance which tends to return to its original size and shape when deforming forces are removed is

termed “elastic”.

For liquids, the speed of sound can be written as

$$c = \sqrt{\frac{1}{\kappa\rho_0}} \quad (3.1)$$

where ρ_0 represents the uncompressed density of the liquid and κ is the adiabatic compressability. The reciprocal of κ is the adiabatic bulk modulus of elasticity of the liquid, B [49]. In Appendix B, Equation 3.1 is derived from Hooke’s Law and Newton’s Second Law of Motion. For multi-component mixtures this equation becomes

$$c = \left[\left(\sum_{i=1}^n \phi_i \kappa_i \right) \left(\sum_{i=1}^n \phi_i \rho_i \right) \right]^{-1/2} \quad (3.2)$$

or, substituting for κ_i

$$c = \left[\left(\sum_{i=1}^n \frac{\phi_i}{c_i^2 \rho_i} \right) \left(\sum_{i=1}^n \phi_i \rho_i \right) \right]^{-1/2} \quad (3.3)$$

Here, n is the total number of components in the mixture, ϕ is the volume fraction of the dispersed component and ρ is the density of that component [53]. This equation assumes that the particles are rigid, are infinitesimally small compared to the wavelength and that the suspension is dilute [27].

Equations 3.1 and 3.3 hold for sound propagation in a stationary medium at small wave amplitudes. However, any sound wave by its very nature produces a flow of the medium, changing in time and space. This is called “bulk streaming” [54]. The velocity of this flow is the particle velocity v .

The dependence of the sound velocity on the particle velocity can be seen from the following equation.

$$c = c_0 + \left(1 + \frac{B}{2A}\right)v \quad (3.4)$$

In Equation 3.4, c_0 is equal to c in the previous two equations. The ratio B/A is referred to as the “nonlinearity parameter.” The terms A and B come from the following Taylor series expansion of the equation of state for an acoustic wave travelling through an isotropic medium [55].

$$P = P_0 + A \left(\frac{\rho - \rho_0}{\rho}\right) + \frac{B}{2} \left(\frac{\rho - \rho_0}{\rho}\right)^2 + \dots \quad (3.5)$$

where

$$A = \rho_0 \left(\frac{\partial P}{\partial \rho}\right)_{0,S} \quad (3.6)$$

and

$$B = \rho_0^2 \left(\frac{\partial^2 P}{\partial \rho^2}\right)_{0,S} \quad (3.7)$$

P and P_0 are the instantaneous and hydrostatic pressures and ρ and ρ_0 are the instantaneous and equilibrium densities. The partial derivatives are taken at equilibrium and at constant entropy, S . Thus, the nonlinearity of the medium can be expressed as B/A such that

$$\frac{B}{A} = \rho_0 c_0 \left(\frac{\partial c}{\partial P}\right)_T + \frac{\beta T \rho_0}{C_P} \left(\frac{\partial c}{\partial T}\right)_P \quad (3.8)$$

The subscript T indicates a partial derivative taken at constant temperature. The subscript P indicates a partial derivative taken at constant pressure. T itself is the temperature, β is the volume coefficient of thermal expansion and C_P is the specific heat at constant pressure. In soft tissue, the second term in Equation 3.8 dominates. For pure water, B/A has been determined experimentally to increase from 4.16 at 0°C to 6.11 at 100°C [55].

Every fat and edible oil contains a number of different fatty acids. These acids are defined by the number of carbon atoms and the number of double bonds between carbon atoms in each molecule. Appendix C shows the exact fatty acid composition of all four fats or edible oils discussed in this thesis. Javanaud [39] reported that the speed of sound through a fat or edible oil can be calculated from knowledge of its fatty acid composition. For example, the speed of sound through a single fatty acid at 20°C can be calculated using the following equation.

$$c = 1333 + 7n + 8m \quad (3.9)$$

where n is the number of carbon atoms present in the molecule, m is the number of double bonds between carbon atoms and c is in units of ms^{-1} . By calculating the velocity of each fatty acid present in an oil separately and then combining the velocities using Equation 3.3, an approximate overall velocity for an edible oil or fat can be calculated in principle.

The attenuation through liquids will adhere to the same equations set forth in Section 2.3. Single-component liquids do not contain particle structures to scatter incident sound. They also do not contain interfaces to reflect sound. In this instance, the measured attenuation coefficient is the same as the absorption coefficient [23].

3.2 Methods and Materials

In order to take accurate measurements of the speed of sound through a substance, it is essential to be able to control pressure and temperature. In the experiments in this chapter, the variation of velocity with temperature was under investigation. Therefore, every step was taken to ensure that temperature was controlled and measured as accurately as possible. Pressure was assumed to be normal atmospheric pressure. However, atmospheric pressure changes over the course of a day. Therefore, a reading of atmospheric pressure was recorded before taking measurements. Atmospheric pressure readings were obtained from the BBC Weather Centre website data for Oxford city centre [56]. This data is updated every hour.

For the experiments involving pure water, a 15-litre temperature-controlled water bath was used. The bath was manufactured by Grant Instruments Ltd. of Cambridge, UK. By means of a dial on the side of the tank, it was pos-

sible to set the water to a specific temperature within $\pm 1^\circ\text{C}$. The bath used an indicator light next to the dial to confirm that it had reached the set temperature. It was soon discovered that this method was highly inaccurate. Therefore, a digital thermometer was used to monitor the temperature within the tank. Using the thermometer in conjunction with the correct dial position, a desired temperature could easily be reached within $\pm 0.1^\circ\text{F}$, or $\pm 0.056^\circ\text{C}$. The water was continually circulated using a Perspex stirring rod. An air pump was not used to circulate the water because the pump would introduce bubbles and would dissolve gases into the liquid. The importance of using distilled degassed water is discussed later.

The two phantoms used to conduct the experiments described in this chapter were contained in Perspex. Perspex was used because it is an inexpensive material whose acoustic properties are known. The velocity of sound through Perspex is approximately 2690ms^{-1} [57]. The first cell in which the velocity of the milk/cream mixture was measured is shown in Figure 3.1.

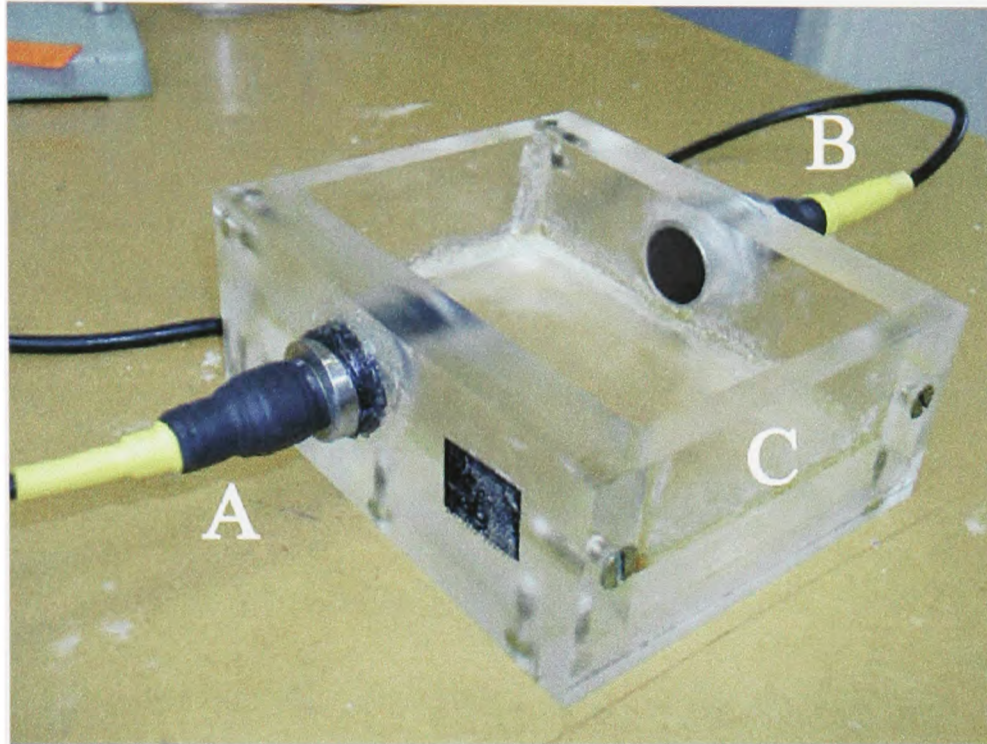


Figure 3.1: Perspex measurement cell. “A” and “B” are the ultrasonic probes. “C” is the Perspex measurement cell.

In Figure 3.1, “A” and “B” are the ultrasonic probes. “C” is the Perspex measurement cell. This cell allowed the transducers to be coupled straight into the liquid. Correct transducer alignment was key to acquiring accurate data. It was important to align the transducer faces in all three dimensions so as to avoid parallax error and inadvertent shifting of the transducers during the experiment. The cell is effectively a rectangular Perspex container with holes drilled through two opposite walls. The diameter of the holes is equal to the diameter of the transducers used. The inner dimensions of the cell are 87.0mm across by 130.0mm wide by a depth of 34.5mm. This gives a total volume of approximately 390.2ml. The cell provided a fixed ultrasound path length of 87.0mm. The transducers were fitted so that the faces of the

transducers aligned with the inside wall of the cell on both sides. Once the transducers were in place, silicone sealant was used to make the cell water tight. When the cell was filled with a liquid, reflections from the bottom of the cell and the surface of the liquid were noticed in the received signal. However, these reflections occurred after the first peak in the received signal. Therefore, they had little bearing on the results presented here. For the calibration measurements presented in the next section, the cell was placed inside the temperature-controlled water bath after the bath was filled with distilled degassed water.



Figure 3.2: Temperature-controlled water bath with Perspex cell inside it.

The water bath's minimum temperature was 25°C . Therefore, in experiments conducted below 25°C , the water bath was not used. Instead, the cell was filled with the liquid under examination and placed in a cooling chamber

for several hours. Measurements were taken as the temperature of the liquid was allowed to rise very slowly. Constant temperature readings were taken using the digital thermometer. Data acquisition was halted as soon as the liquid under examination was within $\pm 0.056^{\circ}\text{C}$ of the target temperature. The data was then saved and acquisition was started once more. This procedure avoided inaccuracies in velocity measurements due to the temperature drifting as the data was saved.

The other phantom was built to mimic more closely the properties of soft tissue. A reticulated foam block was used to simulate a tissue-like structure with tissue-like attenuation. As mentioned earlier, Lerski [52] demonstrated that Bulpren S20 reticulated foam was capable of producing tissue-like attenuation, while the measured velocity drop in distilled water due to the foam was less than 0.1%. The foam is manufactured by Foam Engineers Ltd. of High Wycombe, UK. The Bulpren S20 foam has an open-pore structure and a uniform pore size of 2.5mm. Its industrial application is as an air filter and it contains only open pores. Therefore, it is able to be completely filled with liquid.

A cube of Bulpren S20 was inserted into a Perspex box measuring 117mm by 177mm by a depth of 137mm internally. The box was constructed from 5mm-thick Perspex. The transducers were coupled onto the adjacent sides of the box using ultrasound gel. Thus the total ultrasound path length was

127mm. A cross was etched into the Perspex at the same position on opposite sides of the box. The centre of each transducer face was aligned with the centre of the cross. In this way, accurate transducer alignment was achieved.

The liquid under examination was poured into the box. The foam was then lowered into place. The foam was compressed several times to get rid of any air possibly trapped in voids within the foam. However, it is expected that the mixture was not completely degassed. Velocity measurements were made using milk/cream mixtures of increasing fat content. Temperature was measured by submerging the digital thermometer in the mixture between the edge of the foam cube and an interior wall of the box.

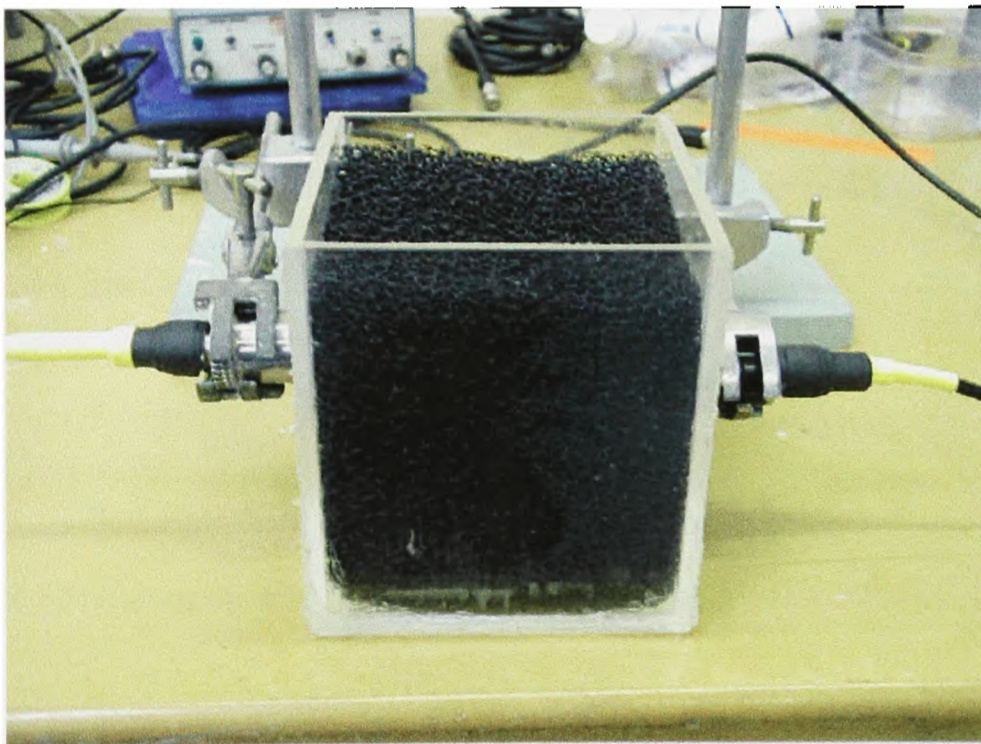


Figure 3.3: Phantom containing a block of reticulated foam.

3.3 Calibration

It was necessary to calibrate the measurement system by using reference media with known acoustic properties. This was done by comparing the system output with known values of the speed of sound in the reference media at the same known temperatures and the same known atmospheric pressures. First, the system was calibrated against a “medical” phantom. A medical phantom is a gel-filled test object with known tissue-like acoustic properties. Distilled degassed water was then chosen as a further reference medium. Distilled degassed water is a medium about which many velocity measurement results have been published. Additionally, measurements were taken to understand the effects of salinity on the speed of sound through sea water. Any ultrasonic system that will be used on live salmon in sea water must calibrate for these effects as well.

3.3.1 Medical Phantom

This type of phantom is used by quality control professionals to calibrate diagnostic ultrasound equipment. The gel within the phantom provides known tissue-like attenuation at a known velocity. The phantom used here was manufactured by Diagnostic Sonar Ltd. as part of the Cardiff Test System group of phantoms. The Cardiff Test System phantoms are used in the British

standard method for calibrating diagnostic ultrasound equipment [58].

The phantom consists of a graphite-loaded gel within a Perspex box. The box has acoustic windows on two adjacent sides. The gel is loaded with graphite at three different concentrations. The graphite particles in each concentration range in size from 15 microns to 44 microns in diameter. This produces three regions of differing attenuation and differing velocity. These properties are summarised in Table 3.1.

	Velocity at 21°C	Attenuation
High Attenuation	1529.8ms ⁻¹	2.56dB cm ⁻¹
Background	1529.1ms ⁻¹	1.84dB cm ⁻¹
Low Attenuation	1531.2ms ⁻¹	0.11dB cm ⁻¹

Table 3.1: Cardiff Test System reference values.

The accuracy of the velocity values is $\pm 0.1\%$, or approximately $\pm 1.5\text{ms}^{-1}$. The velocity at temperatures other than 21°C can be calculated by using a temperature coefficient of $2.4\text{ms}^{-1}\text{°C}^{-1}$. The accuracy of the attenuation values is not stated by the manufacturer. There are structures within the phantom to allow one to take a measurement which incorporates a percentage of each region. In this experiment, measurements were taken on only two regions: the 100% High Attenuation region and the 100% Low Attenuation region. The transducers were coupled to the acoustic windows using ultrasound gel. The digital thermometer was attached to one of the acoustic windows. Twenty measurements were made of each region. The temperature

of the phantom itself was also measured twenty times for each region. The mean temperature of the phantom during measurement of the High Attenuation region was $27.970^{\circ}\text{C} \pm 0.056^{\circ}\text{C}$. The mean temperature of the phantom during measurement of the Low Attenuation region was $26.725^{\circ}\text{C} \pm 0.056^{\circ}\text{C}$. The velocity measurements were then compared to temperature-adjusted expected values. These results are summarised in Table 3.2.

	Expected c	Measured c
High Attenuation	$1546.5\text{ms}^{-1} \pm 1.5\text{ms}^{-1}$	$1546.7\text{ms}^{-1} \pm 1.4\text{ms}^{-1}$
Low Attenuation	$1544.9\text{ms}^{-1} \pm 1.5\text{ms}^{-1}$	$1544.7\text{ms}^{-1} \pm 1.2\text{ms}^{-1}$

Table 3.2: Comparison of expected velocities and measured velocities through the medical phantom.

All measured data in the table above is a mean of 20 measurements. A mean was taken to overcome any coupling problems between the acoustic window of the phantom and the transducer face. Errors in the measured values are standard deviations. These results show that the measured values are approximately in line with expected values. It is reasonable to assume that the measurement system will be able to measure ultrasound velocity to within approximately $\pm 1.5\text{ms}^{-1}$.

Attenuation measurements are compared to expected values in Table 3.3.

	Expected α	Measured α
High Attenuation	2.56dB cm^{-1}	$2.68\text{dB cm}^{-1} \pm 0.31\text{dB cm}^{-1}$
Low Attenuation	0.11dB cm^{-1}	$0.32\text{dB cm}^{-1} \pm 0.25\text{dB cm}^{-1}$

Table 3.3: Comparison of expected attenuations and measured attenuations through the medical phantom.

Again, all measured data in the table is a mean of 20 measurements. Errors in the measured values are standard deviations. Note again that the manufacturer did not state error values for the attenuation through the phantom. However, both of the expected values fall within the error ranges of the measured values. Therefore, it was assumed that the measurement system was capable of measuring attenuation to within approximately $\pm 0.3\text{dB cm}^{-1}$.

3.3.2 Distilled Degassed Water

In 1972, del Grosso and Mader [38] published an equation and tables of data relating the speed of sound in pure water to temperature. However, their equation neglected the pressure dependence of the speed of sound in water. Pierce [59] suggested a pressure dependence term in his 1981 book. Povey [60] has combined the temperature and pressure terms and proposed the following equation, which employs del Grosso and Mader's equation modified by the addition of the pressure dependence term quoted by Pierce.

$$c = 1402.39 + 5.03711T - 0.0580852T^2 + 3.3342 \cdot 10^{-4}T^3 \\ - 1.478 \cdot 10^{-6}T^4 + 3.14643 \cdot 10^{-9}T^5 + 1.6 \cdot 10^{-6} (p_0 - 10^5) \quad (3.10)$$

where T is temperature in degrees Celsius and p_0 is the absolute pressure in Pascals. The temperature coefficients are calculated from empirical data. The equation is accurate to within $\pm 0.015\text{ms}^{-1}$ between 0.001°C and

95.126°C at 10^5 Pa [60]. The objective of this experiment was to obtain an estimate of the error between the results taken with this system on distilled degassed water and the solutions obtained using Equation 3.10 over a 15°C temperature range.

Distilled water was obtained from the Oxford University Biochemistry Department. The water was distilled using the Milli-Q Ultrapure Water machine manufactured by Millipore Incorporated. The purifier output 99.999% pure H₂O. The machine did not, however, degas the water.

It was very important to degas the water to remove dissolved air before measuring the speed of sound through it. Dissolved air generally has very little effect on the speed of sound. However, small changes in pressure can bring dissolved air out of solution, creating bubbles. Similarly, naturally occurring waters often contain microbubbles. They can have a large effect on the velocity of sound in the medium. For example, 10 parts-per-million (ppm) of undissolved air can change the velocity by approximately 8%. Likewise, 0.1ppm of undissolved air has been shown to decrease velocity by approximately 1.4ms^{-1} [60]. Therefore, it was imperative to degas the distilled water before any measurements were taken.

The simplest way to degas a liquid is to place it in an ultrasonic cleaning bath for several minutes. In this experiment, a plastic bottle containing the distilled water was partially submerged in the cleaning bath for fifteen

minutes. The high-power ultrasound of the bath encourages the dissolved air to form bubbles, which then float out of the liquid. The bottle cap was removed so as to let the bubbles escape into the ambient air. The bath itself was supplied by RS Components Ltd. and contained two 75W, 2.5MHz transducers pointed upwards from the floor of the bath.



Figure 3.4: Water bottle containing distilled water inside the ultrasonic cleaning bath.

The water was then carefully transferred to the temperature-controlled water bath. Care was taken to minimise the probability of new gas bubbles being introduced into the liquid during the transfer. The speed of sound was then measured over a temperature range of 25°C to 39°C. This temperature range was chosen so as to allow use of the temperature-controlled water bath. While the temperature of sea water, and thus the temperature of fish tissue,

would in practise be lower, this temperature range is quite satisfactory for calibrating the measurement system. The atmospheric pressure was recorded as 1007mB, or 1.007×10^5 Pa, and rising. The results are shown below.

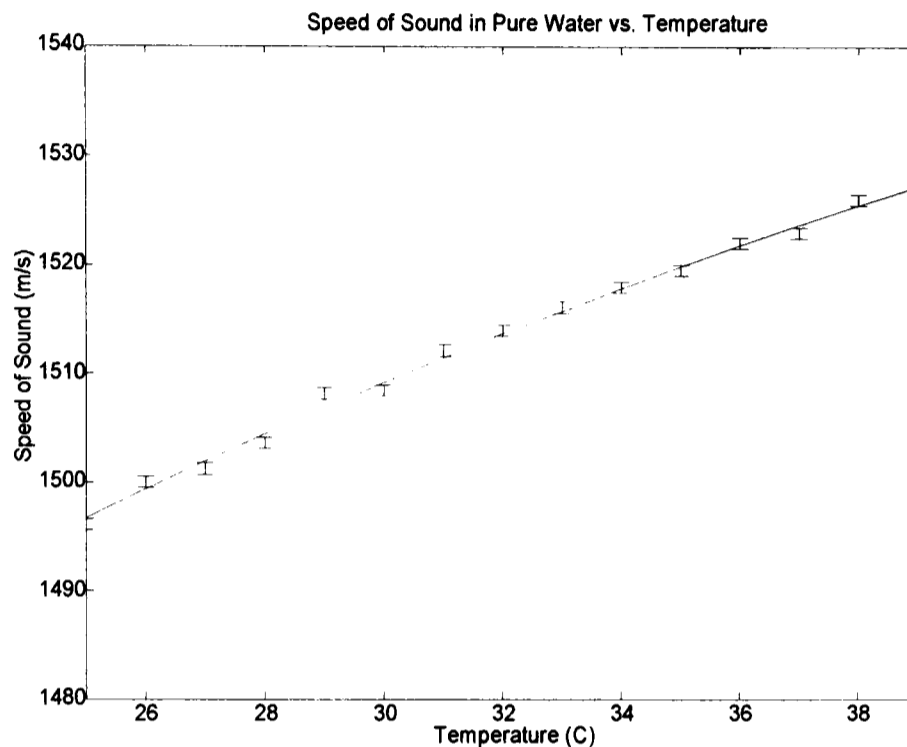


Figure 3.5: Speed of sound in distilled degassed water versus temperature. The dots represent measured values. The solid line is the solution to Equation 3.10.

In the figure above, the dots represent measured values while the solid line is the solution to Equation 3.10. The standard deviation in these measurements is $\pm 0.51 \text{ms}^{-1}$ in relation to expected values from the solution to Equation 3.10.

3.3.3 Salt Water

In the wild, salmon can be found in both salt water and fresh water. However, the majority of commercial fish farms in Europe are located in the salt water of the North Atlantic Ocean. Therefore, it makes sense to investigate the effect that salinity has on the propagation of ultrasound in water.

In 1960, W.D. Wilson [61] published the following equation giving the speed of sound in sea water as a function of temperature, pressure and salinity.

$$V = 1449.22 + \Delta V_T + \Delta V_P + \Delta V_S + \Delta V_{STP} \quad (3.11)$$

where

$$\Delta V_T = 4.6233T - 5.4585 \cdot 10^{-2}T^2 + 2.822 \cdot 10^{-4}T^3 - 5.07 \cdot 10^{-7}T^4 \quad (3.12)$$

$$\begin{aligned} \Delta V_P = 1.60518 \cdot 10^{-1}P + 1.0279 \cdot 10^{-5}P^2 + 3.14151 \cdot 10^{-9}P^3 \\ - 3.503 \cdot 10^{-12}P^4 \end{aligned} \quad (3.13)$$

$$\Delta V_S = 1.391(S - 35) - 7.8 \cdot 10^{-2}(S - 35)^2 \quad (3.14)$$

$$\begin{aligned} \Delta V_{STP} = (S - 35) - (1.197 \cdot 10^{-2}T + 2.61 \cdot 10^{-4}P - 1.96 \cdot 10^{-7}P^2 \\ - 2.09 \cdot 10^{-6}PT) + P(-2.796 \cdot 10^{-4}T + 1.3302 \cdot 10^{-5}T^2 \\ - 6.644 \cdot 10^{-8}T^3) + P^2(-2.391 \cdot 10^{-7}T + 9.286 \cdot 10^{-10}T^2) \\ - 1.745 \cdot 10^{-10}P^3T \end{aligned} \quad (3.15)$$

T is the temperature in degrees Celsius, P is the pressure in kg/cm^2 ($1.02\text{kg}/\text{cm}^2 = 10^5\text{Pa}$) and S represents the salinity of the water in parts-per-thousand (ppt). The equation reflects the speed of sound in sea water in the temperature range -3°C to 30°C , the pressure range $1.033\text{kg}/\text{cm}^2$ to $1000\text{kg}/\text{cm}^2$ and the salinity range 33ppt to 37ppt [61]. Approximately 99.5% of all sea water falls within these three ranges. Equation 3.11 is reported to be accurate to within $\pm 0.22\text{ms}^{-1}$.

The objective of this experiment was to determine the effect that different salinities would have on the ultrasound velocity within the medium as the temperature was increased. In this experiment, the salinity ranged from 33ppt to 37ppt, in 2ppt increments. Synthetic marine salt was purchased from a local aquarium supply shop. The sea salt was a mixture of pharmaceutical grade chemically-pure salts and 70 different trace elements, all of which appear naturally in sea water and remain in solution when dissolved. The salt is produced by Dr. Biener GmbH of Wartenberg, Germany.

An acceptable water temperature range for salmon is 2°C to 22°C [17]. This experiment was conducted over the temperature range from 3°C to 18°C . As described earlier, the temperature-controlled water bath was not used for experiments below 25°C . Instead, the water was cooled, then the temperature was allowed to rise slowly. The water was not degassed, as real sea water would contain microbubbles and dissolved gases [60].

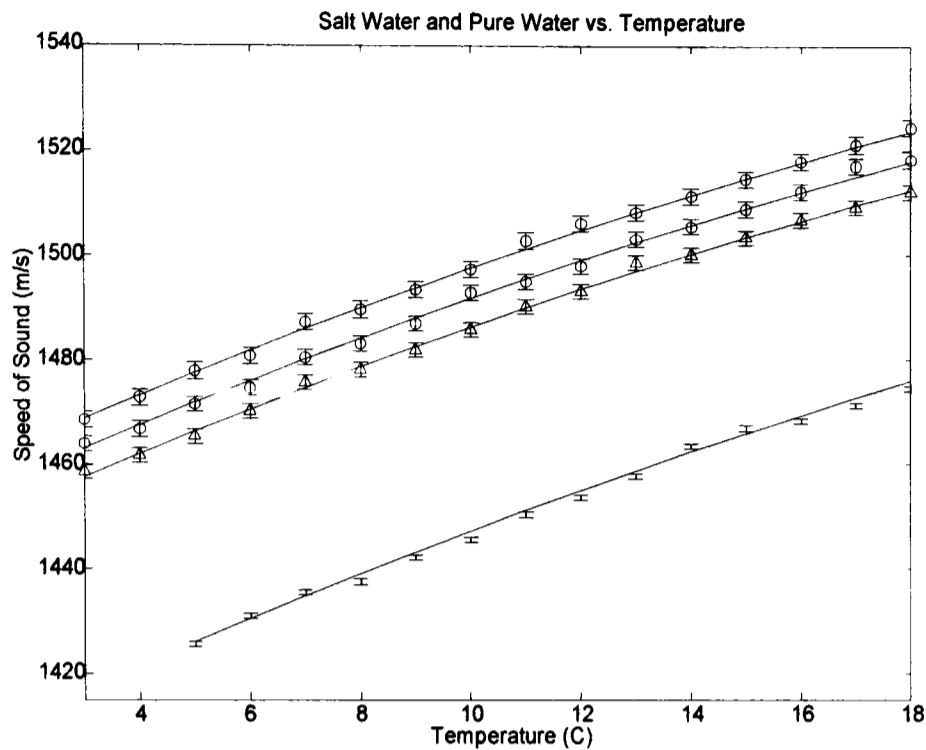


Figure 3.6: The velocity gap between pure water, bottom, and water of various salinities. Shapes represent experimental data. The bottom line is the solution to Equation 3.10 for pure water. The other solid lines are the solutions to Equation 3.11 for the three salinities.

The shapes in the top half of Figure 3.6 show the experimental data for three different salinities: 33ppt represented by triangles, 35ppt represented by circles and 37ppt represented by diamonds. The crosses in the bottom half of the figure represent experimental data for pure water. The top solid lines are the solutions to Equation 3.11 for those three salinities. The bottom solid line is the solution to Equation 3.10 for pure water.

These results demonstrate that the acoustic velocity increases near-linearly with both salinity and temperature within this range. At a concentration of 33ppt, the velocity difference with pure water of the same temperature is approximately $39.85\text{ms}^{-1} \pm 1.36\text{ms}^{-1}$. A concentration of 35ppt yields a

difference of approximately $42.67\text{ms}^{-1} \pm 1.46\text{ms}^{-1}$ with pure water of the same temperature. Finally, a concentration of 37ppt produces a difference of $44.87\text{ms}^{-1} \pm 1.56\text{ms}^{-1}$. All errors are standard deviations from expected values from Equation 3.11. These results show increases of approximately 1.2ms^{-1} per ppt. The changes in velocity with salinity can be attributed to changes in both density and compressibility within the medium [62, 63, 64, 65, 66].

Atmospheric pressure was recorded for each salinity and included in the calculations. However, the pressure range was so small at ground level (0.011kg/cm^2) that the effects of atmospheric pressure change on the results presented here is negligible.

The repeatability of these results will depend on the degree of microbubbles present in the water under investigation. However, an increase in salinity will always cause an increase in acoustic velocity in waters with similar amounts of dissolved air and microbubbles over the range of temperatures seen here. More important is the fact that water salinity and air bubbles will have to be calibrated for in a finished fish fat monitoring system used in sea water.

3.4 Milk/Cream Mixtures

Milk and cream were chosen as the two components for a phantom to investigate whether the system was capable of detecting velocity and attenuation changes due to changes in fat concentration in a dispersed fat system. The milk and cream were obtained from a local supermarket. The milk contained 0.1% fat, while the cream contained 48% fat. Both the milk and the cream contained approximately 3% protein, 5% lactose and 1% of other solids, such as vitamins and minerals. The other 43% of the cream and 90.9% of the milk was water [67]. As both phantom components contained approximately the same levels of protein, lactose and other solids, all velocity and attenuation changes should have been caused by changes in the fat level of the mixtures.

Appendix C shows that there are differences in fatty acid composition between milk fat and salmon oil. Milk fat is high in saturated fatty acids, while salmon oil is high in mono- and polyunsaturated fatty acids. This compositional difference leads to a difference in acoustic velocity. Using Equations 3.3 and 3.9, it is possible to calculate the velocity of sound through milk fat as $1445.05\text{ms}^{-1} \pm 1\text{ms}^{-1}$ and the velocity of sound through salmon oil as $1486.12\text{ms}^{-1} \pm 1\text{ms}^{-1}$, both at 20°C . Despite these differences, milk fat is close enough to salmon oil in composition and acoustic velocity to give a reasonable idea of the behaviour of salmon oil in a dispersed fat system.

The cream was diluted with milk at different concentrations reflecting the range of fat concentrations found in salmon muscle tissue. Measurements were taken with the mixtures inside the Perspex measurement cell. Each mixture was constantly stirred with a Perspex stirring rod so as to keep the mixture as homogenous as possible. It was stirred slowly so that air was not introduced into the mixture. In this section, simulating tissue-like attenuation was not attempted.

3.4.1 Measurement Temperature

An important consideration is the temperature at which one may most easily distinguish between fat levels within the milk/cream mixture. McClements [25] has demonstrated that several edible oils have negative $\frac{dc}{dT}$ values. Many edible oils were reported to have $\frac{dc}{dT}$ values of between $-3.2\text{ms}^{-1}\text{C}^{-1}$ and $-3.4\text{ms}^{-1}\text{C}^{-1}$. Water has a positive $\frac{dc}{dT}$ slope of approximately $3.7\text{ms}^{-1}\text{C}^{-1}$ between 4C and 25C . Therefore, there is a temperature at which the speed of sound in the water content of the mixture and the speed of sound in the fat content of the mixture will be equal. At this temperature, changes in fat content will not be reflected in the measured speed of sound. This experiment aimed to find the intersection temperature. Once the intersection temperature was found, a temperature at which one could more easily dis-

tinguish between velocity changes caused by changes in fat level could be chosen as the temperature at which to conduct future experiments.

Another consideration with respect to temperature is the fact that a significant proportion of the milk fat will be solid within the temperature range for salmon defined in Section 3.3.3 [68]. The amount of solid fat present will decrease as the temperature increases. Other studies have suggested that this behaviour can be overcome by taking measurements above 35°C [60]. At this temperature, one can guarantee that all the fat within the mixture is liquid. It was decided here to take measurements within the temperature range for salmon as the intramuscular fat within salmon would be partially solid as well. In working with these materials over 35°C, one also risks the components denaturing.

The most straight forward approach is to measure the velocities through 100% cream over a range of temperatures, then through 100% milk over the same range of temperatures. Plotting the two curves will yield an intersection temperature. This was attempted here. However, it was found that a usable signal could not be obtained through the 100% cream. This was due to the fact that the signal almost completely attenuated before it could reach the receiving transducer 87mm away. The high degree of attenuation suggests that Equation 3.3 ignores scattering within the mixture.

Therefore, the velocity was measured at six different concentrations, rang-

ing from 0% cream to 50% cream, in 10% increments and over a temperature range from 5°C to 21°C. In theory, all of these plots should also intersect at the temperature at which the velocity in milk fat and the velocity in water are equal. Figure 3.7 shows these results.

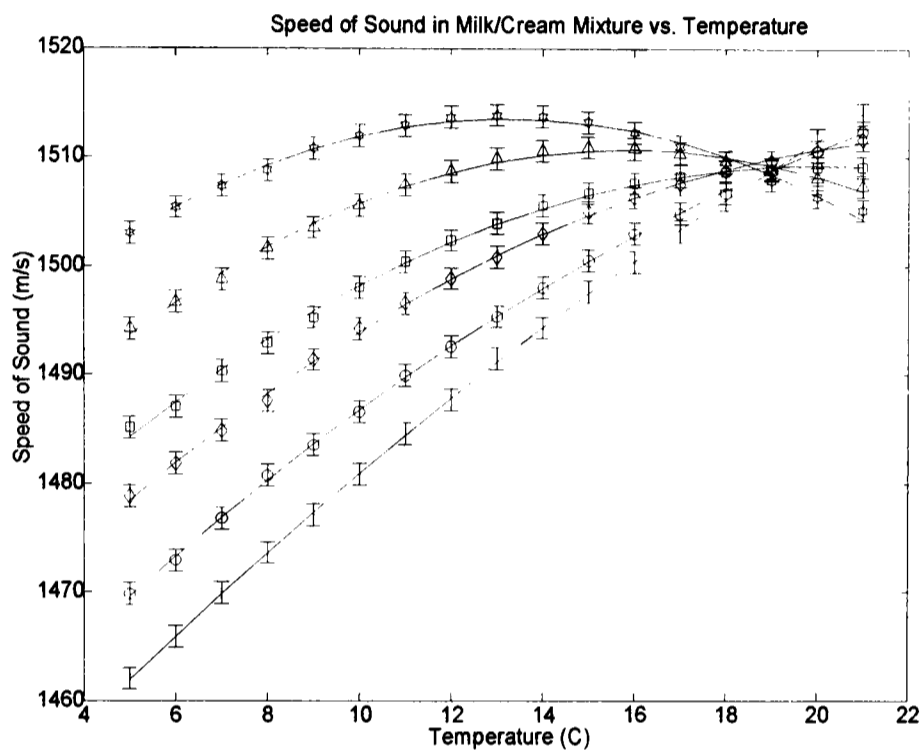


Figure 3.7: Speed of sound versus temperature profiles for cream-in-milk concentrations of 0% (dots), 10% (circles), 20% (diamonds), 30% (squares), 40% (triangles), and 50% (hexagrams). The solid curves are best-fits.

In Figure 3.7, empirical data is represented by shapes. The solid curves are best-fits. As expected, all six plots converged at approximately 19°C. From the graph it is clear that any temperature around 19°C should be avoided for future ultrasound measurements, as there is very little separation in the velocities of different fat contents at this temperature. Therefore, 10°C was chosen as a temperature for future milk/cream experiments, as

there is a good separation of approximately 6ms^{-1} per 10% cream, or approximately 5% fat, at this temperature. Moreover, 10°C is near the middle of the temperature range for salmon.

3.4.2 Measurements at 10°C

Further measurements of the speed of sound and attenuation of the phantom were taken exclusively at 10°C . Data was taken as the fat content of the phantom was raised from 0% cream, or 0.1% fat, to 50% cream, or approximately 24% fat. This fat range is the same as that found in farmed salmon [17]. The results are shown below.

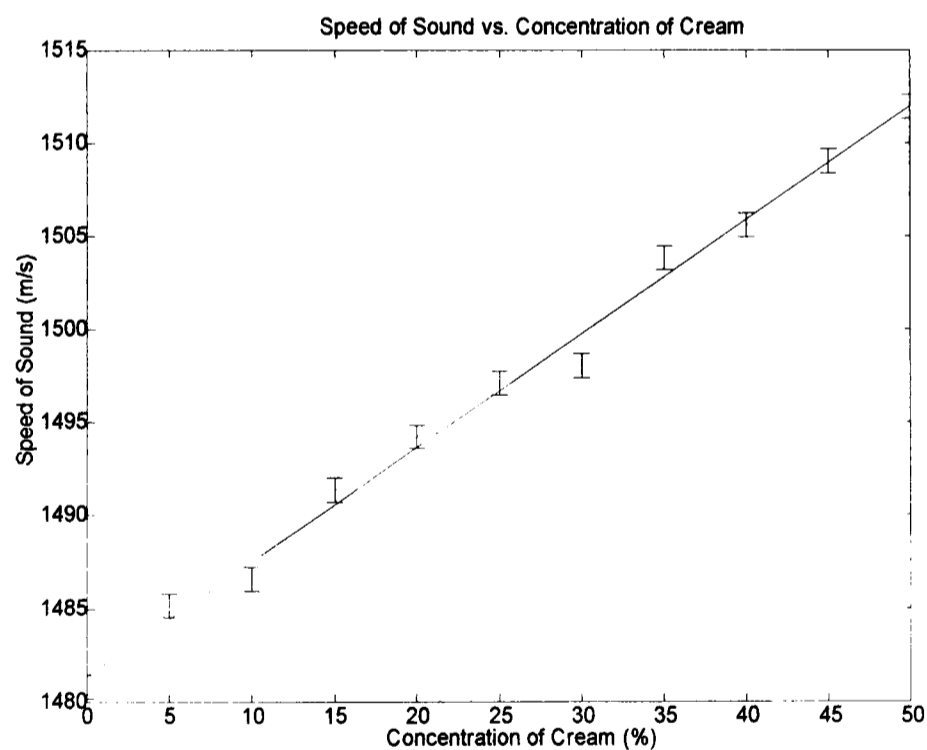


Figure 3.8: Speed of sound versus concentration of 48% fat double cream in 0.1% fat milk at 10°C .

Figure 3.8 demonstrates that the ultrasound system was capable of de-

tecting the velocity changes caused by increased cream concentrations over the entire concentration range. The increase in velocity with concentration is linear. This linear relationship was used to determine the following equation from empirical data.

$$c = 0.61 \cdot \text{cream_percentage} + 1481.37 \quad (3.16)$$

Equation 3.16 is expected to be accurate to within $\pm 1.5\text{ms}^{-1}$. Using Equation 3.16, it is possible to calculate that the velocity through 100% cream is approximately 1542.63ms^{-1} . Using this value and the measured value of 1480.81ms^{-1} through 100% milk, it becomes possible to use a modified version of Equation 3.3 to determine the fat content of a mixture from knowledge of its acoustic velocity alone.

The densities of liquid oils and water are fairly similar [53]. The density of milk fat is 912kg m^{-3} . The density of water is 997kg m^{-3} [46]. Thus, Equation 3.3 can be simplified.

$$c = \left[\left(\sum_{i=1}^n \frac{\phi_i}{c_i^2} \right) \right]^{-1/2} \quad (3.17)$$

It has been shown that this relationship gives a good description of the ultrasonic properties of a mixture in which the density of the various components are similar and scattering is not appreciable [34, 25, 32, 43, 28]. In the case

of a milk/cream mixture, the equation becomes

$$c = \left[\frac{\phi_{milk}}{c_{milk}^2} + \frac{\phi_{cream}}{c_{cream}^2} \right]^{-1/2} \quad (3.18)$$

$$c = \left[\frac{\phi_{milk}}{1480.81^2} + \frac{\phi_{cream}}{1542.63^2} \right]^{-1/2} \quad (3.19)$$

where

$$\phi_{cream} = \frac{fat_percentage_{cream}}{0.48 \cdot 100\%} \quad (3.20)$$

$$\phi_{milk} = \frac{fat_percentage_{milk}}{0.001 \cdot 100\%} \quad (3.21)$$

However, this leaves two unknowns ($fat_percentage_{cream}$ and $fat_percentage_{milk}$) in one equation. Since the amount of fat in the milk component is so small, the total fat in the mixture is approximately equal to the amount of fat in the cream component. Thus, by substituting for ϕ_{milk} , Equation 3.18 becomes usable for fat content prediction.

$$c = \left[\frac{1 - \phi_{cream}}{1480.81^2} + \frac{\phi_{cream}}{1542.63^2} \right]^{-1/2} \quad (3.22)$$

or

$$cream_percentage = (100\%) \left(\frac{\frac{1}{c^2} - \frac{1}{1480.81^2}}{\frac{1}{1542.63^2} - \frac{1}{1480.81^2}} \right) \quad (3.23)$$

recalling that

$$fat_percentage_{cream} = 0.48 \cdot cream_percentage \quad (3.24)$$

The repeatability of using Equation 3.23 to predict cream concentrations, and thus fat levels within a milk/cream mixture, is discussed in the next section.

It was observed that attenuation in the mixture rose with increasing levels of fat. This is shown in Figure 3.9.

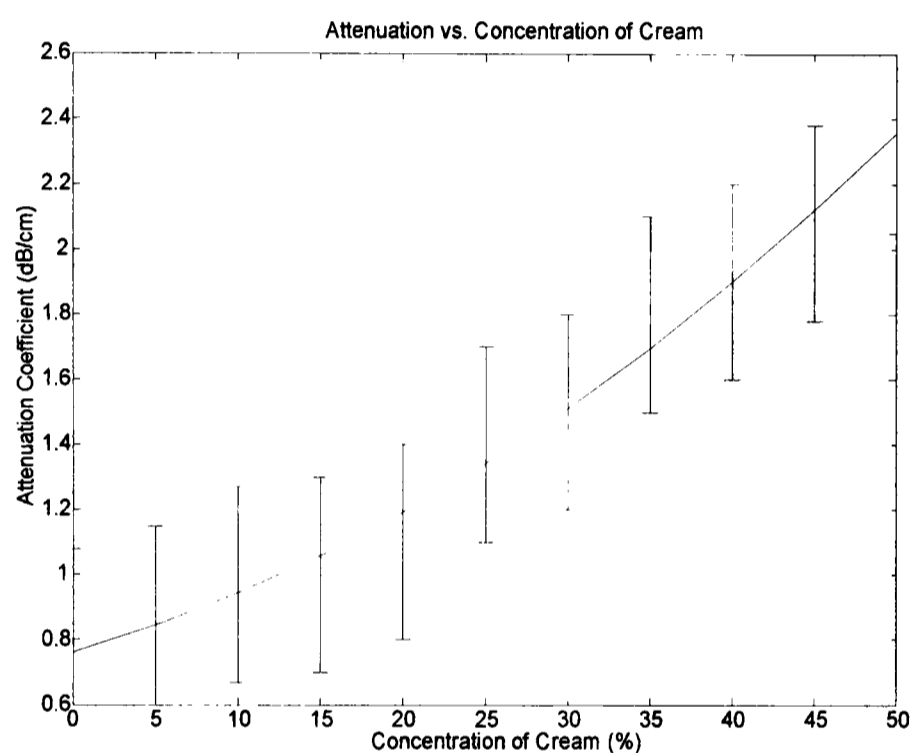


Figure 3.9: Attenuation versus concentration of cream. Dots are experimental data. The solid curve is a best-fit.

Figure 3.9 shows the attenuation recorded over the entire concentration range. As mentioned earlier, this experiment did not attempt to mimic the attenuation caused by soft tissue. However, it is worth noting how the attenuation increases slightly more rapidly as the concentration of cream increases. This increase in attenuation is caused mainly by the fat component of the mixture. Since the milk fat is dispersed in the form of globules, the milk fat

attenuates even more strongly than would pure milk fat [46]. If one assumes that particle size distribution remains roughly constant over the entire concentration range, then the nonlinear increase in attenuation can be attributed to multiple scattering of the ultrasound beam between emulsion droplets [69].

3.4.3 Repeatability

This section discusses experiments which were performed to assess how well Equation 3.23 could predict cream concentrations in milk/cream mixtures. Similar to previous experiments, cream was diluted with milk to create mixtures of seven distinct dispersed fat levels. All velocity measurements were made at 10°C. From this data, an estimate of cream content was calculated. These tests were repeated 10 times. The mean results are shown in the table below.

%Cream	%Measured	%Error	%Standard Deviation
7	5.64	-1.36	±0.78
14	15.84	+1.84	±2.35
19	18.36	-0.64	±2.45
24	25.81	+1.81	±0.71
35	36.63	+1.63	±2.31
40	41.83	+1.83	±1.45
47	48.36	+1.36	±1.73

Table 3.4: Mean repeatability results for seven cream concentrations.

Table 3.4 shows that there is a good correlation ($r=0.998$, $n=7$) between fat content determined by ultrasound measurement and the actual fat content

of the mixture. All mean errors are within $\pm 2.0\%$ cream, or approximately $\pm 0.96\%$ fat. Standard deviations do not vary beyond $\pm 2.5\%$ cream, or approximately $\pm 1.2\%$ fat. It is difficult to tell what portion of these errors is due to experimental error in measuring out exact quantities of liquid and what proportion is due to system error. Still, these results have shown that it is possible to predict fat content of a dispersed fat system to within approximately $\pm 1.5\%$ using only ultrasound velocity measurements at a single temperature.

3.5 Foam Phantom

This section describes experiments in which a cube of Bulpren S20 reticulated foam was inserted into the milk/cream mixture in order to provide tissue-like attenuation. Again, velocity and attenuation measurements were taken to determine if ultrasound was capable of detecting changes in distributed fat level in a more tissue-like phantom.

3.5.1 Calibration

It was necessary to calibrate the phantom to account for the effect on velocity of coupling through the walls of the Perspex box. Each wall is 5mm thick. Therefore, the walls add an additional 10mm of Perspex to the total

ultrasound path. As mentioned earlier, the speed of sound through Perspex is approximately 2690ms^{-1} . This should cause the measured speed of sound to rise, as the velocity of the liquids under investigation all have much lower velocities. An experiment was conducted using only distilled degassed water inside the box at a temperature of 22°C . The expected velocity through distilled degassed water alone at 22°C is 1488.18ms^{-1} . Twenty readings were taken. The expected velocity through the box and water at that temperature was calculated to be 1530.73ms^{-1} using Equation 3.3. The mean measured velocity was $1531.21 \pm 1.00\text{ms}^{-1}$. This showed that the velocity increase due to the Perspex interfaces alone would be approximately 43ms^{-1} .

The velocity decrease due to the addition of the foam block was also investigated. The literature [52] states only that the velocity drop due to the foam is approximately 0.1%. In this experiment, 0.1% is approximately 1.53ms^{-1} . When the foam was inserted into the water, a velocity drop was indeed recorded. Again, twenty readings of the velocity were taken. The mean velocity dropped to $1529.63 \pm 0.30\text{ms}^{-1}$. This is a drop of approximately 1.58ms^{-1} .

Therefore, the total velocity increase in the milk-cream mixtures due to the foam and Perspex was expected to be approximately 41ms^{-1} . Thus, in the experiment described below, the velocity increase due to these materials was subtracted from the measured velocity to yield the velocity through the

milk/cream mixtures alone.

3.5.2 Milk/Cream Mixtures

As in Section 3.4, the velocity of the milk-cream mixture was measured at eleven different concentrations: 0% to 50% cream, or 0.1% to approximately 24% fat, in 5% cream increments. All measurements were taken at a temperature of 10°C. The foam block was inserted into the mixtures to provide a tissue-like structure for the ultrasound to travel through and to provide tissue-like attenuation. The results are shown in Figure 3.10.

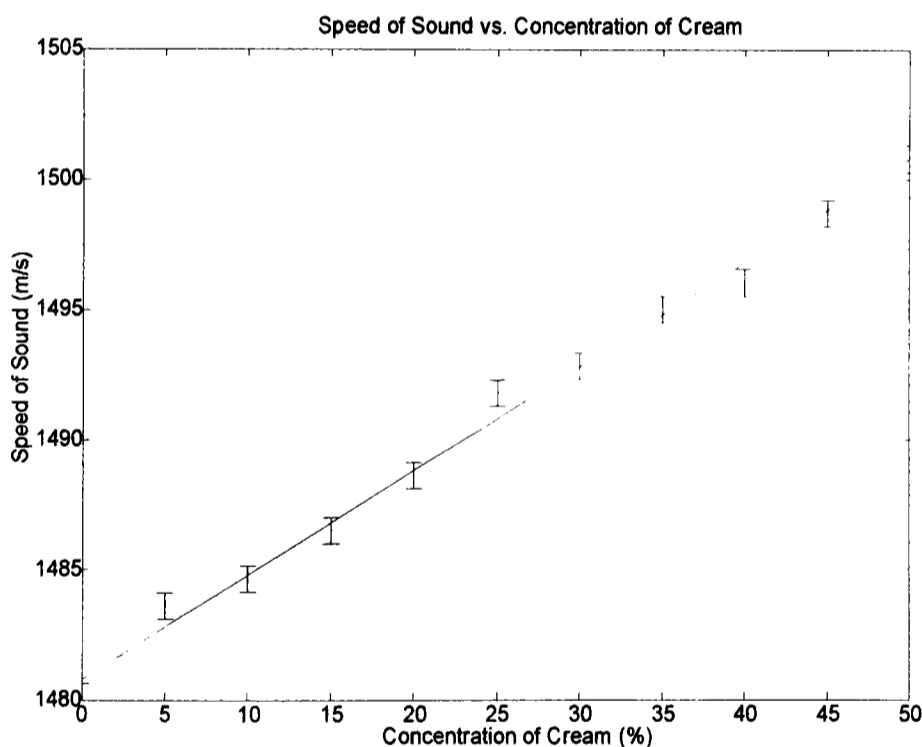


Figure 3.10: Speed of sound versus concentration of 48% fat cream in 0.1% fat milk inside a reticulated foam structure.

These results are very similar to those in Section 3.4. The velocity through milk alone was measured as approximately 1480ms^{-1} in both experiments.

However, the velocity only increases by approximately 2ms^{-1} per 5% increase in cream concentration. This is in contrast to an approximately 3ms^{-1} increase in overall velocity with the same increase in cream concentration observed in Figure 3.8. This change can possibly be explained by the fact that the foam phantom includes two Perspex interfaces as well as the block of foam. The overall elasticity of the system has decreased from the phantom used in Section 3.4. Therefore, a change in fat level will have less of an effect on overall velocity than it had in the previous section.

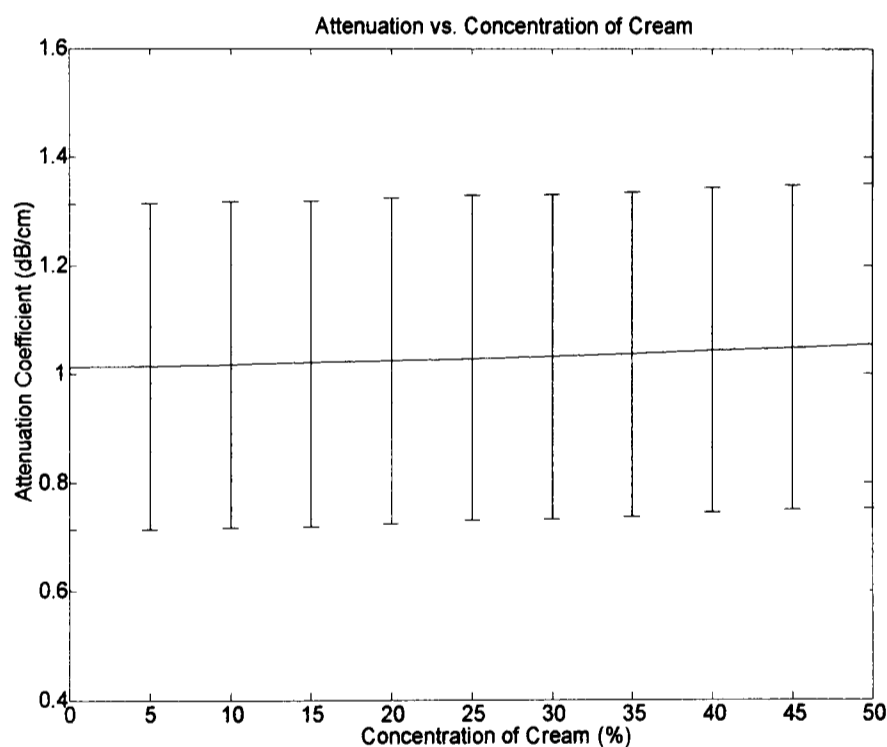


Figure 3.11: Attenuation versus concentration of cream. Dots are experimental data. The curve is a best-fit.

Figure 3.11 illustrates that the attenuation recorded using this phantom was similar in its increase to that in which there was no foam structure. However, the range of attenuation seen with the foam in place is much smaller.

The foam has imposed an attenuation value of approximately 1dB cm^{-1} . The Perspex interfaces can be expected to contribute to the measured attenuation as well. However, these attenuation values are consistent with the attenuation reported by Lerski using Bulpren S20 foam at 2.25MHz [52]. More important is the fact that the ultrasound system was capable of measuring changes in both velocity and attenuation caused by increases in fat concentration in this distributed fat system.

3.6 Conclusion

This chapter has demonstrated three things which are important if one is to make accurate measurements of salmon muscle tissue. First, the measurement system could be calibrated to a maximum error of approximately $\pm 1.5\text{ms}^{-1}$. This should ensure accurate measurements in all experiments using this system. Second, it was shown that measurements well away from 19°C yielded a better separation of the speeds of sound in fat and water within a dispersed fat system. Finally, it has been shown that the ultrasound system is capable of measuring the increases in velocity and attenuation which result from increased concentrations of dispersed fat.

Chapter 4

Salmon Tissue

Chapter 3 demonstrated that ultrasound was capable of detecting changes in dispersed fat concentration in milk/cream mixtures by measuring the mixture's acoustic velocity and attenuation. It was possible to predict the amount of fat in the mixture to within approximately $\pm 1.5\%$. This chapter investigates whether ultrasound can be used to distinguish between fat levels in Atlantic salmon muscle tissue to a similar degree of accuracy. Sigfusson has shown that it is possible to use ultrasound to predict the fat level of Atlantic mackerel and North Atlantic albacore to approximately $\pm 2\%$ [43, 28]. It has also been shown that the acoustic velocity and attenuation through whitefish muscle tissue will change with a change in fat level [21]. Whitefish belong to the *salmonidae* family of fishes and thus have a very similar muscle structure to that of salmon [70].

To interpret the changes in velocity and attenuation due to changes of fat content within the muscle, it is necessary to understand some basic salmon anatomy. The amount of intramuscular fat in salmon muscle tissue varies along the length of the fish [9]. The fat content in certain regions of the salmon is more representative of the overall fat content of the fish than is the fat content in other regions. The quantity of intramuscular bones also varies across the width of the fish. Therefore, it was important to cut samples from a region of the salmon in which there were no bones and the fat content of the tissue represented well the overall fat content of the fish. It was also important to know what types of tissues the ultrasound beam would travel through within each sample. Salmon muscle is not homogenous and contains tendon structures whose acoustic velocity could possibly alter the overall measured velocity through the sample.

In order to measure velocity and attenuation, it was necessary to measure the thickness of each sample. Therefore, a rig was constructed to measure the thickness of the sample at the same moment the time of flight and attenuation through it were measured. It was soon discovered that the rig contained errors in distance measurement. Therefore, several experiments were conducted to calibrate the rig. This yielded correction factors which were then added to the calculation of velocity in software.

Freese and Makow's study of the ultrasonic properties of whitefish [21]

found that compressing the sample by approximately 10% ensured good coupling between the transducers and the samples. It also found that submerging the sample in water of a known temperature was the easiest way of controlling the temperature of the sample. Both of these techniques were used here. In the experiments described below, the rig was partially submerged in a tub of water. The level of the water ensured that the sample was completely submerged, while the metal micrometer used to measure the thickness of the sample was not in contact with the water. This prevented rust. The tub was then placed in a cooling chamber to regulate the temperature of the water. Measurements of velocity were taken over a twenty minute period, as the temperature of the sample dropped to the temperature of the water.

An experiment was conducted to confirm that 10°C was an appropriate temperature at which to conduct tissue measurements. The intersection temperature between distilled degassed water and fish oil was determined so that an appropriate temperature at which to conduct further experiments could be found. An experiment was also conducted to ensure that results on a single sample were repeatable to within $\pm 1\text{ms}^{-1}$. Ten Unilever samples were measured ten times each and the standard deviation in the measurements of each sample was calculated.

Attenuation and velocity measurements were made on 50 different samples. Twenty-five contained approximately 8% $\pm 3\%$ fat and were supplied

by Unilever PLC. The other 25 contained approximately $11\% \pm 3\%$ fat and were supplied by Tesco PLC. Chemical fat extraction was performed on a further 12 samples to more-closely determine the relationship between acoustic velocity and the fat content of the samples.

4.1 Acoustic Properties of Tissue

Many of the acoustic properties of tissue are the same as the acoustic properties of liquids described in Section 3.1. One important difference though is that in isotropic solids both longitudinal waves and shear waves can be propagated [55]. A longitudinal wave is a wave in which the oscillating particles in the medium are displaced parallel to the direction of motion. The longitudinal wave velocity through a solid is given by

$$c_L = \sqrt{\frac{B + \frac{4}{3}G}{\rho}} = \sqrt{\frac{E(1 - \nu)}{\rho(1 - 2\nu)(1 + \nu)}} \quad (4.1)$$

where B is the bulk modulus, G is the shear modulus, ρ is the density, E is Young's modulus and ν is Poisson's ratio. Typical values for the bulk and shear moduli in salmonid muscle tissue are not currently available in the literature.

A shear wave is one in which the particles in the medium are displaced in a direction perpendicular to the motion of the wave. The shear waves created in liquids and gases using low-intensity ultrasound are so small as

to be negligible due to the lack of strong three-dimensional intermolecular coupling forces within the medium. It is this lack of coupling forces which enable liquids and gases to flow [23]. The shear wave velocity through a solid is given by

$$c_S = \sqrt{\frac{G}{\rho}} = \sqrt{\frac{E}{2\rho(1+\nu)}} \quad (4.2)$$

Attenuation in tissues follows the same equations described in Section 2.3. However, attenuation in tissue will be caused by scattering as well as absorption. Scattering occurs when the beam encounters an interface bounded by materials having different acoustic impedances [26]. Most biological material is inhomogeneous. Different tissues have different acoustic impedances and all consist of a meshwork of blood vessels, fibres, connective tissues and different types of cells. Therefore, all tissues are composed of a myriad of reflecting surfaces. If the dimensions of a reflector are smaller than the wavelength of the beam, then the reflector acts as a point source and re-radiates a portion of the energy of the ultrasound beam in all directions [23]. Reflectors which are larger than the wavelength of the beam are usually major internal structures or organs. In this case the amplitude of the backscatter is small, except when the angle of incidence is normal or near-normal [26]. It is difficult to separate the contribution from scattering and the contribution from absorption in the overall attenuation measured. However, the results

from the previous chapter indicate that as the concentration of fat dispersed within a material increases, the overall attenuation through that material increases due to increased scattering of the ultrasound beam by the dispersed fat globules.

All of the salmon muscle tissue samples used in experiments described in this chapter were frozen during shipment and storage. They were left to thaw for approximately three hours before each experiment. It has been shown that the velocity through whitefish, increased by approximately 8% when it was frozen once and then thawed. Similarly, attenuation through the whitefish increased by approximately 2% [21]. This is due to changes in composition when water is lost due to “drip” after freezing and during thawing [71]. The velocity increases because there is a higher concentration of fat and protein in the tissue than there was before the water was lost through drip.

4.2 Target Area for Sample Extraction

For ease of measurement and increased accuracy of results, it was necessary to extract muscle tissue samples from a section of the salmon in which the muscle tissue both represented the overall fat content of the fish and contained the fewest intramuscular bones.

Salmon belong to the taxonomic branch of fish called “teleosts”. Figure 4.1 shows the general anatomy of a teleost [72].

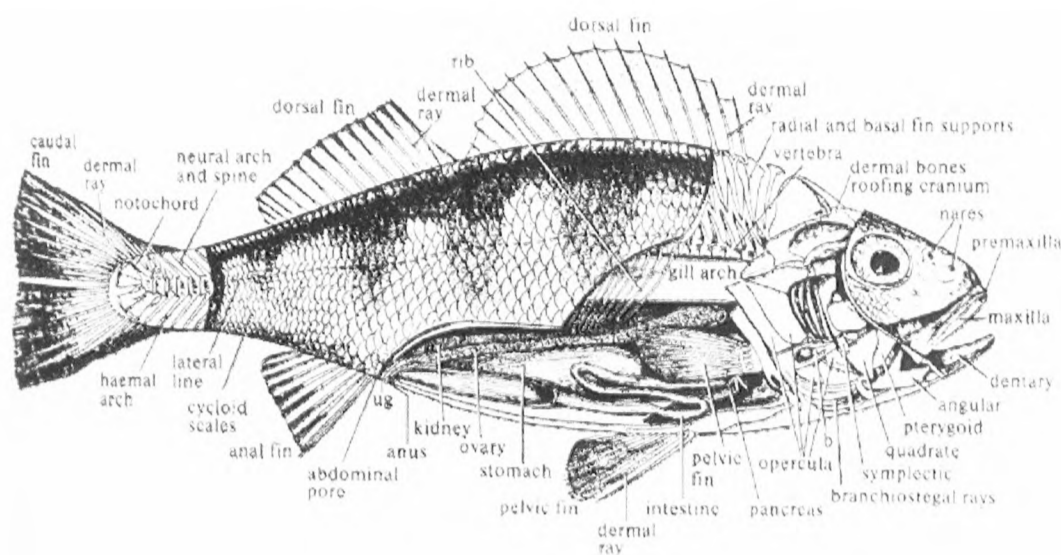


Figure 4.1: General anatomy of a teleost.

At the bottom of the salmon is a thick layer of fat. This is the fish’s extramuscular fat. Above this is the body cavity containing the fish’s internal organs, including the swim bladder. A swim bladder is an air-filled sack which enables a fish to alter its depth in water as it swims by altering the amount of air trapped in it. There is very little actual muscle tissue in this area below the spine. There is only a thin layer of muscle between the body cavity and the dermis on each side of the fish. The bottom half of the fish is therefore an inappropriate place from which to take muscle tissue samples.

A possible target area is the rear of the fish, behind the anal fin. Here the muscles are much more compact, as the muscles fibres and connective tissues

come to a head in this area. However, the fat content of these leaner muscles is much lower than elsewhere on the fish. The fat content of the muscles here does not represent overall fat concentrations as well as those muscle tissues found in centre of the fish, above the spine [9].

Therefore, muscle located between the dorsal fin and the spine was investigated as a possible area from which to take samples. Between the dorsal fin and the spine, there is only bone, muscle and connective tissue. The advantage of taking tissue samples from the area between the dorsal fin and the spine is that the fat content of the muscle tissue in this area is more representative of the overall fat level of the fish [9].

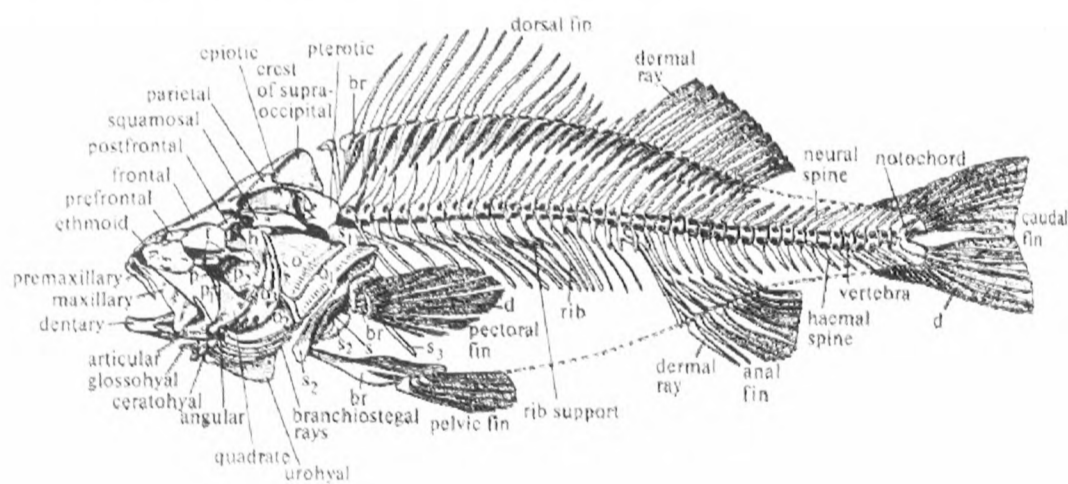


Figure 4.2: Skeletal structure of a teleost.

Figure 4.2 shows the skeletal structure of a teleost [72]. It would appear to suggest that tissue samples taken from anywhere on the fish would unavoidably contain bones as well. However, Figure 4.3 shows that this is not true.

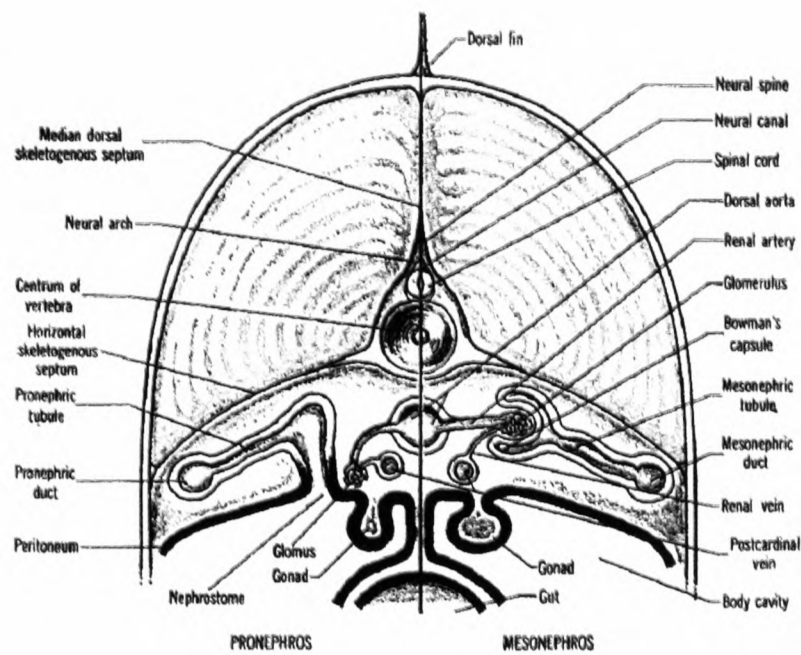


Figure 4.3: Anatomical cross-section of a fish.

Figure 4.3 shows that there is an area on each side of the median dorsal skeletogenous septum which contains only muscle tissue [70]. The figure does not show that there are small intramuscular bones up to approximately the level of the spine. However, above this there is only muscle. Therefore, the tissue samples measured in following sections are cuts from this area between the dorsal fin and the spine and between the median dorsal skeletogenous septum and the dermis of the fish.

The tissue samples themselves were obtained from Unilever PLC and Tesco PLC. The Unilever samples contained approximately $8\% \pm 3\%$ fat and were cut into cubes by the company itself. The Tesco samples contained approximately $11\% \pm 3\%$ fat and were obtained from a local supermarket.

The estimates of fat content were arrived at by performing destructive chemical analysis on muscle tissue from the same area from which the samples used here were extracted. The chemical tests were performed by the companies themselves. In the case of the Tesco samples, this estimate of fat content was printed onto the packaging into which the fish was wrapped. All samples were frozen during shipment then thawed for three hours before each experiment. This was enough time for the sample to reach room temperature. Room temperature was approximately 22°C.

4.3 Muscle Tissue Structure

It was important to understand the structure through which the ultrasound travelled. This section describes the different types of salmon muscle tissue as well as the function of the myosepta in binding the muscles together. It also describes the quantities of fat, water and protein present in typical salmon muscle and reports an equation to predict the quantities of these components within a single tissue sample.

4.3.1 Types of Muscle Tissue

Salmon muscle can be classified as either “red” or “white”. The red muscle is used for everyday swimming and slow propulsion through the water. Figure

4.4 shows that the red muscle layers are very thin and are located just under the dermis [73]. The rest of the muscle in the salmon is white muscle. White muscle is used for rapid high-energy movements, such as jumping up stream or escaping from predators [74].

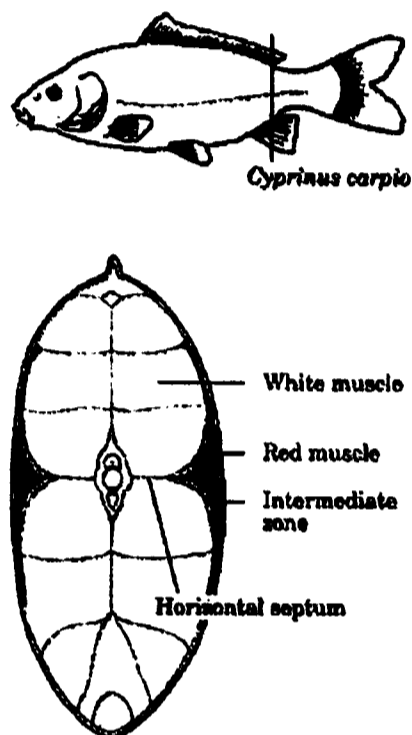


Figure 4.4: Red and white muscle as distributed in teleosts. The fish's spine (centre of the fish) is not labelled.

Although it is called “white”, white muscle in salmon is actually dark pink in colour. The quantities of the pink pigment astaxanthin present in salmon muscle is a function of an individual fish's diet [75]. Many commercial fish farms feed their fish diets high in prawns and other pigment-enhancing foods. The natural astaxanthin in the prawns, for example, deepens the white muscle's pink colour. This, in turn, increases the fish's marketability. If a fish were to be fed on only bugs, for example, this white muscle would

indeed be white [74].

The fat content of red muscle tends to be much higher than that of white muscle. This is dependent on how active the fish was during its life. The layer of red muscle is so thin though, that it does not make much difference to the overall fat content of the fish. A typical red muscle layer is less than 3mm thick. It comprises less than 10% of the overall mass of the fish [74]. In experiments described in this chapter, only white salmon muscle was used.

4.3.2 Myosepta

The muscle itself consists of bundles of muscle fibres which are held together by connective tissue called “myosepta”. The myosepta can be seen in cross-section as a distinctive pattern of curved white streaks or circles amongst the dark pink muscle. Figure 4.5 shows the overlapping meshwork of myosepta onto which the muscle fibres attach [76].

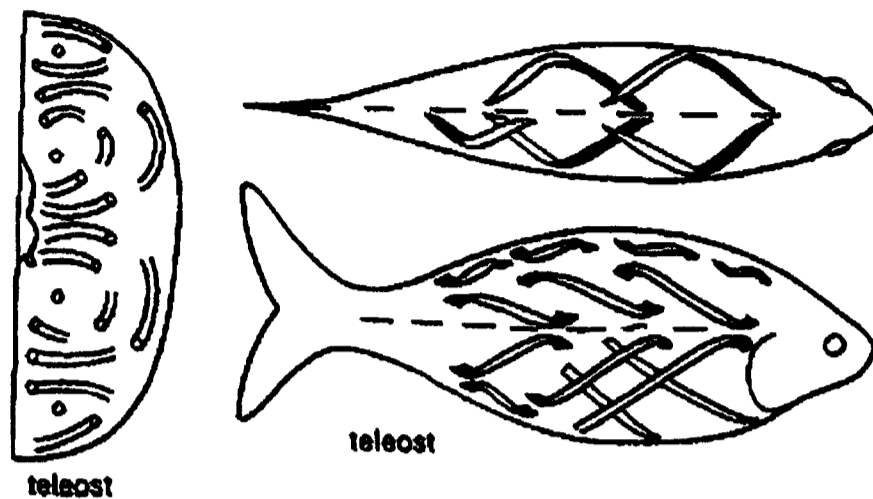


Figure 4.5: Myosepta structure in teleosts.

As a consequence of this meshwork, the myosepta are like loosely woven pieces of cloth which can be deformed but not elongated. In salmon, the myosepta are stiffened by ribs and by smaller intramuscular bones to limit this deformation [76]. These stiffening elements act to permit only lateral movements when the myosepta contract. They also serve to reduce the general flexibility of the body.

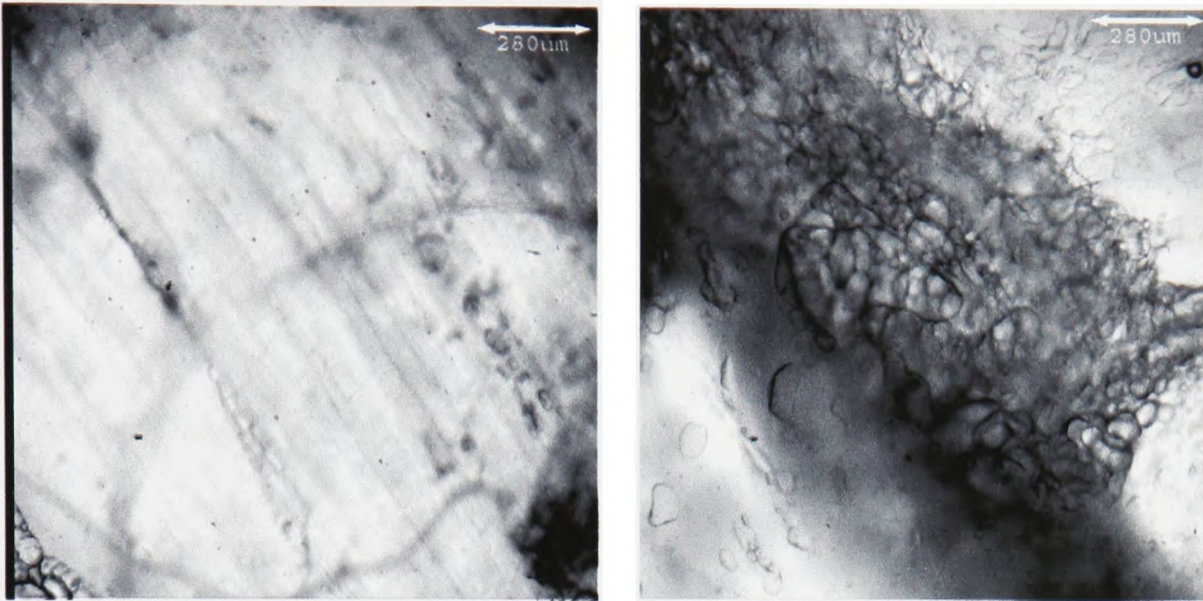


Figure 4.6: View of a single myoseptum (right) and muscle tissue without myosepta (left). Both pictures were taken using a scanning optical microscope. The scale in the top right of each image shows that 200 pixels is equivalent to 280 microns, or 1 pixel is equivalent to 1.4 microns.

In Figure 4.6, the image on the right shows a single myoseptum. The image on the left shows salmon muscle tissue without myosepta. Both of these pictures were taken using an Olympus BX60M scanning optical microscope¹. The myosepta consist of approximately 82% collagen and approximately 18% elastin [77]. However, the right side of Figure 4.6 shows that myosepta are also surrounded by numerous fat globules. These are clearly visible all along its length. Myosepta are the main intramuscular fat depositories in salmon, containing up to 40% of the fat in the muscle [78].

¹This microscope was made available by the Oxford University Scanning Optical Microscopy Group.

4.3.3 Tissue Constituents

As mentioned earlier, the muscle fibres contain proteins (15%-30%), fat in the form of lipids (5%-25%), water (50%-80%) and ash. The term “ash” encompasses all of the non-flammable trace minerals which typically make up between 0.5% and 1% of the total muscle mass. These minerals include calcium, magnesium and various salts.

Katikou [9] found the following empirical relationship between lipid content and water content within salmon muscle tissue.

$$water_percentage = -0.78 \cdot lipid_percentage + 75.23 \quad (4.3)$$

For a group of farmed salmon raised and fed under similar conditions, the above equation will hold to within $\pm 1\%$ water [9]. For such a group, protein levels remain relatively stable, changing only two to three percent overall. This suggests that one need only measure either water level or fat level to know the approximate percentages of all three major constituents of salmon muscle tissue.

4.4 Methods and Materials

In order to measure the speed of sound through a solid, one must be able to measure its thickness as well as the time it takes for the ultrasound to pass

through it. A thickness measurement is also necessary for attenuation measurements. Therefore, a rig was constructed that would allow the thickness of a sample and the time delay through it to be measured at the same time.

As mentioned in Chapter 3, none of the samples was thicker than 25mm. Figure 4.7 shows a diagram of a linear micropositioning stage that formed the core of the tissue measurement rig [79]. The platform on the stage was able to move a maximum of 25mm from its zero position. The exact distance moved was controlled by a micrometer to within $\pm 0.01\text{mm}$.

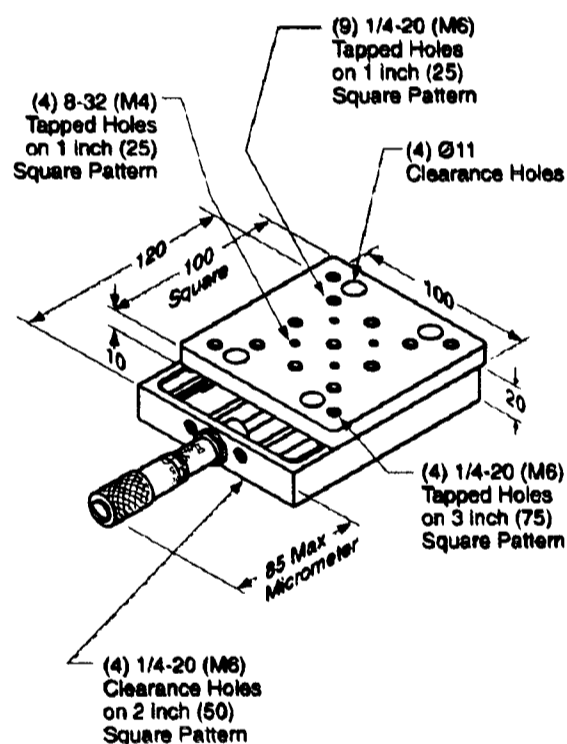


Figure 4.7: Linear micropositioning stage. Units are millimetres.

Assuming an average speed of sound through salmon muscle tissue of approximately 1540ms^{-1} , an error of $\pm 0.01\text{mm}$ in distance measurement can lead to an error of approximately $\pm 0.06\%$ in velocity measurement. This is

equivalent to approximately $\pm 0.9\text{ms}^{-1}$.

A Perspex cube measuring 46mm in all dimensions was cut. A hole was drilled through it so that it could hold one of the transducers. Another hole, perpendicular to the first, was drilled so that the transducer could be secured using a plastic screw. The cube was then fastened onto the platform of the micropositioning stage. A Perspex frame was built to hold both the micropositioning stage and the other transducer. The other transducer was also secured using a plastic screw. The frame was constructed so that both transducers would be aligned in three dimensions. The transducers were sealed in place using silicone sealant. The completed rig is shown below.

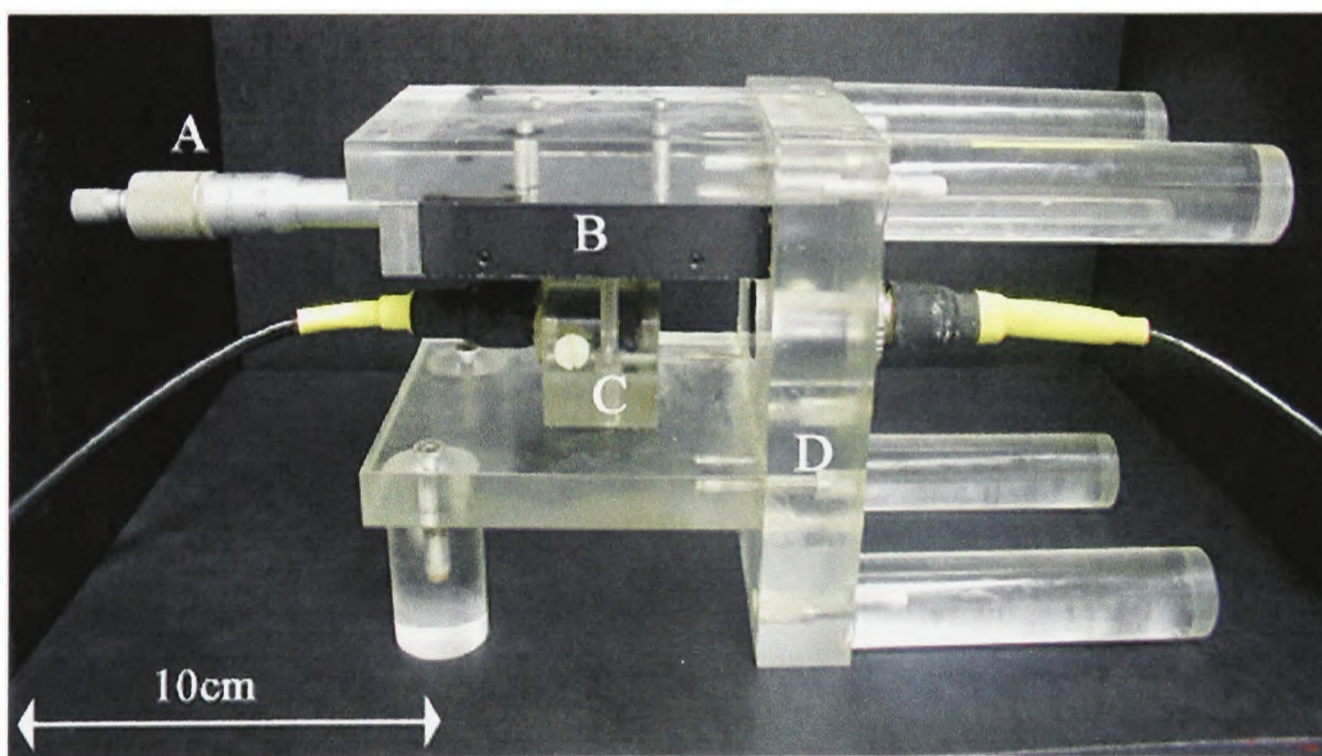


Figure 4.8: The tissue measurement rig.

Figure 4.8 shows the completed rig with major components labelled. “A”

is the micrometer. “B” is the linear micropositioning stage. “C” is the Perspex cube fastened to the stage. It holds one transducer. “D” is the Perspex block holding the other transducer. The tissue samples sat on the Perspex surface between “C” and “D.”

It was necessary to ensure good coupling between the transducers and the samples. Because the samples were malleable and did not have completely straight edges, the following method was used. A thin layer of ultrasound gel was first applied to the surface of both transducers. The rig was then tilted upwards so that a sample could rest on top of the transducer which was fixed in block “D.” The transducer attached to the linear positioning stage was brought closer to the sample until it touched the sample, at which point a signal would appear for the first time on the oscilloscope screen. This distance between transducers was taken to be the uncompressed thickness of the sample.

Freese and Makow [21] observed that compressing samples of whitefish up to 30% improved coupling and lowered the measured velocity by only 0.5%. In their published experiments, they chose to compress the samples by approximately 10%. That technique has been used here as well. All tissue samples used in the experiments described in this chapter were compressed by approximately 10% from their uncompressed thicknesses. This compression also minimised the likelihood of air bubbles being trapped between the

transducer face and the sample. It was assumed that the rig exerted approximately the same amount of pressure on each sample.

A calibration experiment was performed to detect any distance measurement or transducer alignment errors that may have existed in the system. If no errors existed, then a measurement of the speed of sound through distilled degassed water at one temperature should render the same speed for any distance between transducers. Recall that in a previous chapter, a time offset of +531.5ns was incorporated into the calculation of the speed of sound to correct for the inability to measure the distances between the transducer elements and the transducer faces. This experiment aimed to detect any further distance error caused by the rig.

The experiment was conducted at approximately 19°C. The expected speed of sound through water at this temperature is 1479.23ms^{-1} [38]. As in previous experiments, the water was degassed using the ultrasonic cleaning bath. The results are shown in Figure 4.9.

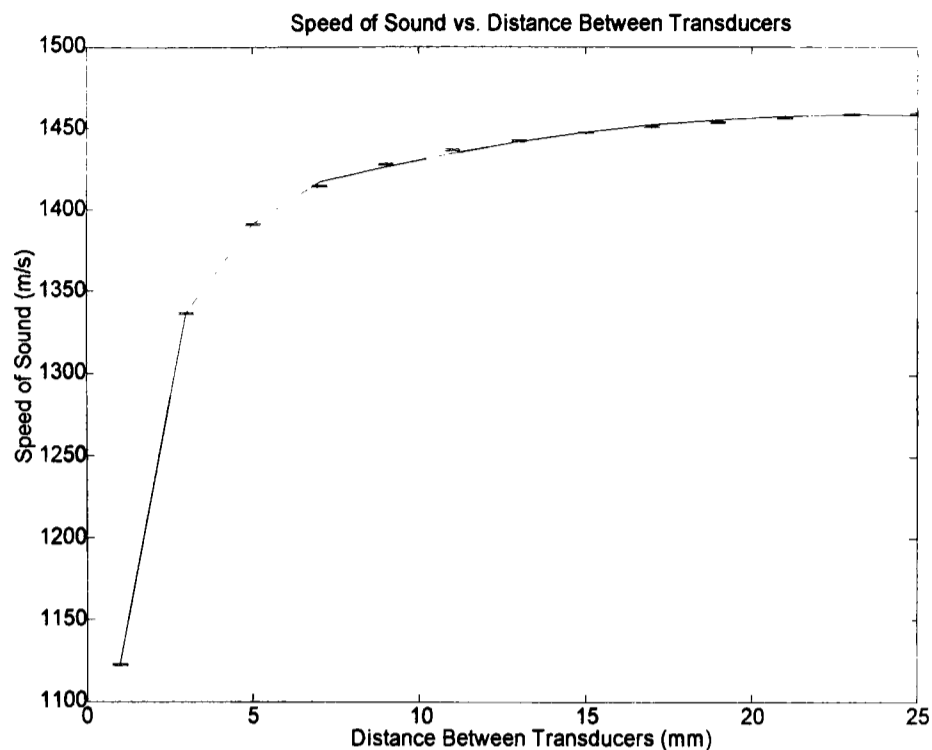


Figure 4.9: Speed of sound versus distance between transducers.

Figure 4.9 shows that there is obviously an error in the system. The largest source of potential error was the discrepancy between the distance that the micrometer read and the actual distance between transducers. This was corrected through a series of measurements using a digital distance gauge. The gauge, which incorporated a microscope, was accurate to within ± 5 microns². Twenty-five measurements were recorded in one-millimetre increments and compared to the distance reading on the micrometer.

Two errors were discovered. The first was a constant distance offset of +0.375mm. The other was a proportional error of +0.060mm per 25mm travelled by the micrometer shaft. Both of these corrections were then applied

²This gauge was made available by the Oxford University Engineering Workshops.

to the data set to yield the results below.

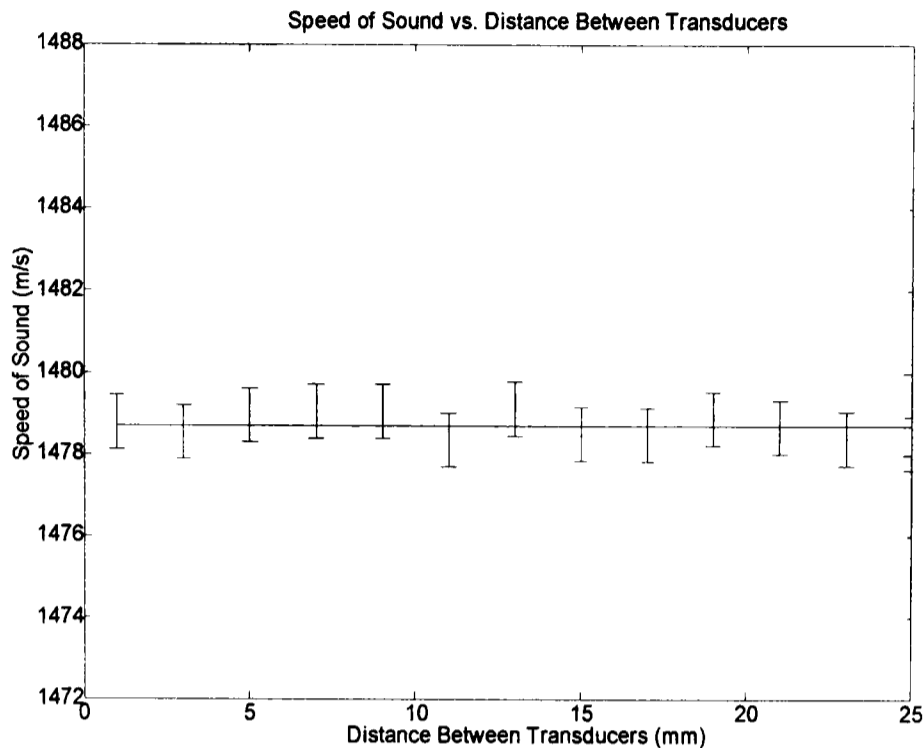


Figure 4.10: Speed of sound versus distance between transducers. This data has been corrected for distance measurement errors.

Figure 4.10 shows the data once the distance corrections were applied. The data deviated only $\pm 0.66 \text{ ms}^{-1}$ from the mean value of 1478.70 ms^{-1} . This is within $\pm 1 \text{ ms}^{-1}$ of the expected value of 1479.23 ms^{-1} .

To maintain the samples at a constant temperature, the rig was placed into a plastic tub as shown in Figure 4.11. The tub was then filled with distilled degassed water up to a level just below the level of the micropositioning stage but above the level of the transducers. This prevented rust on the micropositioning stage but ensured that the transducers and tissue sample were submerged.

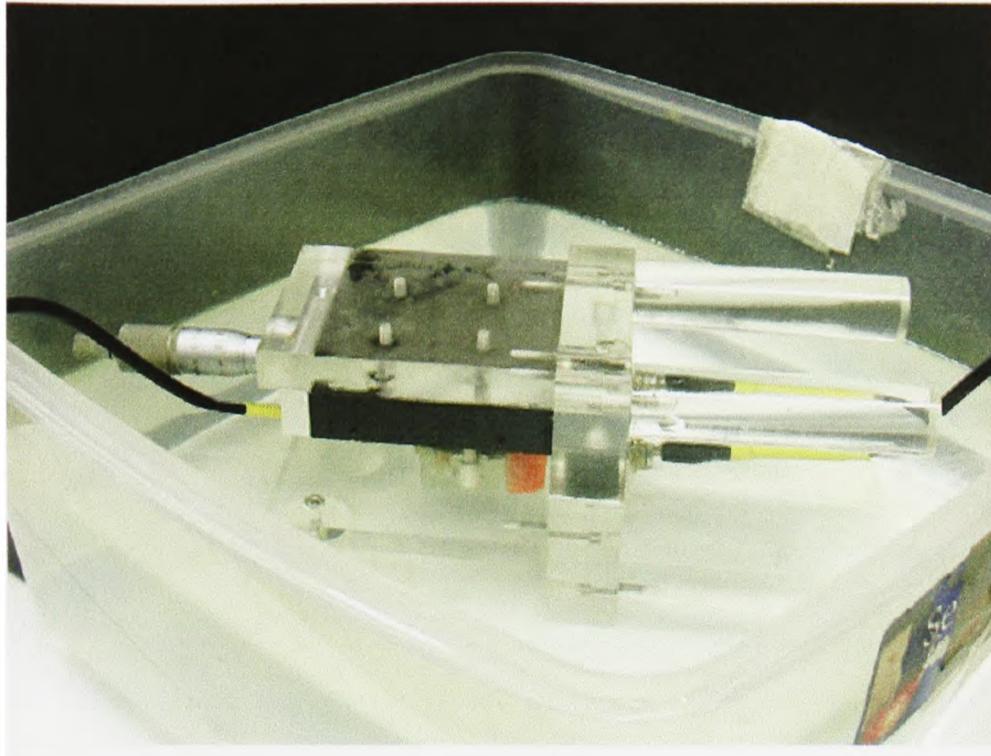


Figure 4.11: Tissue measurement rig holding a tissue sample submerged in the plastic tub of distilled degassed water.

The plastic tub was then placed in a cooling chamber. The velocity through the sample was recorded when the sample reached the target temperature. Section 4.5 explains why 10°C was a good temperature at which to take velocity measurements through salmon muscle tissue. It was assumed that the tissue sample had reached the temperature of the surrounding water, i.e., 10°C , when the measured velocity through it stopped decreasing. The temperature of the water was measured using the same digital thermometer described in the previous chapter.

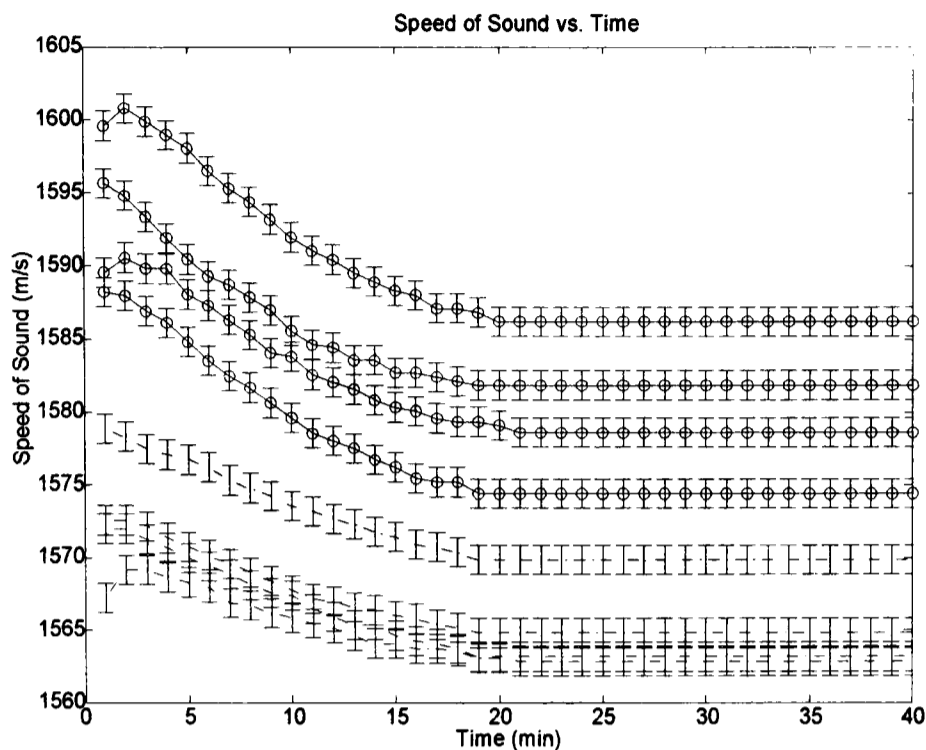


Figure 4.12: Speed of sound versus time for eight tissue samples. The dots represent data for samples containing approximately 11% fat. The circles represent data for samples containing approximately 8% fat.

Figure 4.12 shows that it took approximately 20 minutes for tissue samples to reach the temperature of the water from room temperature. The dots represent data from four representative Tesco samples, containing approximately 11% fat. The circles represent data from four representative Unilever samples, containing approximately 8% fat. The velocity through all samples measured in this chapter was recorded at one-minute intervals over a forty-minute period.

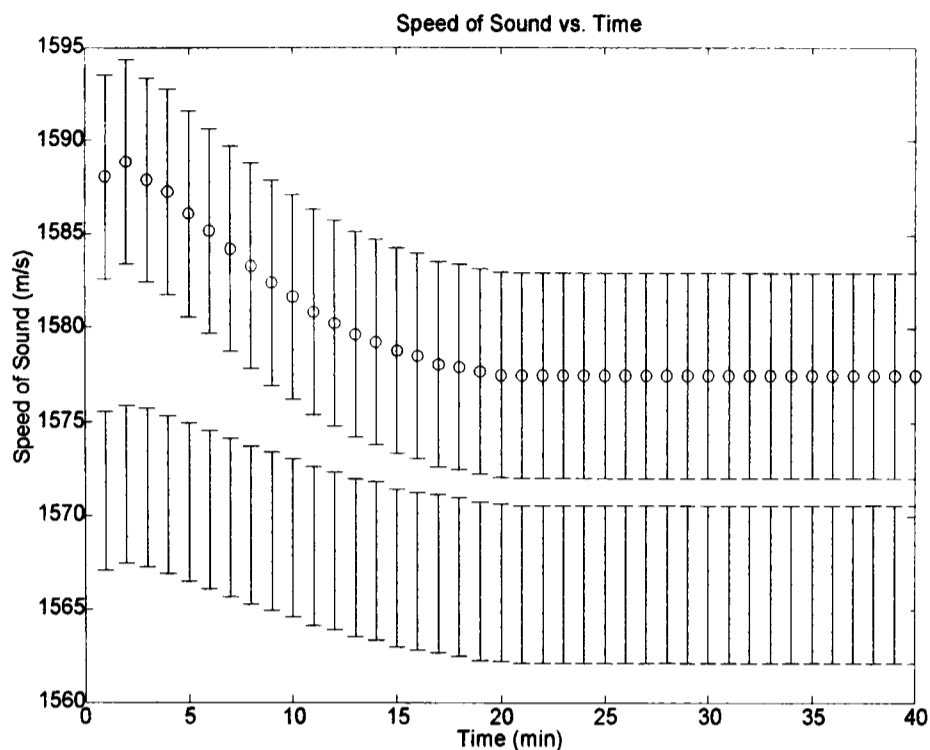


Figure 4.13: Mean velocity versus time results for 50 samples. Mean velocity of Unilever samples is represented by circles. Mean velocity of Tesco samples is represented by dots.

Figure 4.13 shows the mean velocity recorded for each group of 25 as the samples acclimatised to the temperature of the water. The velocity of each sample had stopped falling after approximately 20 minutes. Results presented in Section 4.6 are the velocities and attenuations measured at 10°C, after the sample had been immersed for 20 minutes.

4.5 Measurement Temperature

As in Chapter 3, it was important to determine the intersection temperature of the speed of sound in water and the speed of sound in fish oil before taking measurements of the speed of sound through fish tissue itself. Here

too, it is important to realise that it has been shown that the solid/liquid fat ratio in adipose tissue changes with temperature and affects the ultrasonic velocity through the tissue [32]. The solid fat content is expected to be low at approximately 20°C, but to increase rapidly as the temperature of the tissue drops below 10°C. At 10°C, all of the saturated fat and much of the monounsaturated fat is expected to be solid. At 20°C, all of the monounsaturated fat is expected to be liquid, as will be some of the saturated fat [32, 69].

Ghaedian [34] found the intersection temperature to be approximately 18°C. However, in his experiments, fish oil was not used. Sunflower oil was used instead. Several studies have found the speed of sound through sunflower oil to be approximately 1470.40ms^{-1} at 20°C [39]. Salmon oil is not commercially available, but cod liver oil is. From knowledge of the fatty acid composition of cod liver oil and salmon oil, it is possible to calculate the speed of sound through them as $1479\text{ms}^{-1} \pm 1\text{ms}^{-1}$ and $1486\text{ms}^{-1} \pm 1\text{ms}^{-1}$ respectively at 20°C. The reason that the velocity through cod liver oil is closer to the velocity of salmon oil than is the velocity of sunflower oil is apparent from Appendix C. It shows that the fatty acid composition of cod liver oil is closer to that of salmon oil than is sunflower oil. Since the fatty acid composition of cod liver oil is closer to that of salmon oil, cod liver oil was used here to determine the intersection temperature. Distilled degassed

water and the Perspex measurement cell described in Chapter 3 were used in this experiment as well.

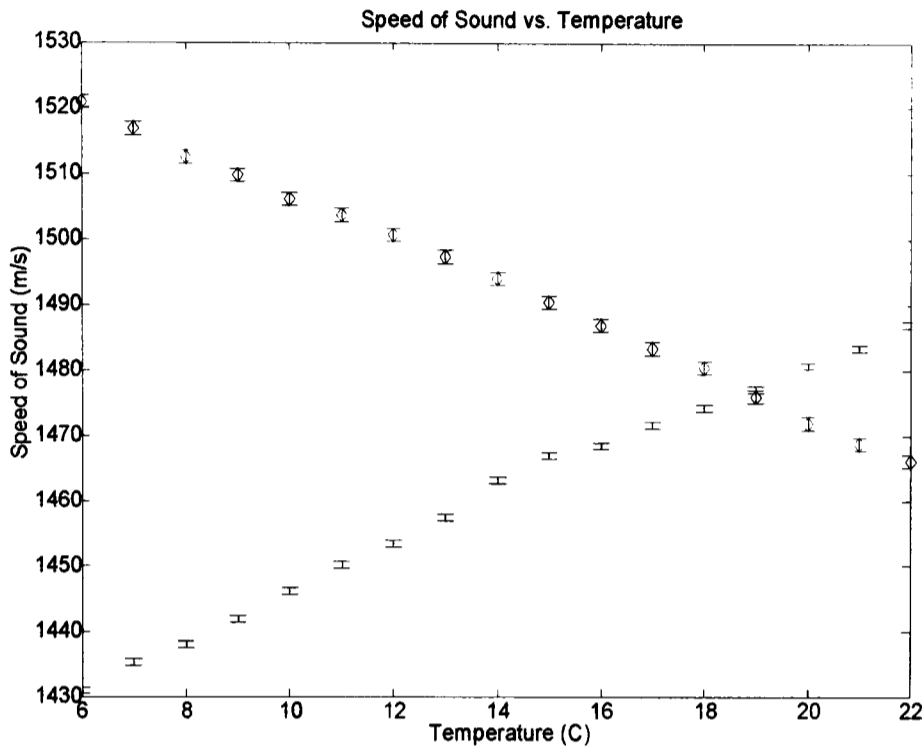


Figure 4.14: Speed of sound through cod liver oil and pure water versus temperature. The diamonds represent cod liver oil data. The dots represent data for pure water.

Figure 4.14 shows that the temperature at which the curves intersect is approximately 19°C. Therefore, it was necessary to take ultrasound measurements in salmon tissue well away from this critical temperature. Raising the temperature to 35°C or 40°C presented difficulties in terms of available hardware. However, the cooling chamber used in several experiments in the previous chapter was already available. Therefore, tissue measurements in the next section were taken at approximately 10°C. At this temperature, there is a separation of approximately 60ms^{-1} between the speed of sound in

these two media.

From the results presented above, it can also be seen that the speed of sound through the cod liver oil was measured as 1472.39ms^{-1} at 20°C . The discrepancy between this measured value and the calculated value is most likely due to slight differences in composition between a commercially available edible oil and a theoretically pure combination of fatty acids. Still, this velocity is closer to that of salmon oil than is the empirically-measured velocity of sunflower oil. Therefore, cod liver oil will still provide a more accurate idea of the intersection temperature than will sunflower oil.

4.6 Tissue Measurements

This section describes further experiments conducted on salmon muscle tissue. Velocity and attenuation measurements were taken to determine if ultrasound was capable of detecting changes in distributed fat level within the tissue and how accurately such determinations could be made.

4.6.1 Sample Orientation

Forty percent of the fat in salmon muscle tissue is contained in the myosepta. Therefore, the amount of myosepta in the ultrasound path can affect the measured velocity through the sample. To ensure that the same approx-

imate myosepta pattern was encountered in all ultrasound measurements, the system of axes in Figure 4.15 was adopted.

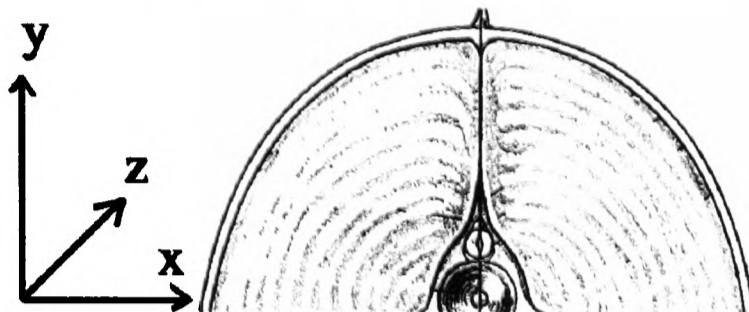


Figure 4.15: System of axes applied to fish samples.

All ultrasound measurements described in this chapter were made in the x-direction, as it is defined in Figure 4.15. Since all samples came from the area of the fish between the dorsal fin and the spine, and since all of the samples were cut from commercially farmed salmon, the thickness of the myosepta in each sample was approximately the same. It was approximately 2.0mm to approximately 2.5mm. A further investigation into the effect that myosepta orientation has on measured velocity was modelled in the next chapter.

4.6.2 Repeatability

Before a large number of samples of different fat contents were measured, it was important to ensure that velocity measurements could be made repeatedly on a single sample with an error no greater than $\pm 1\text{ms}^{-1}$. Velocity

measurements were made on 10 Unilever samples. Each sample was measured 10 times. Each time, one transducer was removed from contact with the sample and then replaced before the next measurement was taken. This was experimentally easier than shifting the sample each time. All measurements were taken at 10°C. Table 4.1 shows these results. Each velocity value is a mean of 10.

Mean c	Standard Deviation
1583.63ms ⁻¹	±0.65ms ⁻¹
1574.61ms ⁻¹	±0.85ms ⁻¹
1571.19ms ⁻¹	±0.26ms ⁻¹
1566.64ms ⁻¹	±0.52ms ⁻¹
1575.82ms ⁻¹	±0.86ms ⁻¹
1589.83ms ⁻¹	±0.83ms ⁻¹
1571.18ms ⁻¹	±0.90ms ⁻¹
1573.15ms ⁻¹	±0.99ms ⁻¹
1567.18ms ⁻¹	±0.51ms ⁻¹
1568.23ms ⁻¹	±0.34ms ⁻¹

Table 4.1: Mean repeatability results for fish tissue samples.

Table 4.1 shows that for each sample the standard deviation was less than $\pm 1\text{ms}^{-1}$ over ten measurements. Therefore, it is reasonable to assume that the velocity measurements taken on tissue with this system did not deviate by more than $\pm 1\text{ms}^{-1}$ within one sample.

4.6.3 Salmon Samples

Velocity and attenuation measurements were made on 50 samples of salmon muscle tissue. Twenty-five of the samples were from those supplied by Unilever. The other 25 samples were from those supplied by Tesco. All measurements were taken at 10°C. The results are shown in the figure below.

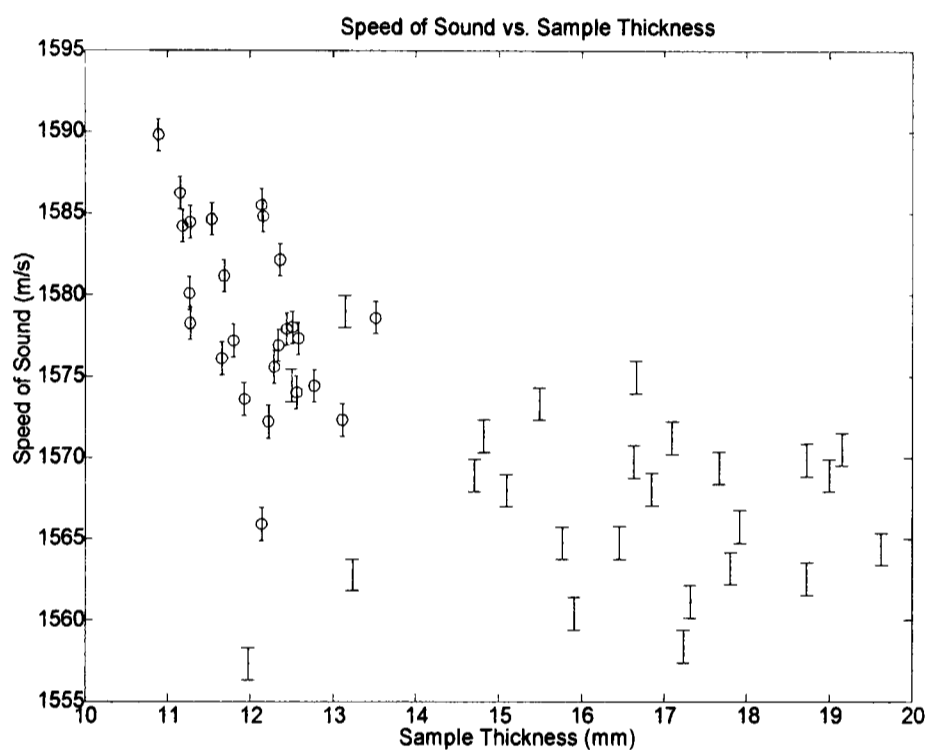


Figure 4.16: Speed of sound versus sample thickness. The circles represent data from Unilever samples. The dots represent data from Tesco samples.

Figure 4.16 shows the speeds of sound recorded for all 50 samples. The circles represent Unilever samples. The dots represent Tesco samples. These results are summarised in Table 4.2. All velocity values are means of 25.

Source	%Fat	Mean c	Standard Deviation
Unilever	8% ± 3%	1578.87ms ⁻¹	±5.48ms ⁻¹
Tesco	11% ± 3%	1568.48ms ⁻¹	±4.23ms ⁻¹

Table 4.2: Variation of velocity with fat content.

The results in Table 4.2 show that there is an approximately 3.5ms^{-1} decrease in velocity with a 1% increase in fat content. This decrease is counter to what was predicted by the milk/cream foam phantom at 10°C . Freese and Makow [21] noted a decrease in velocity with an increase of fat in whitefish over a temperature range from 8°C to 35°C . For muscle tissue, there seems to be no mention in the literature of a “critical temperature” such as that observed for liquids in Section 3.4.1 and Section 4.5. Moreover, if a critical temperature for fish tissue existed between 10°C and 25°C , then the two curves shown in Figure 4.13 should have intersected at some point as the temperature of the samples decreased. No such intersection is seen. This leads to the conclusion that there is no critical temperature between 10°C and 25°C at which the velocities of salmon muscle tissue intersect regardless of fat content. This could be due to structural differences between the liquid and tissue media. This could also be due to changes in the solid/liquid fat ratio with changes in temperature. The variation may also be due to natural variations in fat content in the tissue medium.

The velocity data for both fat levels in Table 4.2 showed large deviations in velocity from their mean. This could in part be due to the natural variation in muscle tissues even between fish raised under similar conditions. It could, as well, be attributed to different quantities of myosepta in the ultrasound path. Whatever the case, these results suggest that there was not

the necessary resolution to distinguish between 1% fat levels in fish tissue using transmission ultrasound at a single temperature. However, it may be possible to perhaps distinguish between “low fat”, “medium fat” and “high fat” salmon. In such a case, the fat range can be split into three divisions. Low fat salmon would be those salmon containing between 0% and 8% intramuscular fat and high fat salmon would be those containing more than 16% fat. Typically, intramuscular fat in salmon does not exceed 25% [17].

Table 4.3 shows the measured attenuation for the same 50 samples. All attenuation values are means of 25.

Source	%Fat	Mean α	Standard Deviation
Unilever	8% \pm 3%	4.11dB cm ⁻¹	0.29dB cm ⁻¹
Tesco	11% \pm 3%	3.42dB cm ⁻¹	0.60dB cm ⁻¹

Table 4.3: Variation of attenuation with fat content.

Table 4.3 shows that the mean attenuation decreased with increasing fat content. This is the opposite of what had been predicted from the milk/cream phantom. However, the trend in this data is the same as that in published attenuation data for whitefish with similar fat levels [21]. Here too though, the size of the deviations suggest that one cannot distinguish between 1% fat levels by attenuation measurements alone. Yet, there may be good enough resolution in these measurements to classify the tissue under examination as either low fat, medium fat or high fat.

Additionally, there may be contact loss between the transducers and the

sample. The attenuation calculation assumes the relationship shown in Equation 2.13. This equation does not account for contact loss. Compressing the sample should have decreased the amount of contact loss, but not eliminated it. As a result, these attenuation results may be artificially high.

4.6.4 Comparison to Chemical Analysis

Chemical analysis was performed on twelve samples. This was done in order to more-clearly determine the relationship between acoustic velocity and the fat content of the salmon muscle samples. Six of the samples used were from those supplied by Unilever. The other six were from those supplied by Tesco. The analysis was performed by Campden & Chorleywood Food Research Association (CCFRA) Technology Limited of Chipping Campden, UK. The Werner Schmid method was used to determine fat levels. As described in Section 1.1, this method involves the use of chemical solvents to extract both polar and nonpolar lipids from the entire sample. Figure 4.17 shows the results.

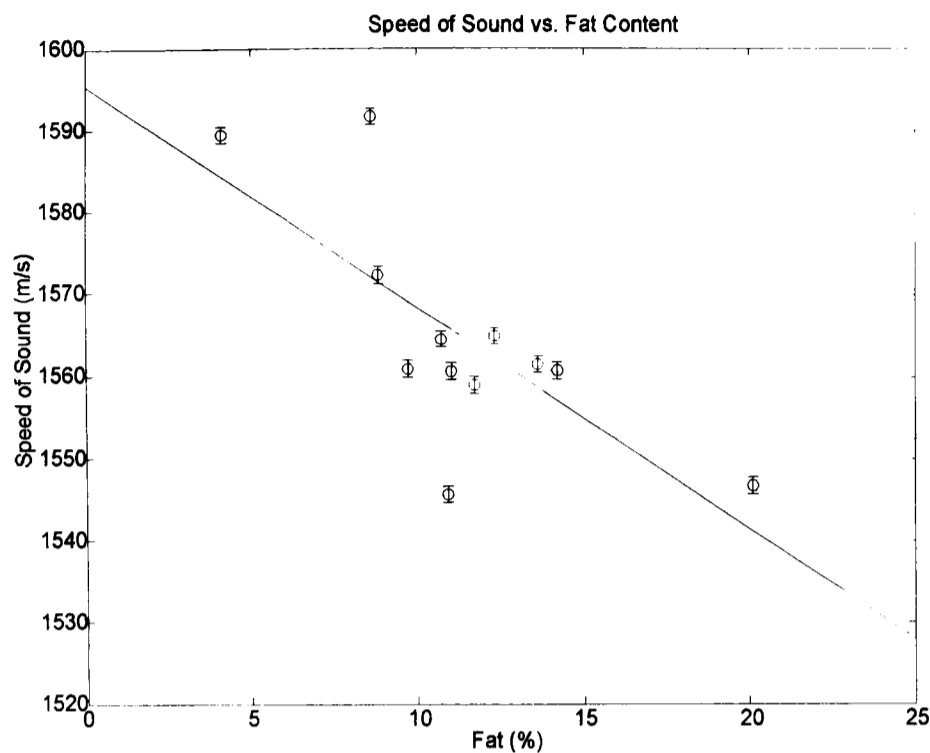


Figure 4.17: Speed of sound versus fat content at 10°C. The line is a best-fit.

Figure 4.17 shows that there is a trend of decreasing speed of sound with an increase in fat level ($r=-0.73$, $n=12$). The mean error in fat measurement using the Werner Schmid method is approximately $\pm 0.6\%$ fat³.

Again, there is not sufficient uniformity in the results to attempt to predict fat content to within 1% fat. However, as suggested in the previous section, it may be possible to place the data into three groups according to fat content. It may be possible to define the following groupings.

³Quality control information supplied by CCFRA.

	Fat	Velocity
Low Fat	0%-8%	$\geq 1575\text{ms}^{-1}$
Medium Fat	8%-16%	$1555\text{ms}^{-1}-1575\text{ms}^{-1}$
High Fat	$\geq 16\%$	$\leq 1555\text{ms}^{-1}$

Table 4.4: Three fat categories for salmon muscle tissue.

Ten of the twelve data points fit to these parameters. The mean velocity data presented in Table 4.2 also fits into these groups. Analysis using t-tests shows that there is a statistically significant difference ($p=0.015$, $\alpha=0.05$) between the mean of the data which fits into the Low Fat group and that of the Medium Fat group. However, there is not a statistically significant difference ($p=0.070$, $\alpha=0.05$) between the mean of the data in the Medium Fat group and that of the High Fat group. The most-reasonable conclusion to draw from this is that many more samples need to be tested before strong differences between these, or other, groupings may appear.

Had sufficient funds existed, chemical analysis would have been performed on a larger number of samples. This is a focus for future work. Here again, the structure of the tissue, the myosepta size and orientation in particular, may be a factor affecting velocity, as two of the points do not lay near the best fit line or within these groups. The affect that myosepta orientation and thickness have on velocity is modelled in the next chapter.

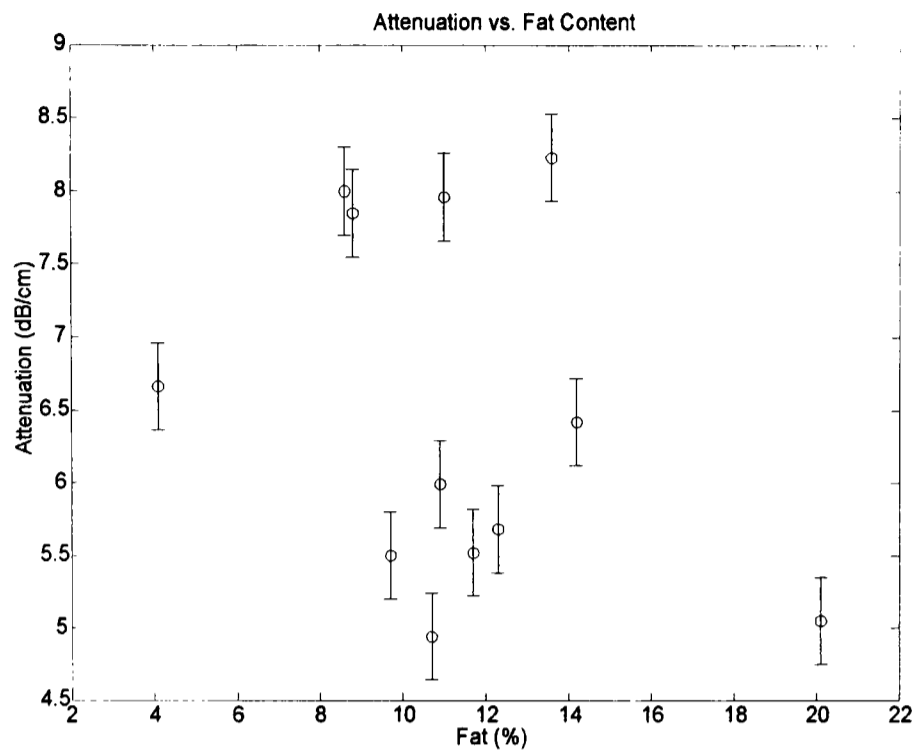


Figure 4.18: Attenuation versus fat content at 10°C.

Figure 4.18 shows the measured attenuation for the twelve samples. A decrease in attenuation with fat content similar to that found in the previous section was expected. However, Figure 4.18 shows that the attenuation measured here has little correlation to the fat level of the sample. Again, a larger sampling group may yet yield this dependence. From this attenuation data, it is not possible to classify the samples according to fat content at all. Here, too, contact loss may be a factor.

4.7 Conclusion

This chapter has shown that the salmon muscle tissue samples used here came from a section of the fish which represented the overall fat content of the fish and contained the fewest intramuscular bones. It has also been shown that it was possible to take velocity measurements on a single sample with an accuracy of approximately $\pm 1\text{ms}^{-1}$. This level of repeatability was important if one was to measure the fat content using velocity measurements. The orientation of each sample was approximately the same in order to have the beam pass through approximately the same myosepta orientation in each sample.

A decrease in both attenuation and velocity were measured as the fat content of the samples increased. However, there was not sufficient resolution using this technique to distinguish between 1% fat levels. It was possible to group the samples into three divisions (high fat, medium fat and low fat) based solely on ultrasound velocity measurements at a single temperature.

Chapter 5

Salmon Tissue Model

The term “mathematical model” can be applied to any set of mathematical equations which is thought to represent another entity, be it physical phenomena, a concept, etc. [80]. This chapter describes a mathematical model which was developed to study the effects of changes in fat content, myoseptum size and myosepta configuration on the speed of sound through a salmon sample. Modelling attenuation was not attempted. Given the biological variation between salmon samples, it was hoped that output from the model would provide an idea of the magnitude of variation in velocity one would expect over a range of samples.

There are several methods and programmes for modelling the propagation of ultrasound through soft tissue. A popular programme for modelling ultrasound propagation in tissue is Field II. It was developed by J.A. Jensen of the

Technical University of Denmark. The main application of this programme is to simulate the image of an ultrasound scanner [81]. The programme runs on top of Matlab and is written in the Matlab programming language. It splits the transducer face into rectangles and a far-field approximation is calculated for each rectangle. The object under examination is created by the user by placing point scatterers at different distances from the transducer and setting various properties of those scatterers [82]. While useful in some situations, Field II is not appropriate here. Just as with ultrasound scanners, Field II assumes a tissue velocity of 1540ms^{-1} . Within the programme, it is not possible to set the speed of sound through different materials. This is a necessity if one is to investigate velocity changes due to changes in the tissue constituents or myosepta size.

A more suitable package is Wave2000. It is a commercially available programme for modelling the propagation of ultrasound in two dimensions. It was developed by CyberLogic Incorporated of New York City, USA [83]. It has been used in previous studies to simulate ultrasound in bone and soft tissues. It operates by solving the two-dimensional elastic wave equation by the finite difference method. Its user interface allows one to graphically create an object for sonification, assign physical properties to that object and place transmitters and receivers at any location around the object. However, purchase of this product was not financially viable. Therefore, a less expensive

alternative was sought.

Since attenuation was not being modelled, it was sufficient to model the path of the wavefront through the sample and the speed of sound through each medium it encountered. A rapid and inexpensive method that would yield the required information is ray tracing. In a ray tracing model, waves are treated as bundles of rays which propagate undeviated until they interact with inhomogeneities within a medium or interfaces between media [84]. Ray theory has been used in the study of wave propagation in isotropic homogeneous and inhomogeneous materials [85, 84, 86]. The Matlab programming language was used to create a two-dimensional ray tracing model. The full Matlab code listing for this model can be found in Appendix D.

5.1 Model Geometry and Methods

With this model, one hoped to understand the variation in velocity caused by changes in fat content, myoseptum thickness and myosepta configuration. All three of these parameters affect measurement repeatability between samples. Changes in velocity caused by a single myoseptum were also investigated so as to understand which myosepta have the greatest effect on measured velocity.

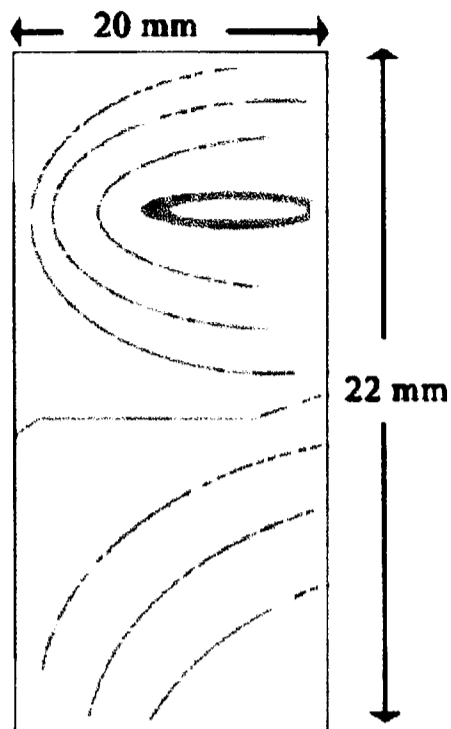


Figure 5.1: Model salmon sample cross-section. This figure is not to scale.

Consider the geometry shown in Figure 5.1. The figure represents a cross-section of one salmon sample cut from the region of interest. The dark curves represent the general shape and number of myosepta found in salmon. The dimensions of the sample being modelled is representative of the size of samples with a similar myosepta pattern. Samples taken from the other side of the spine will have a mirror-image myosepta pattern from the one shown in Figure 5.1. This other pattern was not modelled.

One can see that there are two distinct regions of myosepta. The upper half of the sample consists of myosepta in the form of three concentric half-ellipses with a thicker full ellipse inside them. The myosepta pattern in the bottom half of the sample consists largely of three concentric quarter-ellipses.

A straight myoseptum with its ends at 45-degree angles separates the top and bottom halves of the sample.

The wave travelled from left to right as the sample is shown in Figure 5.1. The wave was split into 122 separate rays. This quantity of rays was convenient from a programming standpoint. A height of 22mm means that there is an initial separation of approximately 0.18mm between rays. A transducer with an element size of 0.5 inches, or 12.7mm, was used in all of the experiments described previously. Thus, a transducer element of the same size was modelled here. An element size of 12.7mm is equivalent to between 70 and 71 rays in terms of beam width. Therefore, 71 rays were used to model the beam from this transducer. A sample thickness of 20mm means that only the Frénel region need be modelled, as the expected Rayleigh distance for such a transducer transmitting into salmon muscle will be between approximately 52mm and 61mm.

The velocity of a single ray can be calculated from knowledge of the quantities of the different media through which the ray passes and knowledge of the speeds of sound in those media. Each medium was considered to be a homogenous mixture with a constant velocity. In this model, the velocity of a single ray is calculated from knowledge of the distance the ray travels through white muscle tissue, the distance it travels through myosepta and the speeds of sound in both of these media at a known temperature. The

mean received velocity was calculated as a mean of the velocities of 71 rays.

Which rays were used was dependent on transducer position.

The thickness of myosepta in salmon is representative of the overall amount of intramuscular fat present. However, myoseptum thickness is also dependent on the growth rate of the salmon. For salmon with similar growth rates, myoseptum thickness increases as the level of overall intramuscular fat within the sample increases [87]. There is little literature relating the thickness of a myoseptum to the overall percentage of intramuscular fat. However, in this model the following relationship was found to yield reasonable results.

$$myoseptum_thickness = 1.8 + 0.01 \cdot fat_percentage \quad (5.1)$$

where *myoseptum_thickness* is in millimetres.

The muscle/myoseptum interfaces were modelled as arrays of angles such that the angle of diffraction of a ray was calculated using Snell's Law. This allowed the geometry of the myosepta to be quickly changed if necessary. The distance between myosepta is not important. There is no difference in terms of calculated velocity if the beam travels through several myosepta, one after the other, and then through white muscle for the rest of its journey, or if the beam travels through myosepta separated by several millimetres of white muscle. Again, attenuation effects, such as scattering caused by inhomogeneity of the media, were not modelled.

5.1.1 Using Snell's Law

Figure 5.2 illustrates a version of Snell's Law. It shows a ray travelling from a source in Medium 1 into Medium 2.

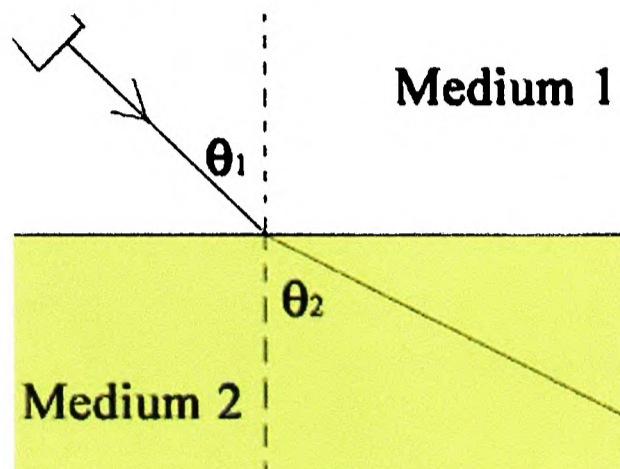


Figure 5.2: A single ray refracting as it enters a medium with a different speed of sound.

Snell's Law states that for the situation illustrated above

$$c_1 \sin \theta_1 = c_2 \sin \theta_2 \quad (5.2)$$

where c_1 and c_2 are the speeds of sound in Medium 1 and Medium 2 respectively [88]. The angle at which the rays refracted when encountering a muscle/myoseptum interface was calculated using Equation 5.2.

Figure 5.3 illustrates the three behaviours of rays encountering a myoseptum.

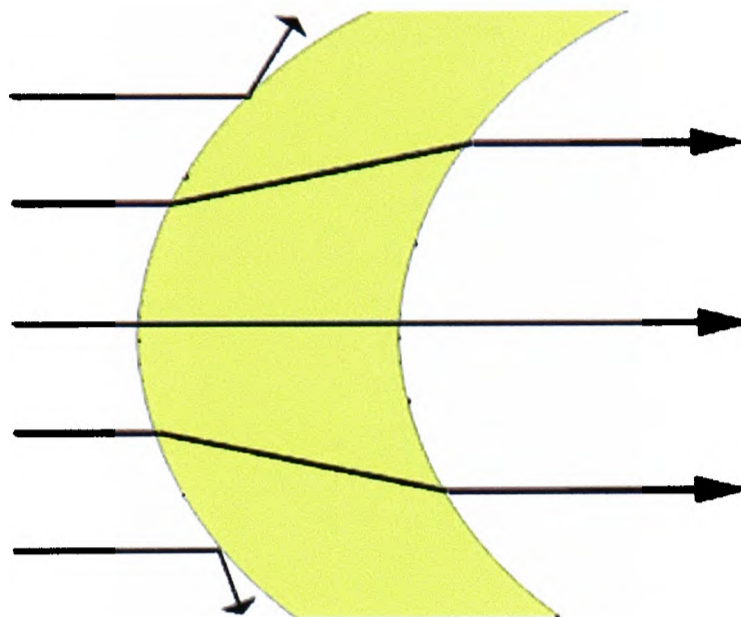


Figure 5.3: Rays encountering a single myoseptum.

The rays illustrated in Figure 5.3 either totally reflect and do not enter the myoseptum, refract, or pass straight through depending on the angle at which they encounter a muscle/myoseptum interface. Experimental simulations showed that rays encountering an interface at an angle of 63° or greater were completely reflected away from the interface. This is due to the velocity ratio between media at the interface. Those rays which encountered an interface at an angle greater than 63° were modelled as having not arrived at the receiver and their data was not included in the calculation of overall velocity.

From knowledge of the refraction angle, it is possible to calculate the path length of the ray within a myoseptum. Figure 5.4 shows the approximation

used here.

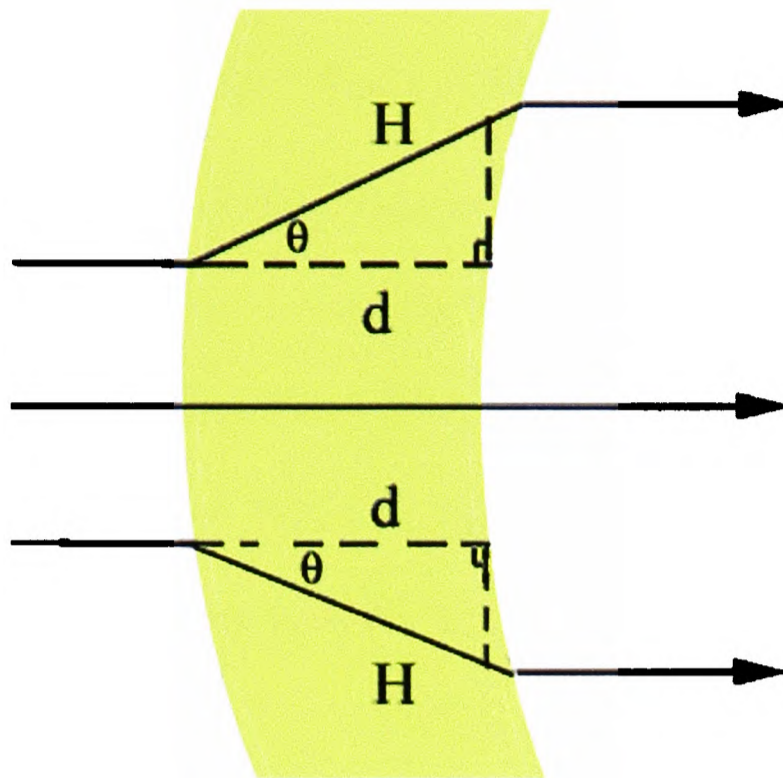


Figure 5.4: Geometry for the calculation of a ray's path length within a myoseptum.

In Figure 5.4, d is the thickness of the myoseptum as defined by Equation 5.1, H is the distance the ray travels within the myoseptum and θ is the refraction angle. H is calculated from d and θ .

It is obvious from Figure 5.4 that the distance travelled by the ray in the myoseptum is slightly greater than the distance H due to the curvature of the myoseptum. Given that a myoseptum is normally less than 3mm thick, this error in H will be much smaller than a wavelength in size, assuming a 2.25MHz frequency. Its precise value will depend on the curvature of the myoseptum and on the angle θ .

The total distance a ray travels through the sample was defined as

$$d_{total} = d_{muscle} + d_{myosepta} \quad (5.3)$$

$d_{myosepta}$ can be found by adding together all of the resultant H terms in the ray's propagation. This should add the errors present in the H terms. However, this error should still be a fraction of a millimetre in size as there will be a maximum number of five H terms. This maximum occurs when a ray travels through all myosepta in the top half of Figure 5.1. d_{muscle} is defined as

$$d_{muscle} = d_{sample} - n_{myosepta} \cdot myoseptum_thickness \quad (5.4)$$

where d_{sample} is the thickness of the sample and $n_{myosepta}$ is the number of myosepta the ray has passed through during its propagation. It is important to note that d_{muscle} is an approximation based on $myoseptum_thickness$ and as such will contain the same errors due to the curvature of the myoseptum.

From this information, Equation 3.3 was used to calculate an overall velocity for a single ray. The velocity of several rays was averaged to yield the mean velocity through a section of the sample.

5.1.2 Speed of Sound Through Salmon Tissue

The percentage of fat in the sample and the temperature of the sample are input by the user when the model is run. This model assumed that all samples

were at an atmospheric pressure of 10^5 Pa, or approximately 1 atmosphere.

The speeds of sound through white muscle and myosepta were each calculated at 20°C and then temperature-corrected to the input temperature. For both myosepta and white muscle, a temperature correction of $2.3 \text{ ms}^{-1}\text{C}^{-1}$ was used. This is the correction found for whitefish over the temperature range of 8°C to 35°C [21]. This approach was taken, because there is not literature regarding the change in the speed of sound with temperature through the elastin and collagen phases of myosepta, nor through the protein phase of white muscle nor through salmon muscle tissue as a whole. However, there was sufficient velocity data on all of the white muscle and myosepta components at approximately 20°C .

White Muscle

As mentioned in Section 4.1, fish muscle tissue can be considered an aqueous mixture since its bulk modulus is much larger than its shear modulus. Therefore, the speed of sound through the white muscle portion of the sample was calculated using the multi-component Equation 3.3. The speed of sound through fat in the sample at 20°C was calculated using Equation 3.9. From the percentage of fat, the percentage of water present in the sample was then calculated using Equation 4.3. The speed of sound in water at a given temperature was calculated using Equation 3.10. It was found that

results closer resembling those from real salmon samples could be achieved by adding 35ms^{-1} to the result of Equation 3.10. This correction could be necessary for three reasons. Perhaps the water within tissue behaves more like salt water due to the various salts and minerals in the tissue. This term could also correct for the effects of freezing on the sample. Both salinity and freezing are known to raise the speed of sound in tissues [71, 61]. A further possible reason for the discrepancy could be the varying amount of solid fat content in real salmon tissue.

The percentage of protein in the sample is the difference of subtracting the percentage of fat and the percentage of water in the sample from 100%. Finding the speed of sound through protein was more difficult. In other studies of fish tissue, it has been the case that the speed of sound through protein was not calculated. Instead, models were based on empirical measurements of the speed of sound through a “fat phase,” generally comprising an edible oil, and the speed of sound through an “aqueous phase,” comprising water and protein [22, 34, 43, 28, 20]. The models ignored any structural effects. Suvanich [20] found that this type of model worked well for cod, flounder, mackerel and catfish. It did not work well for salmon. There was not a good correlation between his predicted velocities for salmon and his measured values.

An alternative approach is to consider the main proteins in salmon white

muscle tissue and the molecular structures of those proteins. The three major proteins in muscle tissue are actin, myosin and collagen. Each protein is made up of up to 20 different amino acids. The U.S. National Center for Biotechnology Information database [89] contains information on the primary protein sequences of all 23 proteins which exist in salmon muscle tissue. A primary protein sequence describes the structure and quantities of amino acids that make up a protein [90]. The overall amino acid composition of salmon muscle tissue has been published by R.P. Wilson [91]. Moreover, Kharakoz [40] has published data on the speed of sound at five different temperatures through 18 of the 20 amino acids which appear in salmon muscle.

However, none of this amino acid data will yield a reasonable idea of acoustic velocity through these proteins. This is because of a difference in molecular structure between amino acids and proteins. It is thought that the bonds in the short-chain amino acids will react differently to ultrasound than will the bonds in the longer-chain proteins made from the same amino acids [92]. Therefore, it would be inappropriate to use Equation 3.3 in combination with Kharakoz's data to yield acoustic velocities for proteins.

Collagen is the most abundant protein in muscle tissue. In humans, collagen constitutes approximately 25% to 30% of the total protein, and thus, about 6% of the total body weight [93]. An increase in collagen concentration has been shown to increase the speed of sound in both suspensions and in

tissue [37, 94, 95, 96]. This suggests that it has a speed of sound greater than both water and fat.

It may be possible to get an idea of the speed of sound through proteins by examining polymers with the same sorts of bonds in their molecular structures as proteins. A polymer is a material with just a few amino acids repeated in its structure. Nylon is an example of this. The speed of sound through nylon at 20°C has been found to be 1800ms^{-1} [97]. Amides such as dimethyl formamide (DMF) may also provide an idea of the speed of sound through proteins as they also contain the same sorts of bonds in their structure as one finds in proteins [92]. In this model, a value of 1750ms^{-1} for protein was found to yield reasonable results.

Finally, Equation 3.3 was used to combine the velocities and volume fractions of each component to yield an overall velocity through salmon white muscle tissue.

Myosepta

A myoseptum is composed primarily of collagen and elastin. The connective tissue of fish contains approximately 82% collagen and approximately 18% elastin [77]. There is no data in the literature for the speed of sound through elastin. Therefore, the myoseptum was treated as a collagen thread. Goss [98], proposed the following empirical equation for the speed of sound through

collagen threads.

$$c = 1588 + 32 \ln C \quad (5.5)$$

where C is the wet weight percentage of collagen in the tissue and c is in units of ms^{-1} . This equation is for collagen threads at a temperature of 22°C . The speed of sound through a single myoseptum at this temperature was calculated to be approximately 1729.02 ms^{-1} .

Figure 4.6 showed that a myoseptum is surrounded by fat. As mentioned earlier, the myosepta contain approximately 40% of the total intramuscular fat. Thus, it is assumed that there exists a higher concentration of fat in myosepta than in the white muscle which they connect. Here, the myosepta were modelled as having twice the volume fraction of fat than that of the overall volume fraction of fat in the sample. Therefore, the speed of sound in the collagen thread was combined with the speed of sound in fat using Equation 3.3 to yield an overall velocity for myosepta.

Summary of Key Assumptions and Equations

Here follows a summary of the key assumptions and equations used to calculate the speed of sound through white muscle tissue and through myosepta. Note again that the percentage of fat in the sample and the measurement temperature are input by the user.

- Atmospheric pressure was 10^5 Pa, or approximately 1 atmosphere.
- The temperature coefficient for white muscle and myosepta was $2.3\text{ms}^{-1}\text{°C}^{-1}$ in both cases.
- White muscle was considered a homogenous aqueous mixture. Therefore, Equation 3.3 was used to calculate the speed of sound through white muscle tissue from the speeds through its three principal components.
- The velocity through the fat component of white muscle was calculated using Equation 3.9 and corrected for temperature.
- The velocity through the water component of white muscle was calculated using Equation 3.10 and 35ms^{-1} was added to the result.
- The velocity through the protein component of white muscle was assumed to be 1750ms^{-1} .
- The percentage of water in the sample was calculated using Equation 4.3.
- The percentage of protein in the sample was the difference of subtracting the percentage of fat and the percentage of water in the sample from 100%.

- The myosepta were treated as collagen threads surrounded by fat. The percentage of fat in a myoseptum was assumed to be approximately twice as much as in white muscle.
- Equation 5.5 was used to calculate the velocity through the collagen thread. The result was then temperature corrected. It was assumed that the myosepta contained 82% collagen.
- The speed of sound in the collagen thread was combined with the temperature-corrected speed of sound in fat using Equation 3.3 to yield an overall velocity for myosepta.

5.2 Results

Five different situations were modelled. First, a situation which resembled the experiments described in Sections 4.6.3 and 4.6.4 was modelled at several different temperatures and fat contents. This was done to ensure that the model would yield results close to those found empirically. The variation in velocity caused by changes in myosepta configuration was then modelled. Next, the variation in velocity caused by changing myoseptum thickness was investigated. The effect on velocity of individual myosepta was investigated by modelling a sample in which only one myoseptum was present. Finally,

the additive contribution of individual myosepta was seen by starting with a myosepta-less sample and then adding myosepta into the model individually. It was hoped that these modelled situations would provide an insight into the magnitude of error one would expect given the natural variation in structure in salmon muscle tissue.

5.2.1 Temperature and Fat Profiles

In the experiments described earlier, all measurements were taken from the upper half of the salmon sample, as represented by top half of Figure 5.1. Therefore, model output for the top 71 rays should resemble data recorded from real salmon muscle. Figure 5.5 shows the model output for temperatures ranging from 5°C to 25°C in 1°C increments and fat contents ranging from 1% to 25% in 2% increments.

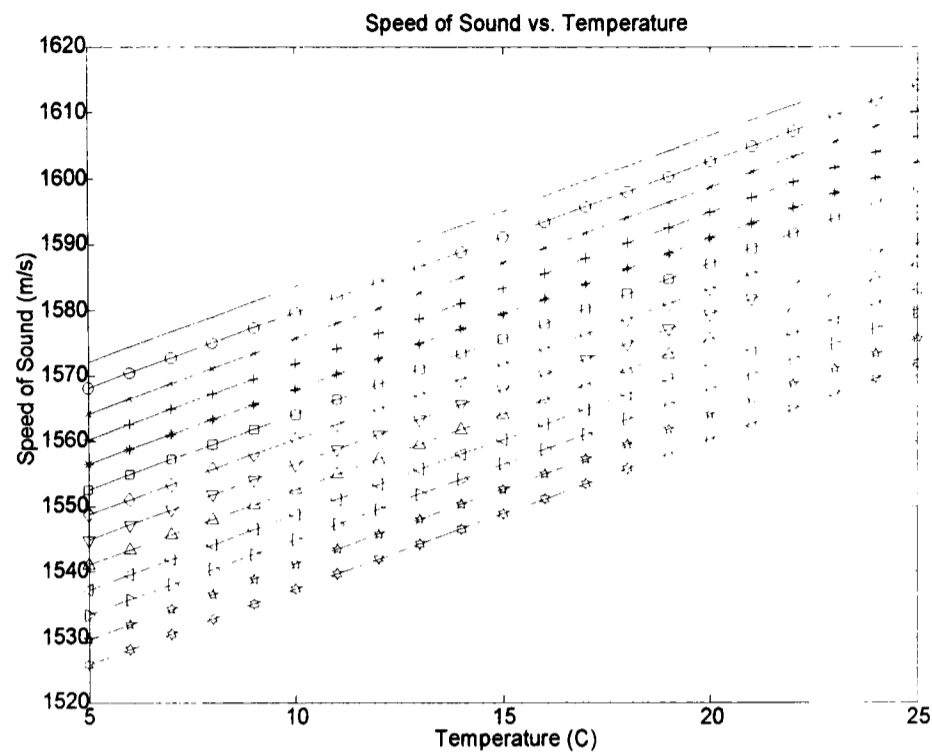


Figure 5.5: Speeds of sound versus temperature for 13 fat levels.

The data in the figure above shows two behaviours which are also seen in results from salmon tissue. The output velocity decreased with increasing fat content. In Figure 5.5, data representing 1% fat is shown at the top of the graph by a solid line with no symbols along its length. The data representing 25% fat is shown at the bottom of the graph by hexagrams. Moreover, the velocity also increased with increasing temperature. Figure 5.6 compares the model output at 10°C to the results from Section 4.6.4.

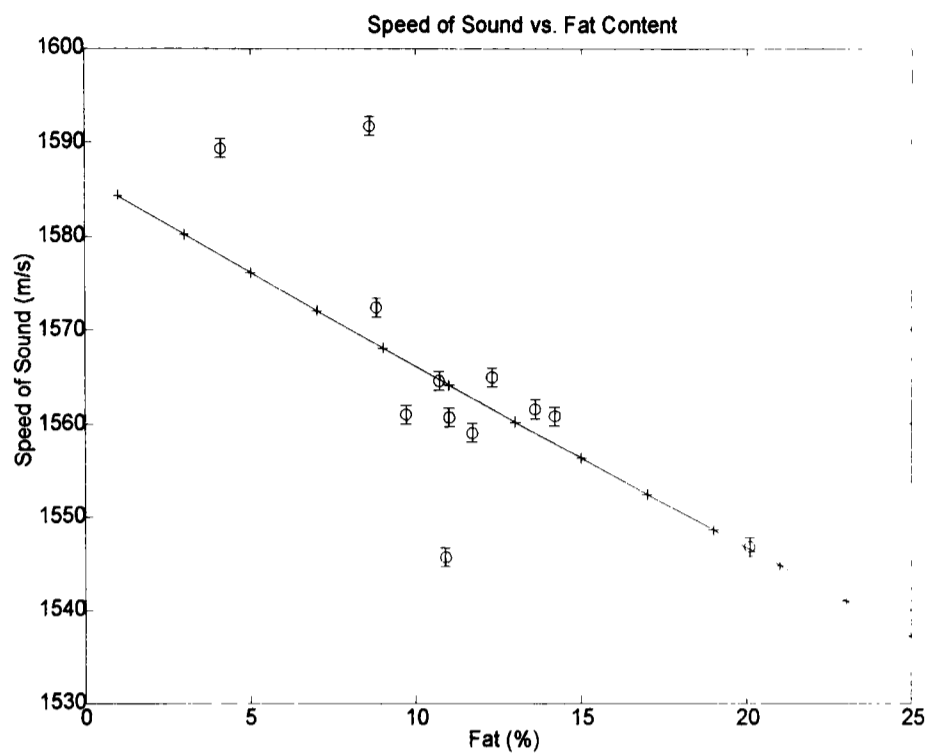


Figure 5.6: Speed of sound versus fat content at 10°C.

In Figure 5.6, the circles represent results from Section 4.6.4. The crosses and solid line represent the output from the model. Bland and Altman have shown that two data sets with a high correlation do not necessarily agree [99, 100]. Data sets which seem to be in poor agreement can produce quite high correlations. The Bland-Altman method of assessing agreement involves first plotting the difference of the data against its mean. Figure 5.7 shows this.

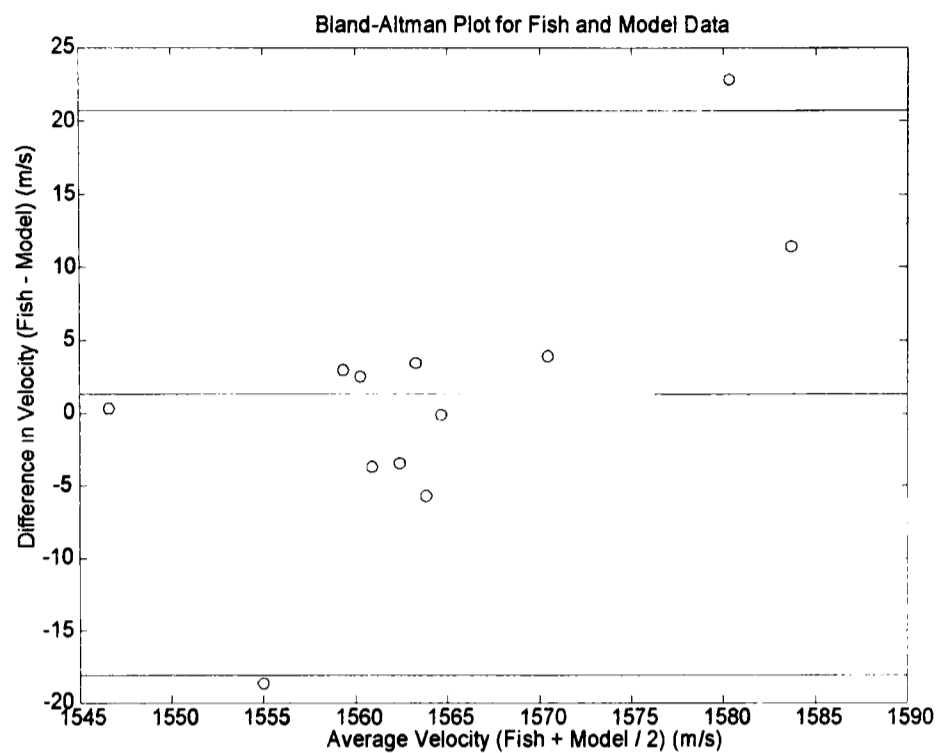


Figure 5.7: A Bland-Altman plot of fish and model data.

The solid line in the middle of Figure 5.7 shows the mean value of approximately 1.3 ms^{-1} . This indicates a positive bias in the measurements. It is difficult to know whether this bias is systemic or arises because the sampling group is so small. If the differences from the mean are normally distributed, 95% of differences should lie between $\text{mean} + 1.96 \cdot \text{sd}$ and $\text{mean} - 1.96 \cdot \text{sd}$, where sd is the standard deviation [99]. In this case, the standard deviation is approximately $\pm 9.9 \text{ ms}^{-1}$. The lines in the top and bottom of Figure 5.7 represent these bounds. From these calculations, it is possible to conclude that output from the model may be approximately 20.7 ms^{-1} above or approximately 18.1 ms^{-1} below the experimental results.

After removing the two outlier values, it appears that the rest of the data falls between approximately $\pm 10\text{ms}^{-1}$ from the mean. However, $\pm 10\text{ms}^{-1}$ is not a small enough bound between the two measurements to enable fat content prediction more accurate than approximately $\pm 8\%$ fat. This degree of accuracy needs to be improved in order for the model to be of more use. This result may be improved by using a larger fish sampling group.

5.2.2 Changing Myosepta Configuration

In this section, the affect on velocity of different myosepta configurations encountered by the ultrasound beam was investigated by moving the transducer down the sample. The temperature of the sample was set to 10°C . The situation being modelled is shown in Figure 5.8.

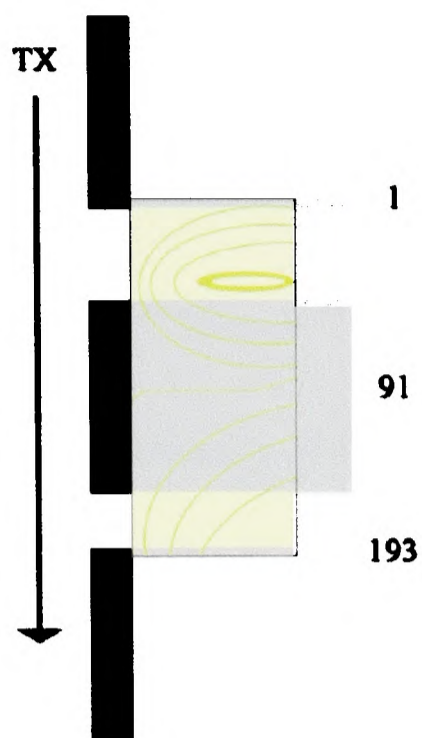


Figure 5.8: Three transducer positions and resultant beams. Parts of the beam outside of the sample are not shown.

In Figure 5.8, the transmitter is represented by a black rectangle to the left of the sample. This illustrates that there are 193 possible transducer positions given the quantisation of the beam width. For example, in position 1, only the bottom ray is transmitted into the sample. In position 91, the entire 71 rays which make up the beam are transmitted into the sample. Finally in position 193, only the top ray is transmitted into the sample. Parts of the beam outside of the sample are not shown. All 193 positions were modelled. The range of fat content modelled is 1% fat to 25% fat in increments of 2% fat. However, for clarity, only the results for fat contents of 1%, 9%, 17% and 25% are presented in Figure 5.9.

Figure 5.9 shows the modelled velocity for all transducer positions at four

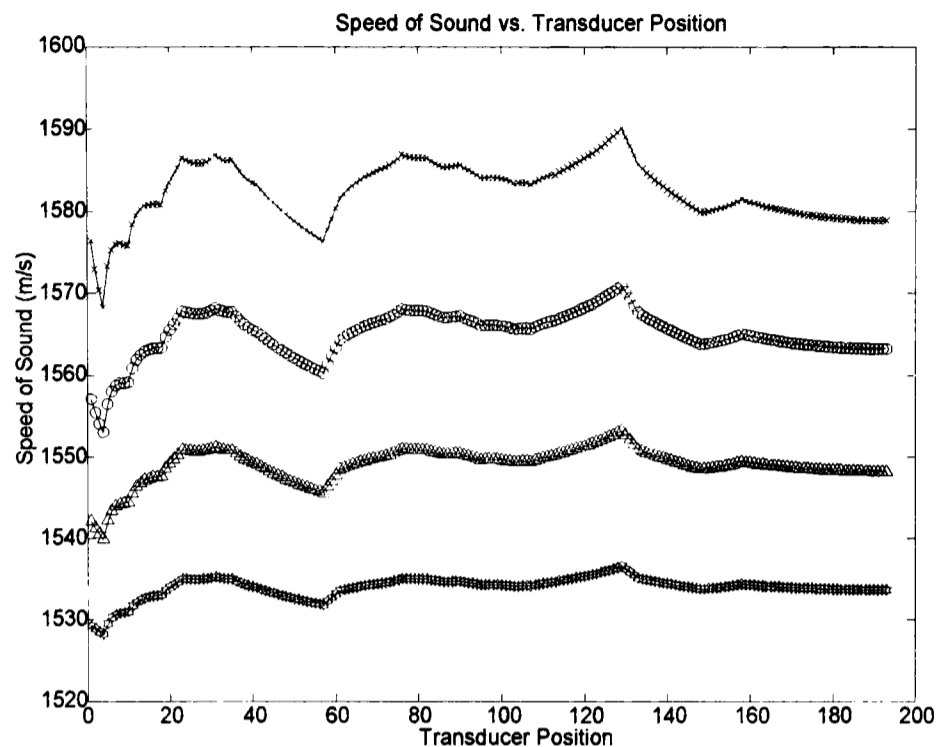


Figure 5.9: Speed of sound versus transducer position for fat contents of 1% (crosses, top), 9% (circles), 17% (triangles), and 25% (hexagrams, bottom).

fat levels. One percent fat is represented by crosses at the top of the graph while 25% fat is represented by hexagrams at the bottom of the graph. This shows that there is a variation in velocity with myosepta configuration. It also shows that this variation decreases with an increase in fat content. This is summarised in the table below.

%fat	Mean c	Standard Deviation
1	1582.45ms^{-1}	$\pm 3.62\text{ms}^{-1}$
9	1565.08ms^{-1}	$\pm 2.87\text{ms}^{-1}$
17	1549.05ms^{-1}	$\pm 2.11\text{ms}^{-1}$
25	1534.00ms^{-1}	$\pm 1.32\text{ms}^{-1}$

Table 5.1: Variation of velocity with fat content over all transducer positions.

Table 5.1 shows that the standard deviation caused by changing myosepta configuration increases near-linearly as fat content decreases. For data over a

fat range such as that in Section 4.6.4, a maximum error of between approximately $\pm 1\text{ms}^{-1}$ and approximately $\pm 4\text{ms}^{-1}$ can be expected from changing myosepta configuration.

5.2.3 Changing Myoseptum Thickness and Myosepta Configuration

The effect of changing myoseptum thickness was investigated in this section. The temperature of the sample was set to 10°C . The fat content of the sample was set to 12.5%. This is a value in the middle of the fat range for salmon. The thickness of all myosepta was increased from 0.1mm to 2.5mm in 0.2mm increments. The results for thicknesses of 0.1mm, 0.9mm, 1.7mm and 2.5mm are shown in Figure 5.10.

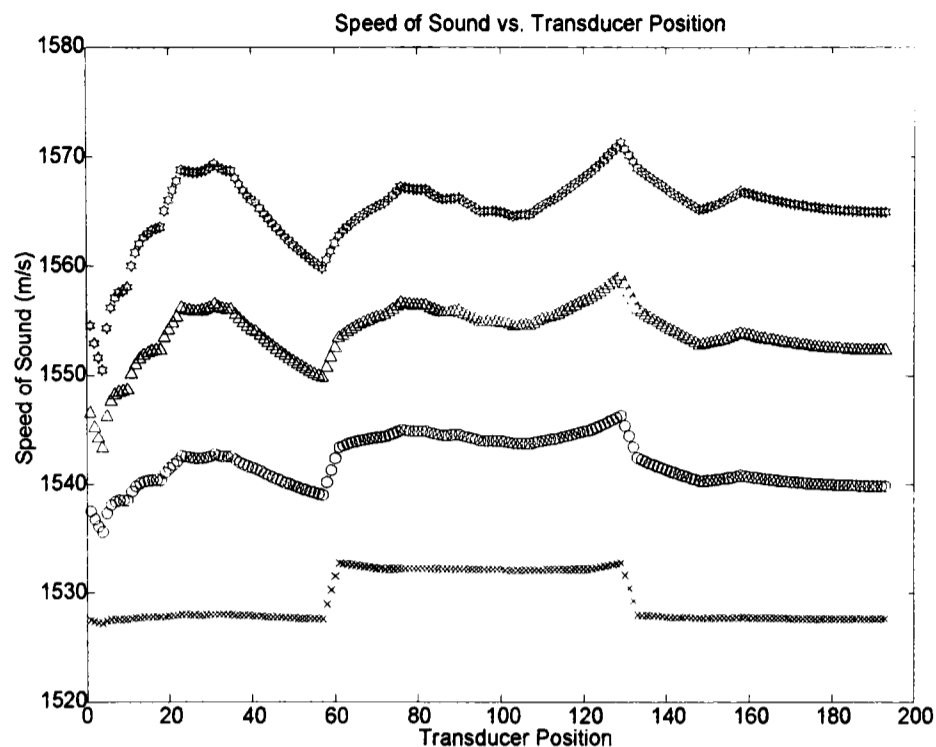


Figure 5.10: Speed of sound versus transducer position for myoseptum thicknesses of 0.1mm (crosses, bottom), 0.9mm (circles), 1.7mm (triangles), and 2.5mm (hexagrams, top).

Figure 5.10 shows the output velocity for all transducer positions at four myoseptum thicknesses. Model output for a thickness of 2.5mm is represented by hexagrams at the top of the graph and output for a thickness of 0.1mm is represented by crosses at the bottom of the graph. This shows that there is a variation in velocity with myoseptum thickness as well as myosepta configuration. One noticeable feature is the rise in velocity of approximately 5ms^{-1} when the horizontal myoseptum is encountered at position 61. This myoseptum constitutes a complete myoseptum path through the sample. Thus, a rise in velocity should be expected where this myoseptum is encountered. It can be seen from Figure 5.10 that the prevalence of this feature to affect

overall velocity decreases as the myosepta thicken. The variation in velocity increases with an increase in myoseptum thickness. Table 5.2 summarises these results.

Myoseptum Thickness	Mean c	Standard Deviation
0.1mm	1529.44ms ⁻¹	±2.16ms ⁻¹
0.9mm	1541.98ms ⁻¹	±2.21ms ⁻¹
1.7mm	1553.89ms ⁻¹	±2.55ms ⁻¹
2.5mm	1565.28ms ⁻¹	±3.28ms ⁻¹

Table 5.2: Variation of velocity with myosepta thickness over all transducer positions.

Table 5.2 shows that over a thickness range such as that seen in most salmon, a maximum variation of between approximately $\pm 2\text{ms}^{-1}$ and approximately $\pm 4\text{ms}^{-1}$ can be expected from changing myoseptum thickness.

5.2.4 Contribution of Individual Myosepta

The contribution of individual myosepta can be seen by modelling a sample with only a single myoseptum present. The temperature of the sample was set to 10°C. Figure 5.11 shows the numbering scheme applied to the myosepta.

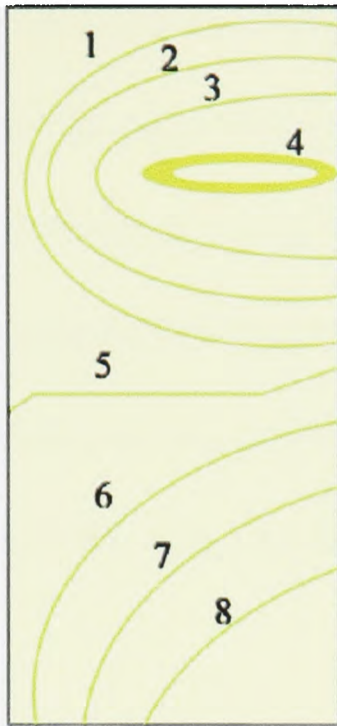


Figure 5.11: Numbering scheme applied to the myosepta.

The average velocity and variation in velocity with position was output for fat contents ranging from 1% to 25% in 2% increments. Table 5.3 summarises the output for 13% fat.

Myoseptum Number	Mean c	Standard Deviation
no myosepta	1529.30ms^{-1}	$\pm 0.00\text{ms}^{-1}$
1	1534.34ms^{-1}	$\pm 5.60\text{ms}^{-1}$
2	1532.77ms^{-1}	$\pm 3.96\text{ms}^{-1}$
3	1531.48ms^{-1}	$\pm 2.68\text{ms}^{-1}$
4	1530.16ms^{-1}	$\pm 1.21\text{ms}^{-1}$
5	1533.21ms^{-1}	$\pm 4.37\text{ms}^{-1}$
6	1534.92ms^{-1}	$\pm 4.54\text{ms}^{-1}$
7	1533.56ms^{-1}	$\pm 4.19\text{ms}^{-1}$
8	1532.82ms^{-1}	$\pm 3.91\text{ms}^{-1}$

Table 5.3: Variation of velocity over all transducer positions with only one myoseptum in the model.

Table 5.3 shows that the addition of a single myoseptum into a sample empty of myosepta increased the mean output velocity. This is what one would expect. The acoustic velocity of a myoseptum is higher than that of the surrounding muscle. It is noticeable that myoseptum number 4 causes the least rise in mean velocity and deviation. At this fat level, all other myosepta cause the mean velocity to rise by approximately 3ms^{-1} to approximately 5ms^{-1} .

The table above shows data for 13% fat only. The figures on the following two pages show velocity versus transducer position for each myoseptum for fat levels of 1%, 9%, 17% and 25% fat over all 193 transducer positions. It can be seen that the same trends are repeated over these fat levels. In all cases, deviation decreases with increasing fat content.

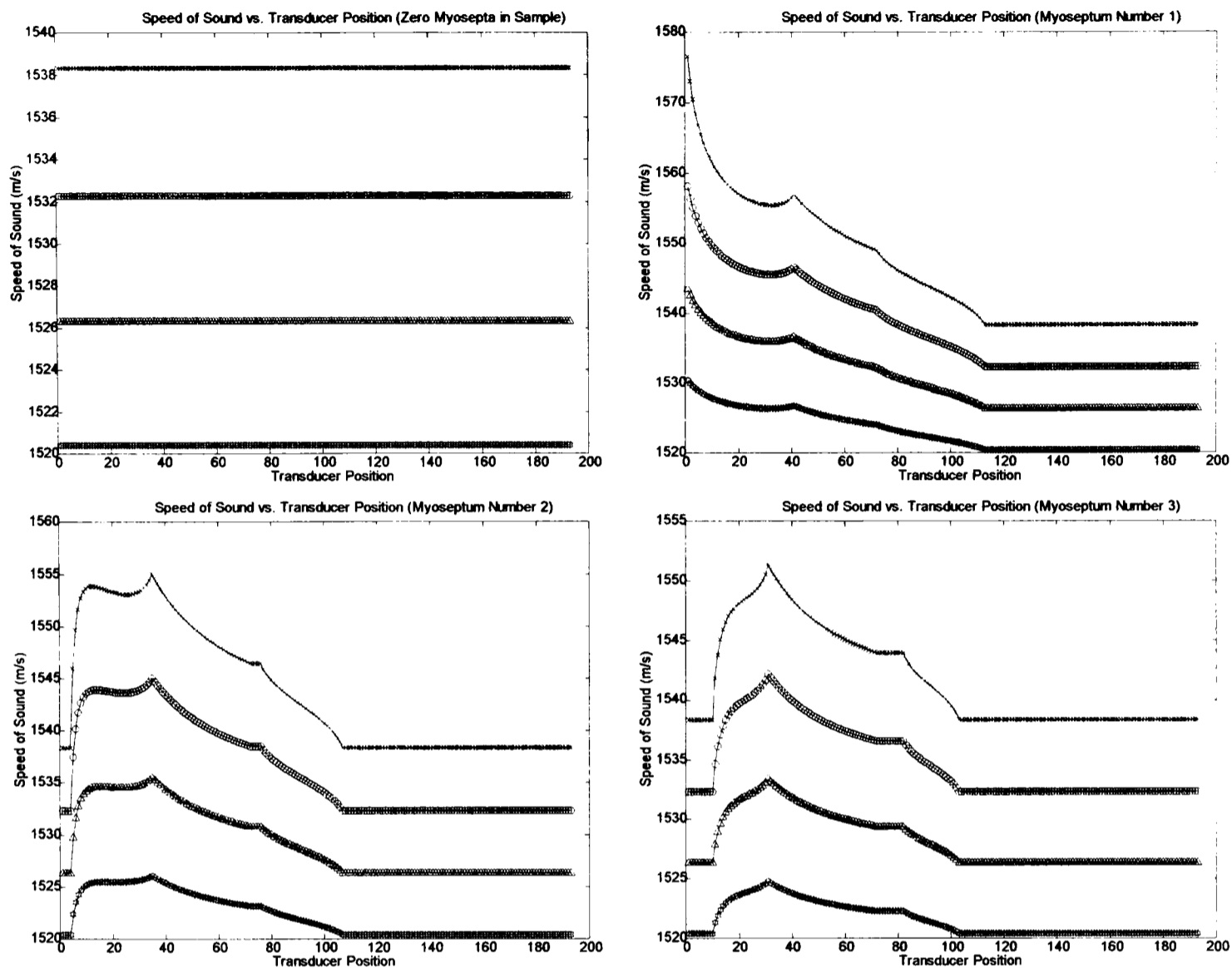


Figure 5.12: Speed of sound versus transducer position for fat contents of 1% (crosses, top), 9% (circles), 17% (triangles) and 25% (hexagrams, bottom). The results for zero myosepta are shown in the graph at the top left. The results for myoseptum number 3 are shown in the graph at the bottom right.

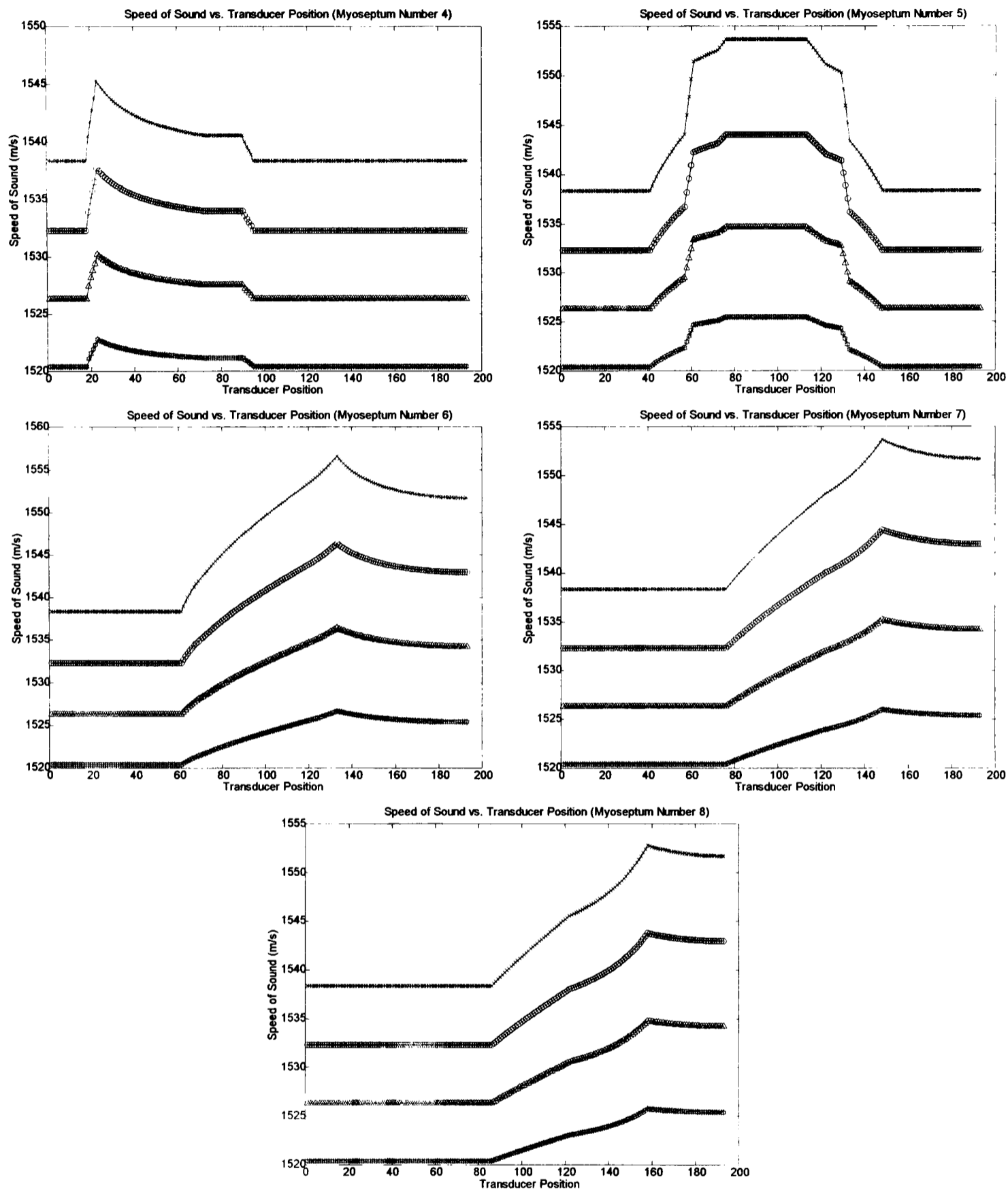


Figure 5.13: Speed of sound versus transducer position for fat contents of 1% (crosses, top), 9% (circles), 17% (triangles) and 25% (hexagrams, bottom). The results for myoseptum number 4 are shown in the graph on the top left. The results for myoseptum number 8 are shown in the graph at the bottom.

5.2.5 Additive Contribution of Individual Myosepta

The additive contribution of individual myosepta can be seen by starting with a myosepta-less piece of tissue and then inserting myosepta into the model one by one. The temperature of the sample was set to 10°C. The same numbering scheme as in Figure 5.11 was used here. Myosepta were added into the model in ascending order according to number.

The average velocity and variation in velocity with position was output for fat contents ranging from 1% to 25% in 2% increments. Table 5.4 summarises the output for 13% fat.

Number of Myosepta	Mean c	Standard Deviation
0	1529.30ms ⁻¹	±0.00ms ⁻¹
1	1534.34ms ⁻¹	±5.60ms ⁻¹
2	1537.66ms ⁻¹	±9.01ms ⁻¹
3	1539.71ms ⁻¹	±11.18ms ⁻¹
4	1540.44ms ⁻¹	±11.99ms ⁻¹
5	1544.35ms ⁻¹	±11.95ms ⁻¹
6	1549.85ms ⁻¹	±7.86ms ⁻¹
7	1555.13ms ⁻¹	±4.46ms ⁻¹
8	1558.67ms ⁻¹	±2.60ms ⁻¹

Table 5.4: Variation of velocity over all transducer positions as myosepta are added into the model.

Again, the addition of myosepta increased the mean output velocity in every case. Table 5.4 also shows that the addition of certain myosepta had little effect on the output velocity. Myoseptum number 4 had the least effect on velocity. The addition of myoseptum number 4 increased the output

velocity by less than 1ms^{-1} . The other myosepta each raised the output velocity by between approximately 2ms^{-1} and approximately 6ms^{-1} . This is similar to what was seen in the previous section.

The table also shows that the deviation in velocity along the length of the sample was significantly affected by the number of myosepta present. The deviation increased and then decreased as more myosepta were added. This can be explained by the fact that the deviation increases as the amount of collagen and fat in the ultrasound path in the top half of the sample increases. The deviation then decreases as the amount of fat and collagen in the bottom half increases. Again, myoseptum number 4 seems to have had the least effect on the deviation of velocity with position.

From the model output, one may infer that salmon samples in which the number of myosepta are the not same between the top and bottom of the sample can expect larger differences in velocity along the length of the sample than those in which there is an equal number of myosepta in each part of the sample.

The table above shows data for 13% fat only. The graphs on the following two pages show velocity versus transducer position for each quantity of myosepta for fat levels of 1%, 9%, 17% and 25% fat over all 193 transducer positions. Again, it can be seen that the same trends are repeated over these fat levels. In all cases, deviation decreases with increasing fat content.

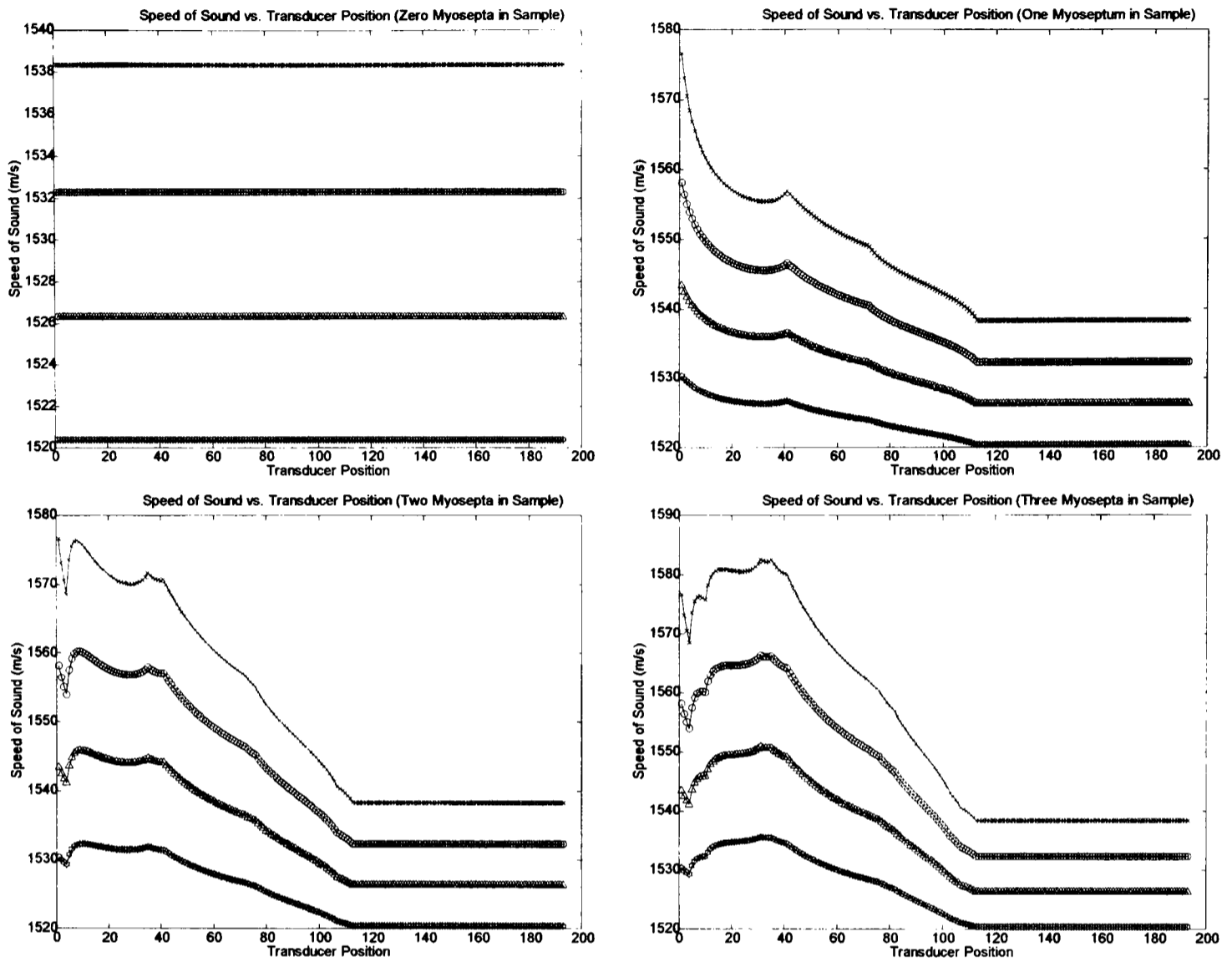


Figure 5.14: Speed of sound versus transducer position for fat contents of 1% (crosses, top), 9% (circles), 17% (triangles) and 25% (hexagrams, bottom). The results for zero myosepta are shown in the graph at the top left. The results for three myosepta are shown in the graph at the bottom right.

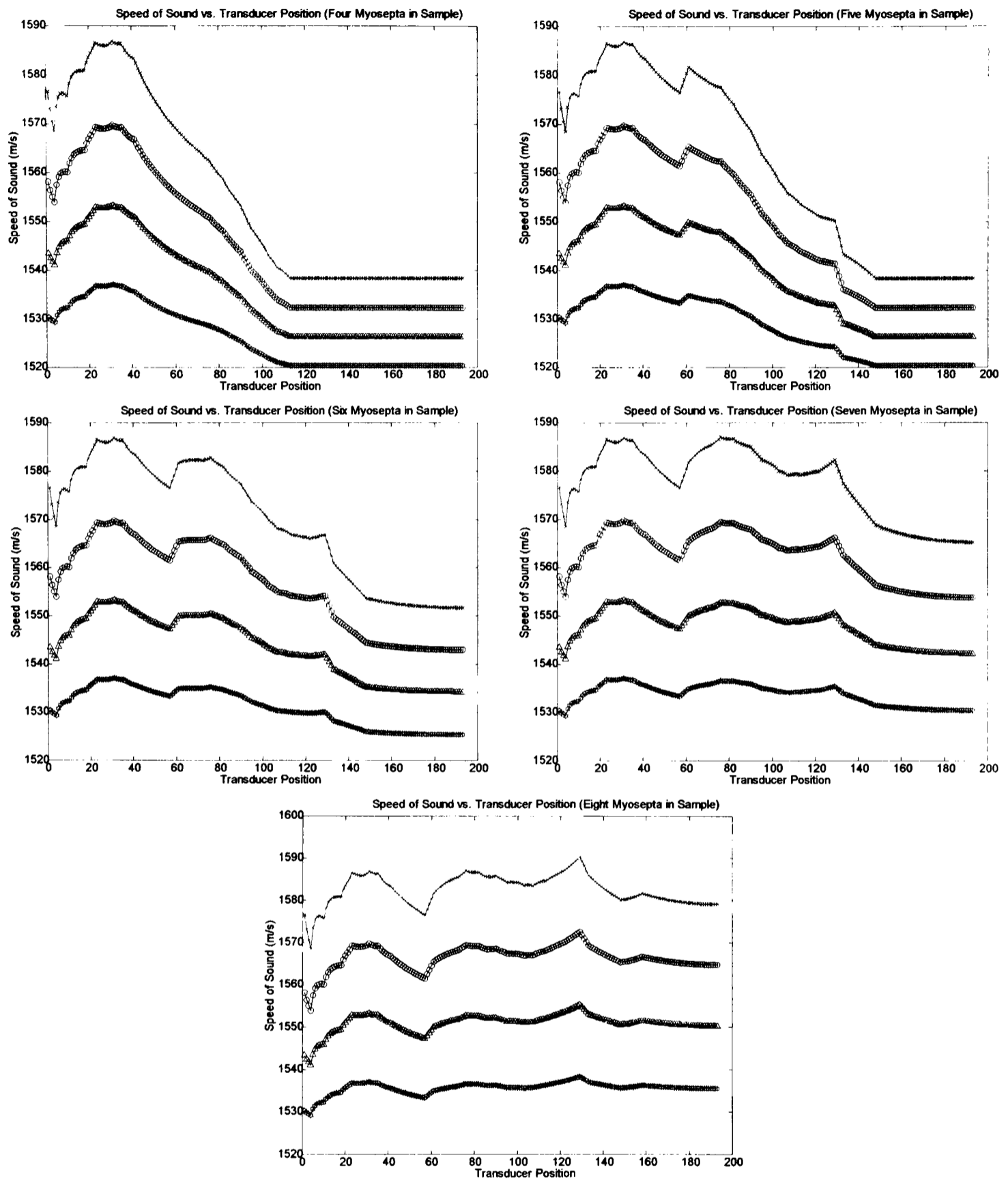


Figure 5.15: Speed of sound versus transducer position for fat contents of 1% (crosses, top), 9% (circles), 17% (triangles) and 25% (hexagrams, bottom). The results for four myosepta are shown in the graph on the top left. The results for eight myosepta are shown in the graph at the bottom.

5.3 Validity of Model with Respect to Wavelength

As stated in Table 2.1, the wavelength of the beam in salmon muscle and myosepta is expected to be approximately 0.7mm. This means that the beam will probably not detect myosepta which are smaller than this thickness. This will affect results in Section 5.2.3 only. In Section 5.2.3, samples with a myoseptum thickness of less than approximately 0.7mm should be expected to have a similar acoustic velocity to that calculated for muscle tissue without myosepta. The simulations described in other results sections in this chapter used a minimum myoseptum thickness of 1.8mm as defined by Equation 5.1.

It was assumed that the transmission of the beam could be modelled using Snell's Law. This is valid when the wavelength of the beam is long compared to the surface roughness of the interface. In general, the behaviour of a wave at an interface is dependent on surface roughness in comparison to wavelength [101]. Specular, or coherent, scattering occurs if the interface appears smooth on the scale of the wavelength. Diffuse, or noncoherent, scattering occurs if the interface appears rough on the scale of the wavelength. Figure 4.6 shows that the surface of a myoseptum is a myriad of fat globules. From the scales in Figure 4.6 it can be seen that most individual fat globules are less than 0.14mm in size. Thus the surface of a myoseptum should appear smooth to

a beam with a wavelength of approximately 0.7mm. Therefore, one would expect specular reflection to occur at these interfaces. In future, modelling specular reflection in addition to refraction at myoseptum interfaces may yield a more accurate model.

5.4 Conclusion

In this chapter, a ray tracing model was constructed. While the pattern, thickness and fat content of myosepta in salmon will vary according to the fish's diet and level of activity during life, this model provides an idea of the magnitude of errors to expect from ultrasound measurements as these characteristics vary. The model output was similar to results from salmon tissue measurements at 10°C ($r=0.73$, $n=12$).

The model has shown that there will be a change in velocity with changes in myosepta configuration, myoseptum size and fat content. The expected variation in velocity with a change in myosepta configuration is between approximately $\pm 1\text{ms}^{-1}$ and approximately $\pm 4\text{ms}^{-1}$ depending on fat content at 10°C. The expected variation in velocity due to changes in myoseptum size and myosepta configuration at that same temperature is between approximately $\pm 2\text{ms}^{-1}$ and approximately $\pm 4\text{ms}^{-1}$ at 12.5% fat. This variation is expected to decrease as the fat content in the myoseptum increases. The

model has also demonstrated that certain myosepta have more of an influence on received velocity and total deviation of velocity along the sample than do other myosepta. This influence decreases as fat content increases.

The accuracy of the model may be improved by changing the code to take the wavelength of the beam into account and model specular reflections in addition to refraction.

Chapter 6

Discussion

6.1 Overview and Analysis of Results

Pulse transit time and intensity methods were chosen for measuring the speed of sound and the attenuation. Before measuring tissue, it was important to show that low-intensity ultrasound could be used to detect changes in fat level of a distributed fat system. Milk and cream were chosen as media whose mixing could provide a distributed fat medium of several different fat levels. It was shown that the fat content of a milk/cream medium could be predicted to approximately $\pm 1.5\%$ fat accuracy ($r=0.998$, $n=7$).

The velocity of the mixture at various fat levels was shown to converge at approximately 19°C . This was illustrated in Figure 3.7. It was assumed that at this temperature the velocity in the fat component of the mixture was

approximately equal to the velocity in the water component of the mixture. Thus, the velocity of the mixture was independent of the proportions of these two components present. This temperature was termed the “crossover temperature.” At a temperature lower than the crossover temperature the velocity of the fat component was greater than the velocity of the water component. At temperatures higher than the crossover temperature, it was *vice versa*. Therefore, measurements were made at 10°C as this was far enough away from the crossover temperature to ensure that there was a measurable difference in velocities between fat levels.

A block of reticulated foam was inserted into the mixture to simulate tissue-like attenuation. The foam was seen to impose an attenuation of approximately 1dB cm⁻¹ on the system. However, attenuation was still seen to increase with fat content.

Once changes in velocity due to the Perspex interface were corrected for, the speed of sound in the mixture was again seen to increase with an increase in fat content. However, the rate at which the velocity increased with increasing levels of fat was slowed from approximately 3ms⁻¹ per 2.5% fat to approximately 2ms⁻¹ per 2.5% fat. These results suggested that one should expect the velocity in salmon muscle tissue to increase with an increase in fat content at 10°C. This increase was expected to be less than 2ms⁻¹ per 2.5% fat due to the muscle tissue being more dense and less compressible than the

foam phantom.

It was thought that the same temperature used to measure the liquid mixtures should be used to measure salmon muscle. Previous studies used liquid mixtures of proteins, water and fats to represent fish tissue. Such mixtures were shown to have a similar crossover temperature to that observed for the milk/cream mixture [22, 34]. An experiment using distilled degassed water and cod liver oil showed that their acoustic velocities intersected at approximately 19°C. This can be seen in Figure 4.14. This is the same temperature at which the velocities in the milk/cream mixtures intersected. Therefore, salmon tissue samples were measured at 10°C as this was well away from the crossover temperature.

Data recorded as the temperature of the samples fell from room temperature to 10°C showed no evidence to suggest a crossover temperature. This could be due to the fact that the density and the compressability of the liquids changes more with temperature than does the density and the compressability of solids. Without a crossover temperature between room temperature and 10°C, one would expect the velocity of salmon tissue to drop with an increase in fat content. This is indeed what was seen here. A trend of decreasing velocity with an increase in fat content was recorded for twelve salmon samples ($r=-0.73$, $n=12$). This is shown in Figure 4.17. This suggests that perhaps it is not valid to simulate salmon tissue as a liquid

mixture of fats, proteins and water.

It was not possible to predict the fat content in salmon muscle with the same degree of accuracy as that in the milk/cream mixtures. Compression and similar sample orientation were both used to provide some degree of uniformity between measured samples. Still, the accuracy with which one could predict the fat content of salmon muscle further suffered from natural biological variation between samples. The variations in myoseptum thickness and in myosepta configuration are thought to have been causes of nonuniformity in the velocity measurements of samples with similar fat content. The myosepta structures inside the muscle tissue are the major difference between what was modelled in the phantoms and the salmon muscle itself. Therefore, fitting an empirical equation to the data was not attempted.

It was suggested that the data could be grouped into three categories: high fat, medium fat and low fat. The range of fat content for salmon was split into three sections. These groups are defined in Table 4.4. Ten of the twelve data points fit into these groups. Analysis suggested that to know the true validity of these groupings, it is necessary to do the same analysis on a much larger number of samples. This will also help to minimise the effects of biological variation between samples on the overall trend of the data.

In salmon muscle, attenuation decreased with an increase in fat. This is the opposite behaviour from that of the foam phantom. A decrease in

attenuation with an increase in fat content had been expected as a similar decrease has been recorded for whitefish muscle tissue [21]. In the group of samples which were tested using chemical analysis, there was no trend of increasing or decreasing attenuation with fat content, even though compression was used to obtain good coupling. Equation 2.13 does not take contact loss into account. As well as accounting for this mathematically, better results may have been obtained by using a thin layer of ultrasound gel between the transducers and the sample.

A ray tracing model was created to model the propagation velocity of ultrasound through a sample of salmon muscle tissue. No attenuation effects of any kind were modelled. The model gives a good idea of the magnitudes of deviation in velocity to expect over a range of fat levels, myoseptum thicknesses and myosepta configurations. It is a good starting point for understanding the effect that these parameters will have on the measured speed of sound through salmon muscle. However, a more complete model may include the myosepta pattern from the other side of the fish and the small intramuscular bones which exist in the lower half of the sample shown in Figure 5.1. The accuracy of the model can be improved by making it three-dimensional. The myosepta pattern in the tissue cannot be completely represented in two dimensions. Figure 4.5 shows the three-dimensional overlapping meshwork of myosepta as it exists in teleosts.

6.2 Conclusions

From the information presented in this thesis, it is possible to conclude several things. The following are results which are consistent with prior studies.

- Milk/cream mixtures can be used to simulate a liquid dispersed fat system.
- It is possible to measure the fat content in a milk/cream mixture to an accuracy of approximately $\pm 1.5\%$ using ultrasound at a single temperature away from the crossover temperature.
- Attenuation is a useful parameter for characterising the quantity of fat in liquid dispersed fat mixtures.
- There exists a trend of increasing velocity with increasing temperature in salmonid muscle tissue.

The following are results which are original findings of this thesis.

- No crossover temperature exists in salmon muscle tissue between 10°C and approximately 22°C . Therefore, it may not be appropriate to model salmon muscle as a liquid mixture of tissue components.
- It has been possible to see a trend of decreasing velocity with increasing fat content in the salmon muscle tissue examined using ultrasound at

a single temperature.

- With the samples which were tested, it has proven possible to group the velocity results into three broad bands of fat content. As explained in Section 4.6.3, each band covers approximately 8% fat.
- Here, attenuation was not useful for characterising the amount of fat in salmon muscle tissue. However, decreases in attenuation with increases in fat content have been observed for other other salmonids at 22°C [21].
- A ray tracing model has proven useful for estimating the speed of sound through salmon muscle tissue.
- The velocity through a salmon sample is affected by the fat level and myoseptum thickness of the sample, as well as the configuration of the myosepta with respect to the transducer. Hence, measurements of the speed of sound through salmon muscle should ensure an approximately similar myosepta pattern between samples.

The accuracy of this method may improve if one examines salmon from a single stock, or salmon which have all been raised under similar feeding regimes. Such salmon would have similar myosepta patterns and myoseptum thicknesses. It would then be possible to perhaps calibrate for a single stock and thus be able to detect differences in fat levels with more confidence.

6.3 Future Work

The chemical analysis on 12 samples in Section 4.6.4 was all that could have been done within the financial constraints of the project. This number of samples was sufficient to highlight a trend of decreasing velocity with increasing fat content. It is expected that a group of between 50 to 100 salmon samples would yield a better correlation than the one found here. A larger sampling group would also minimise the effect of slight biological variations in the muscle structure between individual samples. This would allow an empirical equation to be fit to the data in order to relate velocity to fat content.

More accurate results may also be obtained by lowering the operating frequency so that the wavelength of the beam is much larger than the thickness of a myoseptum. It is expected that increasing wavelength will eliminate some of the variation in velocity due to myosepta configuration predicted by the model.

A three-dimensional ray tracing model would provide results closer to reality than does the current two-dimensional one. This is because of the shape of the myosepta within the muscle tissue. As shown in Figure 4.5, myosepta form an overlapping meshwork which is almost conical in shape. A three-dimensional model would more fully represent the changes in shape

of myosepta along the sample. The ray tracing model could be altered to include further biological corrections such as the small intramuscular bones which appear in the lower half of the sample. The model could also include an option to use the myosepta pattern from the other side of the spine which is a mirror image of the one used here. Moreover, further research on the speed of sound through proteins in solution would enable a more accurate calculation of the speed of sound through the protein component of the tissue. Accuracy of the model may be further improved by modelling specular reflections at myoseptum interfaces in addition to refraction. In future, it may be possible to build a larger geometry for the model which includes bone and other near anatomical features, such as red muscle layers, dermis or subdermal fat layers.

The prospect of measuring the fat content of a whole salmon using ultrasound is something which may be achievable with more research. Measuring the speed of sound through muscle tissue which contains bone is a logical next step. The effects on ultrasound of other materials such as scales, dermis and the thin red muscle and fat layers just under the dermis of a salmon need to be investigated. Only one attempt has been made to measure attenuation through layers of salmonid dermis [21].

The feasibility of correlating the fat content of a whole salmon to the speed of sound through the fish may be improved by averaging velocity mea-

surements along a single fish. Measurements on live fish would necessitate the incorporation of a vision system, such as a stereo camera, to track the position of the fish as the measurements are taken. This thesis is a necessary a first step in the process of accurately and nondestructively measuring the fat content of whole salmon.

Appendix A

Velocity and Attenuation

Calculation Code

The following Matlab code was used to calculate velocity and attenuation from raw oscilloscope data. The two raw data files and the distance between transducers were input to the programme.

```
%Programme for determining speed of sound and attenuation from
%transmission data.
path(path, '\\Octavia\shared\Russ\Data\28_may_2002')
%path(path, 'c:\windows\desktop\chirp\28_may_2002')
clear
close all
format long g
Lsys=11.35; %Distance between transducers in mm
%Lsys=Lsys*1.00275+0.375 %Correct distance offset errors
%for micrometer only
Lsys=Lsys*1e-3; %Lsys in m
Lcm=Lsys*100; %Lsys in cm
```

```

time_range=1e-4;           %Time range of raw data in seconds
%-----
load tx.m                  %Load TX raw data
load f111.m                %Load RX raw data
rx=f111;
N=length(rx);
cut=2.5e3;
y1=tx(1:cut);              %Cut TX data to include only TX pulse
y2=rx(cut+1:length(rx));  %Cut RX data to include only RX signal
%-----
resolution=time_range/N;  %Calculate resolution of raw data
%-----
[m3,n3]=max(y1);          %Record position of TX maximum
b=1;
e=2050;
[m4,n4]=max(y2(b:e));
n4=n4+cut+b;              %Record position of RX first maximum

Offset=531.5e-9;          %Time offset in seconds
dT=((n4-n3)*resolution)-Offset %Calculate time of flight
c=Lsys/dT                  %Calculate speed of sound (m/s)
%-----
                                %Calculate attenuation (dB/cm)
alpha=(-20*log10((max(rx))/250)/Lcm)/2
%-----
figure(1)                  %Visual confirmation that
plot(y2(b:e))              %first RX maximum was used

```

Appendix B

One-dimensional derivation of the equation for longitudinal wave velocity in an elastic medium

In this section the equation for the velocity of a longitudinal wave in an elastic medium is derived from Hooke's Law and Newton's Second Law of Motion. Hooke's Law states that stress is proportional to strain within a medium such that

$$\textit{stress} = \textit{modulus} \cdot \textit{strain} \tag{B.1}$$

where “stress” is defined as the force applied per unit area and “strain” pertains to any change occurring in the relative positions of parts of the elastic body under the action of stress. The “modulus” is a constant representing the linear relationship between stress and strain.

A strain that consists of a change in volume of a body without a change in shape is called a “volume strain.” It can be expressed as $\frac{\Delta V}{V_0}$. Hooke’s Law can be applied to volume strain such that

$$\Delta P = -B \left(\frac{\Delta V}{V_0} \right) \quad (\text{B.2})$$

where ΔP is a change in pressure from equilibrium, $\frac{\Delta V}{V_0}$ is the fractional change in volume and B is a modulus called the adiabatic bulk modulus of elasticity. The above equation can be rewritten as $\Delta P \rightarrow 0$

$$B = -V_0 \left(\frac{dP}{dV} \right) \quad (\text{B.3})$$

For liquids and gases, it is customary to state the compressability, κ , rather than B , where

$$\kappa = \frac{1}{B} \quad (\text{B.4})$$

Thus, the more difficult it is to compress a substance, the larger the value of B and the smaller the value of κ .

Consider the system shown in Figure B.1 [49]. It illustrates particle displacement, ξ , due to a one-dimensional longitudinal wave passing through a

cylinder of cross-sectional area A , in the x direction.

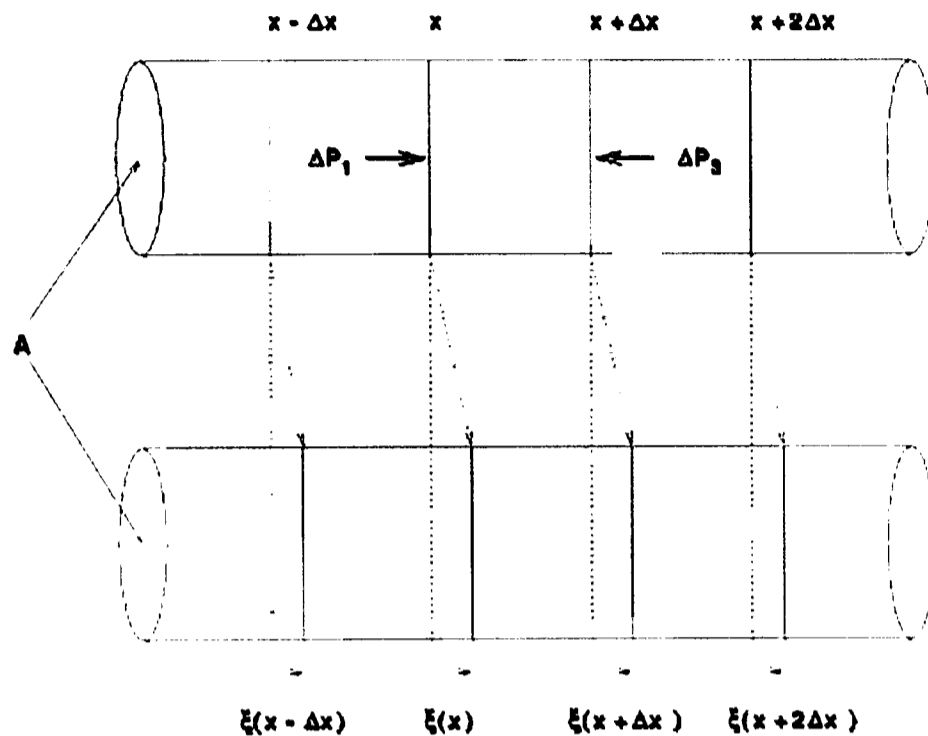


Figure B.1: Particle displacement due to a one-dimensional longitudinal wave passing through a cylinder.

From Figure B.1, it is possible to see that the mass in any slice is

$$\Delta m = A\rho_0\Delta x \quad (\text{B.5})$$

where ρ_0 is the equilibrium density. Now, consider the motion of a point at $x + x/2$. The acceleration of this point is given by the second derivative of position with time.

$$a = \frac{\partial^2}{\partial t^2} \left(\frac{\xi(x) + \xi(x + \Delta x)}{2} \right) \quad (\text{B.6})$$

Therefore, by Newton's Second Law of Motion ($F = ma$) it is possible to write

$$\Delta m \frac{\partial^2}{\partial t^2} \left(\frac{\xi(x) + \xi(x + \Delta x)}{2} \right) = A(\Delta P_1 - \Delta P_3) \quad (\text{B.7})$$

where ΔP_1 and ΔP_3 are the changes in excess pressure in the volume elements between $x - \Delta x$ and x , and between $x + \Delta x$ and $x + 2\Delta x$ respectively, due to deformation. From the definition of B , these are

$$\Delta P_1 = -B \left(\frac{\xi(x) - \xi(x - \Delta x)}{\Delta x} \right) \quad (\text{B.8})$$

$$\Delta P_3 = -B \left(\frac{\xi(x + 2\Delta x) - \xi(x + \Delta x)}{\Delta x} \right) \quad (\text{B.9})$$

Therefore, the equation of motion can be rewritten

$$\Delta m \frac{\partial^2}{\partial t^2} \left(\frac{\xi(x) + \xi(x + \Delta x)}{2} \right) = AB \left(\frac{\xi(x + 2\Delta x) - \xi(x + \Delta x)}{\Delta x} - \frac{\xi(x) - \xi(x - \Delta x)}{\Delta x} \right) \quad (\text{B.10})$$

$$\rho_0 x \frac{\partial^2}{\partial t^2} \left(\frac{\xi(x) + \xi(x + \Delta x)}{2} \right) = B \left(\frac{\xi(x + 2\Delta x) - \xi(x + \Delta x)}{\Delta x} - \frac{\xi(x) - \xi(x - \Delta x)}{\Delta x} \right) \quad (\text{B.11})$$

Recalling that

$$\frac{\Delta y}{\Delta x} = f'(x_0) + C \text{ where } \lim_{\Delta x \rightarrow 0} C = 0 \quad (\text{B.12})$$

The equation becomes

$$\rho_0 x \frac{\partial^2}{\partial t^2} \left(\frac{\xi(x) + \xi(x + \Delta x)}{2} \right) = B \left(\frac{\partial \xi(x)}{\partial x} \Big|_{x+\Delta x} + \epsilon_1 - \frac{\partial \xi(x)}{\partial x} \Big|_x + \epsilon_2 \right) \quad (\text{B.13})$$

taking $\lim \Delta x \rightarrow 0$

$$\frac{\partial^2 \xi(x)}{\partial t^2} = \frac{B}{\rho_0} \frac{\partial^2 \xi(x)}{\partial x^2} \quad (\text{B.14})$$

thus

$$c = \sqrt{\frac{B}{\rho_0}} \quad (\text{B.15})$$

or, for liquids and gases

$$c = \sqrt{\frac{1}{\kappa\rho_0}} \quad (\text{B.16})$$

Appendix C

Fatty Acids

This section presents fatty acid composition data for salmon oil, cod liver oil, sunflower oil and milk fat. Many fatty acids contained in food lipids have a straight molecular chain and an even number of carbon atoms. The fatty acids having two hydrogen atoms bonded to each carbon atom in the chain are termed “saturated.” They have no double bonds between carbons. Fatty acids that contain double bonds between carbon atoms are termed “unsaturated.” The degree of unsaturation of a fatty acid is dependent on the number of double bonds in the molecule. Monounsaturated fatty acids have one double bond. Polyunsaturated fat acids have more than one double bond [51].

All data presented below is from *Bailey's Industrial Oil & Fat Products* [51]. All units are g/100g. The number preceding the colon in the first

column represents carbon chain length. The number following the colon is the number of double-bonds present in the chain.

Name (carbons:double bonds)	Salmon Oil	Cod Liver Oil	Sunflower Oil	Milk Fat
Saturated Fat (total)	19.87	21.67	11.67	62.41
Butyric (4:0)	-	-	-	3.24
Caproic (6:0)	-	-	-	1.92
Caprylic (8:0)	-	-	-	1.12
Capric (10:0)	-	-	-	2.50
Lauric (12:0)	-	-	-	2.81
Myristic (14:0)	3.28	3.57	0.08	10.1
Pentadecylic (15:0)	1	-	-	1.02
Palmitic (16:0)	9.84	10.6	5.9	26.3
Margaric (17:0)	1.5	-	-	0.925
Stearic (18:0)	4.25	2.8	4.5	12.1
Arachidic (20:0)	-	-	0.44	0.37
Behenic (22:0)	-	4.7	0.59	-
Lignoceric (24:0)	-	-	0.168	-
Monounsaturated Fat (total)	28.52	46.74	20.74	28.71
No Name (14:1)	-	-	-	1.2
Palmitoleic (16:1)	4.82	8.31	0.44	2.31
Elaidic (18:1)	17	20.7	19.5	25.2
Gadoleic (20:1)	3.86	10.4	0.8	-
Erucic (22:1)	3.38	7.33	-	-
Polyunsaturated Fat (total)	40.27	22.58	66.08	3.72
Linoleic (18:2)	1.54	0.935	65.7	2.26
Linoleic (18:3)	1.06	0.935	0.384	1.46
No Name (18:4)	2.8	0.935	-	-
Arachidonic (20:4)	0.675	0.935	-	-
EPA (20:5)	13	6.9	-	-
No Name (22:5)	2.99	0.935	-	-
Cervonic (22:6)	18.2	11	-	-
Omega 3 fatty acids	32.3	18.8	-	1.46
Omega 6 fatty acids	2.22	1.87	65.7	2.26

Table C.1: Comparison of fatty acid content. The number preceding the colon in the first column represents carbon chain length. The number following the colon is the number of double-bonds present in the chain.

Appendix D

Salmon Tissue Model Code

Here follows a complete code listing for the ray tracing model described in Chapter 5.

D.1 Temperature and Fat Profiles

D.1.1 allmuscle.m

```
close all
format long g
percent_fat=1;           %Set percent_fat to 1%
for n2=1:13;            %1%-25% fat by 2% increments
    for T=1:40;         %1C-40C in 1-degree increments
        muscleworks;   %Call to muscleworks.m
        speeds(n2,T)=average_c; %Save speed at a single fat level
                                %and temperature
    end
    percent_fat=percent_fat+2; %Increment percent_fat by 2%
end
figure
```

```

plot(5:25,speeds(1,5:25),'.-',5:25,speeds(2,5:25),'o-',5:25,
     speeds(3,5:25),'x-',5:25,speeds(4,5:25),'+-',5:25,
     speeds(5,5:25),'*-',5:25,speeds(6,5:25),'s-',5:25,
     speeds(7,5:25),'d-',5:25,speeds(8,5:25),'v-',5:25,
     speeds(9,5:25),'^-',5:25,speeds(10,5:25),'<-',5:25,
     speeds(11,5:25),'>-',5:25,speeds(12,5:25),'p-',5:25,
     speeds(13,5:25),'h-')
xlabel('Temperature (C)')
ylabel('Speed of Sound (m/s)')
title('Speed of Sound vs. Temperature')

```

```

figure                                %Plot modelled and measured
                                       %velocities at 10C
plot(1:2:25,speeds(1:13,10),'red+-')
xlabel('Fat (%)')
ylabel('Speed of Sound (m/s)')
title('Speed of Sound vs. Fat Content')
hold
f=[4.1 8.6 8.8 9.7 10.7 10.9 11 11.7 12.3 13.6 14.2 20.1];
c=[1589.40 1591.72 1572.42 1560.99 1564.61 1545.68 1560.68
   1559.04 1565.00 1561.54 1560.82 1546.78];
plot(f,c,'o')
hold

```

D.1.2 muscleworks.m

```

%--Input parameters-----
sample_thickness=20;                                %Sample thickness set
                                                    %to 20mm
myosepta_thickness=1.8+.01*percent_fat;            %Myosepta thickness adjusted
                                                    %for fat content
%--Sample Properties-----
Tw=20;                                              %Initial temperature
                                                    %set to 20C
cw=1402.39+5.03711*Tw-0.0580852*Tw^2+3.3342e-4*Tw^3
   -1.478e-6*Tw^4+3.14643e-9*Tw^5;
cw=cw+35;                                          %Velocity of water in
                                                    %white muscle at 20C
cp=1750;                                          %Assumed velocity of

```

```

cf=1486; %protein in 20C
vf_fat=percent_fat/100; %Velocity in fat at 20C
vf_water=(vf_fat*-.78)+.7523; %Volume fraction fat in
%white muscle
vf_protein=1-vf_fat-vf_water; %Volume fraction water
%in white muscle
percent_collagen=82; %Volume fraction protein
%in white muscle
vf_myof=vf_fat*2; %Percent collagen in myosepta
vf_myopro=1-vf_myof; %Volume fraction fat in myosepta
%Volume fraction protein
%in myosepta
c_myosepta=((vf_myopro/(1588+(32*log(percent_collagen)))^2)
+((vf_myof)/cf^2)).^(1/2); %Velocity of myosepta at 20C
c_muscle=((vf_fat/cf^2)+(vf_water/cw^2)+(vf_protein/cp^2)).^(1/2);
%Velocity of white muscle at 20C

%--Temperature Adjustment-----
dT=T-20;
fishT_adjust=2.3*dT; %Temperature adjustment
c_muscle=c_muscle+fishT_adjust; %Velocity in white muscle
%at input temperature
c_myosepta=c_myosepta+fishT_adjust; %Velocity in myosepta at
%input temperature

%--Do Calculations-----
TopHalf; %Call TopHalf.m
BottomHalf; %Call BottomHalf.m

%--Output-----
temp_average_c(1:length(c_route2))=c_route2;
temp_average_c(length(c_route2)+1:length(c_route2)+10)=c_route(1:10);
average_c=mean(temp_average_c); %First 71 rays averaged

```

D.1.3 TopHalf.m

```

%myoseptum #1
theta1=-60:3:60;
theta2=asind((c_myosepta/c_muscle).*sind(theta1));
H=(myosepta_thickness./cosd(theta2))*1;
theta3=asind((c_muscle/c_myosepta).*sind(theta2));
d_travelled2=H+(sample_thickness-myosepta_thickness*1);

```

```

%myoseptum #2
theta1=-60:4:60;
theta2=asind((c_myosepta/c_muscle).*sind(theta1));
H_my=1*myosepta_thickness./cosd(theta2);
theta3=asind((c_muscle/c_myosepta).*sind(theta2));
d_travelled2(5:35)=d_travelled2(5:35)+H_my;
H(5:35)=H(5:35)+H_my;

%myoseptum #3
theta1=-60:6:60;
theta2=asind((c_myosepta/c_muscle).*sind(theta1));
H_my=1*myosepta_thickness./cosd(theta2);
theta3=asind((c_muscle/c_myosepta).*sind(theta2));
d_travelled2(11:31)=d_travelled2(11:31)+H_my;
H(11:31)=H(11:31)+H_my;

%Begin Full Circle = equivalent to 2 myosepta of same orientation
theta_circle=-50:25:50;
theta2_circle=asind((c_myosepta/c_muscle).*sind(theta_circle));
H_circle=2*myosepta_thickness./cosd(theta2_circle);
theta3_circle=asind((c_muscle/c_myosepta).*sind(theta2_circle));
d_travelled2(19:23)=d_travelled2(19:23)+H_circle;
H(19:23)=H(19:23)+H_circle;
%End Full Circle

Number_of_myosepta=1;
for n=1:4
    c_route2(n)=(((H(n)/c_myosepta)+((sample_thickness-
        myosepta_thickness*Number_of_myosepta)/c_muscle))
        /(H(n)+(sample_thickness-myosepta_thickness*
        Number_of_myosepta))).^-1;
end
Number_of_myosepta=2;
for n=5:9
    c_route2(n)=(((H(n)/c_myosepta)+((sample_thickness-
        myosepta_thickness*Number_of_myosepta)/c_muscle))/(H(n)+
        (sample_thickness-myosepta_thickness*Number_of_myosepta))).^-1;
end
Number_of_myosepta=3;

```

```

for n=10:18
    c_route2(n)=(((H(n)/c_myosepta)+((sample_thickness-
        myosepta_thickness*Number_of_myosepta)/c_muscle))/(H(n)+
        (sample_thickness-myosepta_thickness*Number_of_myosepta))).^-1;
end
Number_of_myosepta=4;
for n=19:23
    c_route2(n)=(((H(n)/c_myosepta)+((sample_thickness-
        myosepta_thickness*Number_of_myosepta)/c_muscle))/(H(n)+
        (sample_thickness-myosepta_thickness*Number_of_myosepta))).^-1;
end
Number_of_myosepta=3;
for n=24:31
    c_route2(n)=(((H(n)/c_myosepta)+((sample_thickness-
        myosepta_thickness*Number_of_myosepta)/c_muscle))/(H(n)+
        (sample_thickness-myosepta_thickness*Number_of_myosepta))).^-1;
end
Number_of_myosepta=2;
for n=32:35
    c_route2(n)=(((H(n)/c_myosepta)+((sample_thickness-
        myosepta_thickness*Number_of_myosepta)/c_muscle))/(H(n)+
        (sample_thickness-myosepta_thickness*Number_of_myosepta))).^-1;
end
Number_of_myosepta=1;
for n=36:41
    c_route2(n)=(((H(n)/c_myosepta)+((sample_thickness-
        myosepta_thickness*Number_of_myosepta)/c_muscle))/(H(n)+
        (sample_thickness-myosepta_thickness*Number_of_myosepta))).^-1;
end

%--Begin 45 degree object-----
g=42;
h=57;
Number_of_45degree_objects=1;
theta1(g:h)=45;
theta2(g:h)=asind((c_myosepta/c_muscle).*sind(theta1(g:h)));
H(g:h)=myosepta_thickness./cosd(theta2(g:h)); %d for 1 myosepta
H(g:h)=H(g:h)*Number_of_45degree_objects;
%Layer 2 - out of myosepta
theta3(g:h)=asind((c_muscle/c_myosepta).*sind(theta2(g:h)));
d_travelled2(g:h)=H(g:h)+(sample_thickness-myosepta_thickness

```

```

        *Number_of_45degree_objects);
for n=g:h
    c_route2(n)=(((H(n)/c_myosepta)+((sample_thickness-
        myosepta_thickness*Number_of_45degree_objects)/c_muscle))/(H(n)+
        (sample_thickness-myosepta_thickness*Number_of_45degree_objects))).^-1;
end
%--End 45 degree object-----
%--Begin solid line of myosepta, 1 ray, 3/4 sample thickness
g=58;
h=61;
theta1(g:h)=90;
H(g:h)=sample_thickness*.75;
c_route2(g:h)=(((H(g:h)/c_myosepta)+((sample_thickness*.25)/c_muscle))
        /(sample_thickness)).^-1;
d_travelled2(g:h)=H(g:h);
%--End solid line of myosepta, 1 ray, 3/4 sample thickness
c_route2=real(c_route2);

```

D.1.4 BottomHalf.m

```

theta1=0:1:60;
%--Begin 0-35 degree region-----
g=1;
h=36;
Number_of_myosepta=3;
theta2(g:h)=asind((c_myosepta/c_muscle).*sind(theta1(g:h)));
H(g:h)=myosepta_thickness./cosd(theta2(g:h));
H(g:h)=H(g:h)*Number_of_myosepta;
theta3(g:h)=asind((c_muscle/c_myosepta).*sind(theta2(g:h)));
d_travelled(g:h)=H(g:h)+(sample_thickness-myosepta_thickness
        *Number_of_myosepta);
for n=g:g+length(theta1(g:h))-1
    c_route(n)=(((H(n)/c_myosepta)+((sample_thickness-
        myosepta_thickness*Number_of_myosepta)/c_muscle))
        /(H(n)+(sample_thickness-myosepta_thickness*
        Number_of_myosepta))).^-1;
end
%--End 0-35 degree region-----
%--Begin 36-45 degree region---

```

```

g=37;
h=46;
Number_of_myosepta=2;
theta2(g:h)=asind((c_myosepta/c_muscle).*sind(theta1(g:h)));
H(g:h)=myosepta_thickness./cosd(theta2(g:h));
H(g:h)=H(g:h)*Number_of_myosepta;
%Layer 2 - out of myosepta
theta3(g:h)=asind((c_muscle/c_myosepta).*sind(theta2(g:h)));
d_travelled(g:h)=H(g:h)+(sample_thickness-myosepta_thickness*
    Number_of_myosepta);
for n=g:g+length(theta1(g:h))-1
    c_route(n)=(((H(n)/c_myosepta)+((sample_thickness-myosepta_thickness*
        Number_of_myosepta)/c_muscle))/(H(n)+(sample_thickness-
        myosepta_thickness*Number_of_myosepta))).^-1;
end
%--End 36-45 degree region-----
%--Begin 46-60 degree region----
g=47;
h=61;

%00Begin 45 degree object00000000
Number_of_45degree_objects=1;
theta2(g:h)=asind((c_myosepta/c_muscle).*sind(45));
H_temp=myosepta_thickness./cosd(theta2(g:h));
H_temp=H_temp*Number_of_45degree_objects;
theta3(g:h)=asind((c_muscle/c_myosepta).*sind(theta2(g:h)));
%00End 45 degree object00000000

Number_of_myosepta=2;
theta2(g:h)=asind((c_myosepta/c_muscle).*sind(theta1(g:h)));
H(g:h)=myosepta_thickness./cosd(theta2(g:h));
H(g:h)=H(g:h)*Number_of_myosepta;
theta3(g:h)=asind((c_muscle/c_myosepta).*sind(theta2(g:h)));
d_travelled(g:h)=H(g:h)+H_temp+(sample_thickness-myosepta_thickness
    *(Number_of_myosepta+Number_of_45degree_objects));
for n=g:g+length(theta1(g:h))-1
    c_route(n)=((((H(n)+H_temp(n-g+1))/c_myosepta)+((sample_thickness
        -myosepta_thickness*(Number_of_myosepta+
        Number_of_45degree_objects))/c_muscle))/((H(n)+H_temp(n-g+1))
        +(sample_thickness-myosepta_thickness*(Number_of_myosepta+
        Number_of_45degree_objects))))).^ -1;

```

```

end
c_route=real(c_route);
c_route=reverse(c_route);
%--End 46-60 degree region-----

```

D.2 Changing Transducer Position

D.2.1 change_position.m

```

close all
percent_fat=1;
for n2=1:13;                                %1%-25% fat by 2% increments
    for T=1:40;                               %1C-40C in 1-degree increments
        muscleworks;                          %Call muscleworks.m
        speeds(n2,T)=average_c;               %Save speed at a single fat level
                                                %and temperature
        TransducerDown;                       %Call TransducerDown.m
    end
    percent_fat=percent_fat+2;                %Increment percent_fat by 2%
end
figure
plot(1:193,allspeeds(1,:),'-x',1:193,allspeeds(5,:),'-redo',
     1:193,allspeeds(9,:),'-green^',1:193,allspeeds(13,:),'-blackh')
xlabel('Transducer Position')
ylabel('Speed of Sound (m/s)')
title('Speed of Sound vs. Transducer Position')

```

D.2.2 muscleworks.m

```

%--Input parameters-----
sample_thickness=20;                          %Sample thickness set
                                                %to 20mm
myosepta_thickness=1.8+.01*percent_fat;       %Myosepta thickness adjusted
                                                %for fat content
%--Sample Properties-----
Tw=20;                                         %Initial temperature

```

```

                                                    %set to 20C
cw=1402.39+5.03711*Tw-0.0580852*Tw^2+3.3342e-4*Tw^3
  -1.478e-6*Tw^4+3.14643e-9*Tw^5;
cw=cw+35;                                                    %Velocity of water in
                                                            %white muscle at 20C
cp=1750;                                                    %Assumed velocity of
                                                            %protein in 20C
cf=1486;                                                    %Velocity in fat at 20C
vf_fat=percent_fat/100;                                     %Volume fraction fat in
                                                            %white muscle
vf_water=(vf_fat*-.78)+.7523;                               %Volume fraction water
                                                            %in white muscle
vf_protein=1-vf_fat-vf_water;                               %Volume fraction protein
                                                            %in white muscle
percent_collagen=82;                                       %Percent collagen in myosepta
vf_myof=vf_fat*2;                                         %Volume fraction fat in myosepta
vf_myopro=1-vf_myof;                                       %Volume fraction protein
                                                            %in myosepta
c_myosepta=((vf_myopro/(1588+(32*log(percent_collagen)))^2)
            +((vf_myof)/cf^2)).^(1/2);                    %Velocity of myosepta at 20C
c_muscle=((vf_fat/cf^2)+(vf_water/cw^2)+(vf_protein/cp^2)).^(1/2);
                                                            %Velocity of white muscle at 20C

%--Temperature Adjustment-----
dT=T-20;
fishT_adjust=2.3*dT;                                       %Temperature adjustment
c_muscle=c_muscle+fishT_adjust;                             %Velocity in white muscle
                                                            %at input temperature
c_myosepta=c_myosepta+fishT_adjust;                         %Velocity in myosepta at
                                                            %input temperature

%--Do Calculations-----
TopHalf;                                                    %Call TopHalf.m
BottomHalf;                                                %Call BottomHalf.m
%--Output-----
AverageTop=mean(c_route2);
AverageBottom=mean(c_route);
average_c=(AverageTop+AverageBottom)/2;
total_route(1:length(c_route2))=c_route2;
total_route(length(c_route2)+1:length(c_route2)+length(c_route))=c_route;

```

D.2.3 TopHalf.m

See Section D.1.3.

D.2.4 BottomHalf.m

See Section D.1.4.

D.2.5 TransducerDown.m

```
position=1;
n_speeds=1;
while position<=71
    total=0;
    for n=1:position
        total=total+total_route(n);
    end
    allspeeds_temp(n_speeds)=total/position;
    n_speeds=n_speeds+1;
    position=position+1;
end

while position<=122
    total=0;
    for n=position-71:position
        total=total+total_route(n);
    end
    allspeeds_temp(n_speeds)=total/72;
    n_speeds=n_speeds+1;
    position=position+1;
end

while position<=193
    total=0;
    for n=position-71:122
        total=total+total_route(n);
    end
```

```

    allspeeds_temp(n_speeds)=total/length(position-71:122);
    n_speeds=n_speeds+1;
    position=position+1;
end
if T == 10
    allspeeds(n2,:)=allspeeds_temp;
end

```

D.3 Changing Myoseptum Thickness and Transducer Position

D.3.1 allmuscle_myo.m

```

close all
percent_fat=12.5;
myosepta_thickness=.1;
for n2=1:13;                                %1%-25% fat by 2% increments
    for T=1:40;                               %1C-40C in 1-degree increments
        muscleworks_myo;                     %Call muscleworks.m
        speeds(n2,T)=average_c;              %Save speed at a single fat level
                                                %and temperature
        TransducerDown;                      %Call TransducerDown.m
    end
    myosepta_thickness=myosepta_thickness+.2; %Increment thickness by .2mm
end
figure
plot(1:193,allspeeds(1,:), 'x', 1:193,allspeeds(5,:), 'redo',
     1:193,allspeeds(9,:), 'green^', 1:193,allspeeds(13,:), 'blackh')
xlabel('Transducer Position')
ylabel('Speed of Sound (m/s)')
title('Speed of Sound vs. Transducer Position')
axis([0 200 1520 1580])

```

D.3.2 muscleworks_my0.m

See Section D.2.2.

D.3.3 TopHalf.m

See Section D.1.3.

D.3.4 BottomHalf.m

See Section D.1.4.

D.3.5 TransducerDown.m

See Section D.2.5.

D.4 Contribution of Individual Myosepta

D.4.1 single_my0.m

```
close all
percent_fat=1;
for n2=1:13;                                %1%-25% fat by 2% increments
    for T=1:40;                               %1C-40C in 1-degree increments
        %myo_zero;
        %myo_one;
        %myo_two;
        %myo_three;
        %myo_four;
        %myo_five;
```

```

    %myo_six;
    %myo_seven;
    myo_eight;           %Call myo_eight.m
    speeds(n2,T)=average_c; %Save speed at a single fat level
                        %and temperature
    TransducerDown;     %Call TransducerDown.m
end
percent_fat=percent_fat+2; %Increment percent_fat by 2%
end
figure
plot(1:length(allspeeds(1,:)),allspeeds(1,:),'-x',1:length
     (allspeeds(5,:)),allspeeds(5,:),'-redo',1:length(allspeeds(9,:)),
     allspeeds(9,:),'-green^',1:length(allspeeds(13,:)),
     allspeeds(13,:),'-blackh')
xlabel('Transducer Position')
ylabel('Speed of Sound (m/s)')
title('Speed of Sound vs. Transducer Position (Myoseptum Number 8)')

```

D.4.2 myo_zero.m to myo_eight.m

```

%--Input parameters-----
sample_thickness=20;           %Sample thickness set
                                %to 20mm
myosepta_thickness=1.8+.01*percent_fat; %Myosepta thickness adjusted
                                %for fat content

%--Sample Properties-----
Tw=20;                         %Initial temperature
                                %set to 20C
cw=1402.39+5.03711*Tw-0.0580852*Tw^2+3.3342e-4*Tw^3
    -1.478e-6*Tw^4+3.14643e-9*Tw^5;
cw=cw+35;                       %Velocity of water in
                                %white muscle at 20C
cp=1750;                         %Assumed velocity of
                                %protein in 20C
cf=1486;                         %Velocity in fat at 20C
vf_fat=percent_fat/100;          %Volume fraction fat in
                                %white muscle
vf_water=(vf_fat*-.78)+.7523;   %Volume fraction water
                                %in white muscle

```

```

vf_protein=1-vf_fat-vf_water;           %Volume fraction protein
                                         %in white muscle
percent_collagen=82;                    %Percent collagen in myosepta
vf_myof=vf_fat*2;                       %Volume fraction fat in myosepta
vf_myopro=1-vf_myof;                    %Volume fraction protein
                                         %in myosepta
c_myosepta=((vf_myopro/(1588+(32*log(percent_collagen)))^2)
            +((vf_myof)/cf^2)).^(1/2);   %Velocity of myosepta at 20C
c_muscle=((vf_fat/cf^2)+(vf_water/cw^2)+(vf_protein/cp^2)).^(1/2);
                                         %Velocity of white muscle at 20C

%--Temperature Adjustment-----
dT=T-20;
fishT_adjust=2.3*dT;                    %Temperature adjustment
c_muscle=c_muscle+fishT_adjust;         %Velocity in white muscle
                                         %at input temperature
c_myosepta=c_myosepta+fishT_adjust;     %Velocity in myosepta at
                                         %input temperature

%--Do Calculations-----
%TopHalf_zero;
%TopHalf_one;
%TopHalf_two;
%TopHalf_three;
%TopHalf_four;
%TopHalf_five;
%TopHalf_six;
%TopHalf_seven;
TopHalf_eight;                          %Call TopHalf_eight.m
%BottomHalf_zero;
%BottomHalf_one;
%BottomHalf_two;
%BottomHalf_three;
%BottomHalf_four;
%BottomHalf_five;
%BottomHalf_six;
%BottomHalf_seven;
BottomHalf_eight;                       %Call BottomHalf_eight.m
%--Output-----
AverageTop=mean(c_route2);
AverageBottom=mean(c_route);
average_c=(AverageTop+AverageBottom)/2;
total_route(1:length(c_route2))=c_route2;

```

```
total_route(length(c_route2)+1:length(c_route2)+length(c_route))=c_route;
```

D.4.3 TopHalf_zero.m to TopHalf_eight.m

See Section D.1.3.

Sections of the code not dealing with the velocity in the myoseptum under examination were deleted, or commented out of the .m file.

D.4.4 BottomHalf_zero.m to BottomHalf_eight.m

See Section D.1.4.

Sections of the code not dealing with the velocity in the myoseptum under examination were deleted, or commented out of the .m file.

D.4.5 TransducerDown.m

See Section D.2.5.

D.5 Additive Contribution of Individual Myosepta

D.5.1 additive_my.o.m

```
close all
percent_fat=1;
for n2=1:13;           %1%-25% fat by 2% increments
    for T=1:40;       %1C-40C in 1-degree increments
        %add_my_o_zero;
```

```

    %add_myo_one;
    %add_myo_two;
    %add_myo_three;
    %add_myo_four;
    %add_myo_five;
    %add_myo_six;
    %add_myo_seven;
    add_myo_eight;           %Call add_myo_eight.m
    speeds(n2,T)=average_c; %Save speed at a single fat level
                           %and temperature
    TransducerDown;        %Call TransducerDown.m
end
percent_fat=percent_fat+2; %Increment percent_fat by 2%
end
figure
plot(1:length(allspeeds(1,:)),allspeeds(1,:),'-x',1:length
     (allspeeds(5,:)),allspeeds(5,:),'-redo',1:length(allspeeds(9,:)),
     allspeeds(9,:),'-green^',1:length(allspeeds(13,:)),
     allspeeds(13,:),'-blackh')
xlabel('Transducer Position')
ylabel('Speed of Sound (m/s)')
title('Speed of Sound vs. Transducer Position (Myoseptum Number 8)')

```

D.5.2 add_my_zero.m to add_my_all.m

```

%--Input parameters-----
sample_thickness=20;           %Sample thickness set
                               %to 20mm
myosepta_thickness=1.8+.01*percent_fat; %Myosepta thickness adjusted
                               %for fat content

%--Sample Properties-----
Tw=20;                         %Initial temperature
                               %set to 20C
cw=1402.39+5.03711*Tw-0.0580852*Tw^2+3.3342e-4*Tw^3
  -1.478e-6*Tw^4+3.14643e-9*Tw^5;
cw=cw+35;                      %Velocity of water in
                               %white muscle at 20C
cp=1750;                       %Assumed velocity of
                               %protein in 20C

```

```

cf=1486; %Velocity in fat at 20C
vf_fat=percent_fat/100; %Volume fraction fat in
%white muscle
vf_water=(vf_fat*-.78)+.7523; %Volume fraction water
%in white muscle
vf_protein=1-vf_fat-vf_water; %Volume fraction protein
%in white muscle
percent_collagen=82; %Percent collagen in myosepta
vf_myo_f=vf_fat*2; %Volume fraction fat in myosepta
vf_myo_pro=1-vf_myo_f; %Volume fraction protein
%in myosepta
c_myosepta=((vf_myo_pro/(1588+(32*log(percent_collagen)))^2)
+((vf_myo_f)/cf^2)).^(1/2); %Velocity of myosepta at 20C
c_muscle=((vf_fat/cf^2)+(vf_water/cw^2)+(vf_protein/cp^2)).^(1/2);
%Velocity of white muscle at 20C

%--Temperature Adjustment-----
dT=T-20;
fishT_adjust=2.3*dT; %Temperature adjustment
c_muscle=c_muscle+fishT_adjust; %Velocity in white muscle
%at input temperature
c_myosepta=c_myosepta+fishT_adjust; %Velocity in myosepta at
%input temperature

%--Do Calculations-----
%add_TopHalf_zero;
%add_TopHalf_one;
%add_TopHalf_two;
%add_TopHalf_three;
%add_TopHalf_four;
%add_TopHalf_five;
%add_TopHalf_six;
%add_TopHalf_seven;
add_TopHalf_all; %Call TopHalf_all.m
%add_BottomHalf_zero;
%add_BottomHalf_one;
%add_BottomHalf_two;
%add_BottomHalf_three;
%add_BottomHalf_four;
%add_BottomHalf_five;
%add_BottomHalf_six;
%add_BottomHalf_seven;
add_BottomHalf_all; %Call BottomHalf_all.m

```

```
%--Output-----  
AverageTop=mean(c_route2);  
AverageBottom=mean(c_route);  
average_c=(AverageTop+AverageBottom)/2;  
total_route(1:length(c_route2))=c_route2;  
total_route(length(c_route2)+1:length(c_route2)+length(c_route))=c_route;
```

D.5.3 add_TopHalf_zero.m to all_TopHalf_all.m

See Section D.1.3.

Sections of the code not dealing with the velocity in the myosepta under examination were deleted, or commented out of the .m file.

D.5.4 add_BottomHalf_zero.m to add_BottomHalf_all.m

See Section D.1.4.

Sections of the code not dealing with the velocity in the myosepta under examination were deleted, or commented out of the .m file.

D.5.5 TransducerDown.m

See Section D.2.5.

D.6 Utility Functions

D.6.1 reverse.m

```
function y = reverse_me(x)
l=length(x);
for i=1:l
    y(i)=x(l+1-i);
end
```

D.6.2 sind.m

```
function y=sind(x)
y=sin(x.*pi./180);
```

D.6.3 cosd.m

```
function y=cosd(x)
y=cos(x.*pi./180);
```

D.6.4 asind.m

```
function y=asind(x)
y=asin(x).*(180./pi);
```

D.6.5 acosd.m

```
function y=acos(x)
y=acos(x).*(180./pi);
```

Bibliography

- [1] R.J. Henderson and S. Almatar. Seasonal changes in the lipid composition of herring (*clupea harengus*) in relation to gonad maturation. *Journal of the Marine Biological Association of the UK*, 69:323–334, 1989.
- [2] R.J. Henderson, J.R. Sargent and C.C.E. Hopkins. Changes in the content and fatty acid composition of lipid in an isolated population of capelin (*mallothus villosus*) during sexual maturation and spawning. *Marine Biology*, 78:255–263, 1984.
- [3] C.T. Marshall, N.A. Yaragina, Y. Lambert and O.S. Kjesbu. Total lipid energy as a proxy for total egg production in fish stocks. *Nature*, 402:288–290, 1999.
- [4] V. Neufeldt and D.B. Guralnik, editors. *Webster's New World Dictionary of American English*. Webster's New World, New York, 3rd college edition, 1988.

- [5] S.C. Kestin and P.D. Warriss, editors. *Farmed Fish Quality*. Fishing News Books, Oxford, 2001.
- [6] A.R. Crossland and N. Bratchell. An evaluation and comparison of the CEM meat analysis system with official standard methods for the determination of moisture and fat in meat and meat products. *Journal of the Association of Public Analysts*, 26:89–95, 1988.
- [7] AOAC. *Official Methods of Analysis*. Association of Official Analytical Chemists, Arlington, 15th edition, 1990.
- [8] BSI. *BSI4401: Methods of Test for Meat and Meat Products, Part 5: Determination of Free Fat Content*. British Standards Institution, London, 1970.
- [9] P. Katikou. The distribution of lipids in the fillets of farmed Atlantic salmon (*salmo salar*): Determination by means of a rapid extraction method. Master's thesis, University of Bristol, 1998.
- [10] M.R. Sahasrabudhe and B.W. Smallbone. Comparative evaluation of solvent extraction methods for the determination of neutral and polar lipids in beef. *Journal of the American Oil Chemists Society*, 60, 1983.

- [11] E.G. Bligh and W.J. Dyer. A rapid method of total lipid extraction and purification. *Canadian Journal of Biochemistry and Physiology*, 37, 1959.
- [12] C.S. James. *Analytical Chemistry of Foods*. Blackie Academic & Professional, London, 1995.
- [13] J.A. Mathias, P.C. Williams and D.C. Sobering. The determination of lipid and protein in freshwater fish using near-infrared reflectance spectroscopy. *Aquaculture*, 61:303–311, 1987.
- [14] T. Isaksson, G. Togersen, A. Iversen and K. I. Hildrum. Non-destructive determination of fat, moisture and protein in salmon fillets by use of near-infrared diffuse spectroscopy. *Journal of the Science of Food and Agriculture*, 69:95–100, 1995.
- [15] M.H. Lee. Noninvasive short-wavelength near-infrared spectroscopic method to estimate the crude lipid content in the muscle of intact rainbow trout. *Journal of Agriculture and Food Chemistry*, 40, 1992.
- [16] M. Kent. Hand-held instrument for fat/water determination in whole fish. Technical report, Distell Industries Ltd., UK, 1990.
<http://www.distell.com>.
- [17] J. Lines of Silsoe Research Institute. Private correspondence, 2000.

- [18] N. Kim, D.E. Amin, D. Wilson and G. H. Rouse. Application of newer signal and image-processing techniques for ultrasound beef quality evaluation research. In *A.S. Leaflet R1331*. Center for Animal Science, Iowa State University, 1996.
- [19] V. Amin, D. Wilson and G.H. Rouse. An ultrasound image analysis software for beef quality research. In *A.S. Leaflet R1437*. Center for Animal Science, Iowa State University, 1996.
- [20] V. Suvanich, R. Ghaedian, R. Chanamai, E.A. Decker and D.J. McClements. Prediction of proximate fish composition from ultrasound properties: Catfish, cod, flounder, mackerel and salmon. *Journal Food Science*, 63(6):966–968, 1998.
- [21] M. Freese and D. Makow. High-frequency ultrasonic properties of freshwater fish tissue. *Journal of the Acoustical Society of America*, 44:1282–1289, 1968.
- [22] R. Ghaedian, E.A. Decker and D.J. McClements. Use of ultrasound to determine cod fillet composition. *Journal of Food Science*, 62(3):500–504, 1997.
- [23] A.R. Williams. *Ultrasound: Biological Effects and Potential Hazards*. Academic Press, London, 1983.

- [24] P.N.T. Wells. *Reports on Progress in Physics*, chapter Ultrasonic Imaging of the Human Body, pages 673–681. IOP Publishing Ltd., 1999.
- [25] D.J. McClements and M.J.W. Povey. Ultrasound analysis of edible fats and oils. *Ultrasonics*, 30(6):383–388, 1992.
- [26] P.N.T. Wells. *Biomedical Ultrasonics*. Academic Press, London, 1977.
- [27] D.J. McClements and M.J.W. Povey. Solid fat content determination using ultrasonic velocity measurements. *International Journal of Food Science and Technology*, 22:491–499, 1987.
- [28] H. Sigfusson, E.A. Decker, M. Morrissey and D.J. McClements. Ultrasonic characterization of north Pacific albacore (*thunnus alalunga*). *Journal of Aquatic Food Product Technology*, 49:4372–4377, 2001.
- [29] B.S. Park, A.D. Whittaker, R.K. Miller and D.S. Hale. Predicting intramuscular fat in beef longissimus muscle from speed of sound. *Journal of Animal Science*, 72:109–116, 1994.
- [30] G.A. Fursey, C.A. Miles, S.J. Page and A.V. Fisher. Speed of ultrasound in Hereford bulls and its correlation with carcass composition. *Animal Production*, 52:263–269, 1991.
- [31] C.A. Miles and G.A. Fursey. Measurement of the fat content of meat using ultrasonic waves. *Food Chemistry*, 2:107–118, 1977.

- [32] C.A. Miles, G.A.J. Fursey and R.C.D. Jones. Ultrasonic estimation of solid/liquid ratios in fats, oils and adipose tissue. *Journal of the Science of Food and Agriculture*, 36:215–228, 1985.
- [33] H. Sigfusson, E.A. Decker and D.J. McClements. Rapid prediction of Atlantic mackerel (*somber scombrus*) composition using a hand-held ultrasonic device. *Journal of Aquatic Food Product Technology*, 9(3):27–38, 2000.
- [34] R. Ghaedian, J.N. Coupland, E.A. Decker and D.J. McClements. Ultrasound determination of fish composition. *Journal of Food Engineering*, 35:323–337, 1998.
- [35] C.R. Mol and P.A. Breddels. Ultrasound velocity in muscle. *Journal of the Acoustical Society of America*, 71(2):455–461, 1982.
- [36] H. Hafsteinsson, K. Parker, R. Chivers and S.S.H. Rizvi. Application of ultrasonic waves to detect sealworms in fish tissue. *Journal of Food Science*, 54:244–247, 1989.
- [37] S.A. Goss and F. Dunn. Ultrasonic propagation properties of collagen. *Physics in Medicine and Biology*, 25(5):827–837, 1980.
- [38] V.A. Del Grosso and C.W. Mader. Speed of sound in pure water. *Journal of the Acoustical Society of America*, 52:1442–1446, 1972.

- [39] C. Javanaud and R.R. Rahalkar. Velocity of sound in vegetable oils. *Fat Science Technology*, 90(2):73–75, 1988.
- [40] D.P. Kharakoz. Volumetric properties of proteins and their analogues in distilled water solutions. 2. partial adiabatic compressibilities of amino acids at 15-70C: Supplement 1. experimental data on sound velocity numbers of amino acids. *The Journal of Physical Chemistry*, 95:5634–5642, 1991.
- [41] C.A. Miles, G.A.J. Fursey, A.V. Fisher and S.J. Page. Estimation of lamb carcass composition from measurements of the speed of ultrasound in the soft tissues of live animals and carcasses. *Meat Science*, 30:245–256, 1991.
- [42] R. Chanamai and D.J. McClements. Ultrasonic determination of chicken composition. *Journal of Agriculture and Food Chemistry*, 47:4686–4692, 1999.
- [43] H. Sigfusson, E.A. Decker and D.J. McClements. Ultrasonic characterization of Atlantic mackerel (*scomber scombrus*). *Food Research International*, 34:15–23, 2001.
- [44] <http://www.cygnus-instruments.com> Cygnus Instruments Limited Website, 1999.

- [45] M. Hussey. *Basic Physics and Technology of Medical Diagnostic Ultrasound*. Macmillan, London, 1985.
- [46] C.A. Miles. Attenuation of ultrasound in milks and creams. *Ultrasonics*, 28:394–400, 1990.
- [47] J. Lee. Determination of torso thickness of live fish using ultrasound. MEng Project Report, University of Oxford, 2000.
- [48] http://www.rfcafe.com/references/electrical/coax_chart.htm
RF Café Electrical Reference Website, 2001.
- [49] D.T.J. Linley. The physics of diagnostic ultrasound. <http://marr.bsee.swin.edu.au/~dtl/het408/ultrasound.pdf>, 1998.
- [50] H. Seki, A. Granato and R. Truell. Diffraction effects in the ultrasonic field of a piston source and their importance in the accurate measurement of attenuation. *Journal of the Acoustical Society of America*, 28(2):230–238, 1956.
- [51] Y.H. Hui, editor. *Bailey's Industrial Oil and Fat Products*, volume 1. John Wiley & Sons, Inc., New York, fifth edition, 1996.
- [52] R.A. Lerski, T.C. Duggan and J. Christie. A simple tissue-like ultrasound phantom material. *British Journal of Radiology*, 55:156–157, 1982.

- [53] D.J. McClements and M.J.W. Povey. Ultrasonic velocity measurements in some liquid triglycerides and vegetables oils. *Journal of the American Oil Chemists Society*, 65(11):1787–1790, November 1988.
- [54] K.G. Baker, V.J. Robertson and F.A. Duck. A review of therapeutic ultrasound: Biophysical effects. *Physical Therapy*, 81(7):1351–1358, 2001.
- [55] F.A. Duck. *Physical Properties of Tissue: A Comprehensive Reference Book*. Academic Press, London, 1990.
- [56] <http://www.bbc.co.uk/weather> BBC Weather Centre Website, 2000.
- [57] <http://www.ndt.com> Non-Destructive Testing Website, 2001.
- [58] BSI. *BS5724: Method for Declaring Parameters for Ultrasonic Diagnostic Equipment Using Test Objects*, chapter 3.26. British Standards Institution, London, 1990.
- [59] A.D. Pierce. *Acoustics: An Introduction to its Physical Properties and Applications*. McGraw-Hill, New York, 1981.
- [60] M.J.W. Povey. *Ultrasonic Techniques for Fluid Characterization*. Academic Press, London, 1997.

- [61] W.D. Wilson. Speed of sound in sea water as a function of temperature, pressure and salinity. *Journal of the Acoustical Society of America*, 32(6):641–644, 1960.
- [62] B.E. Conway and R.E. Verrall. Partial molar volumes and adiabatic compressibilities of tetraalkylammonium and aminium salts in water. i. compressibility behavior. *The Journal of Physical Chemistry*, 70(12):3952–3961, December 1966.
- [63] United States Naval Academy Weapons and Systems Engineering Department. *Fundamentals of Naval Weapons Systems*, volume 1. United States Department of Defence, Washington D.C., 1960.
- [64] D.K. Jha and B.L. Jha. Ultrasonic velocity and related parameters of aqueous solutions of some group i salts. *Acustica*, 68:67–71, 1989.
- [65] F.J. Millero, G.K. Ward and P.V. Chetirkin. Relative sound velocities of sea salts at 25c. *Journal of the Acoustical Society of America*, 61(6):1492–1497, June 1977.
- [66] M. Sakurai, T. Nakajima, T. Komatsu and T. Nakagawa. Apparent molal compressibility of sodium chloride in water. *Chemistry Letters*, pages 971–976, 1975.

- [67] F. Harding, editor. *Milk Quality*. Aspen Publishers Inc., Gaithersburg, Maryland, USA, 1999.
- [68] J.W. Fitzgerald, G.R. Ringo and W.C. Winder. An ultrasonic method for measurement of solids-not-fat and milk fat in fluid milk. i. acoustic properties. *Journal of Dairy Science*, 44:1165, 1961.
- [69] M.J.W. Povey of the Univeristy of Leeds Proctor Department of Food Science. Private correspondence, 2001.
- [70] K.F. Lagler. *Ichthyology*. John Wiley & Sons Inc., New York, 2nd edition, 1977.
- [71] H. Sigfusson, V. Suvanich, N. Herrmann, E. A. Decker and D. J. McClements. Ultrasonic properties of atlantic mackerel (*scomber scombrus*) - influence of composition, storage and freezing. In *1999 Annual Meeting Book of Abstracts*, Chicago, 1999. Institute of Food Technologists.
- [72] J.Z. Young. *The Life of Vertebrates*. Clarendon Press, Oxford, 1981.
- [73] W. Stoiber, J.R. Haslett and A.M. Sanger. Myogenic patterns in teleosts: What does the present evidence really suggest? *Journal of Fish Biology*, 55(a):84–99, 1999.

- [74] M.E. Brown (Now M.E. Varley), editor of *The Physiology of Fishes* (1958). Private correspondence, 1999.
- [75] D.H.F. Robb. *Some Factors Affecting the Flesh Quality of Salmonoids: Pigment, Composition and Eating Quality*. PhD thesis, University of Bristol, UK, 1998.
- [76] Q. Bone. *Biology of Fishes*. Blackie Academic & Professional, London, 1995.
- [77] Y. Tsuchiya and I. Takahashi. The content of connective tissue in fish muscles. *The Tôhoku Journal of Agricultural Research*, 1:209–213, 1950.
- [78] D. Tocher of the University of Stirling Institute of Aquaculture. Private correspondence, 2000.
- [79] <http://www.coherentinc.com> Coherent Incorporated Website, 2002.
- [80] R. Aris. *Mathematical Modelling Techniques*. Dover Publications Inc., New York, 1994.
- [81] J.A. Jensen. Field: A program for simulating ultrasound systems. *Medical and Biological Engineering and Computing*, 34(Supplement 1):351–353, 1996.

- [82] J.A. Jensen and S.I. Nikolov. Fast simulation of ultrasound images. In *Proceedings of IEEE International Ultrasonics Symposium*, pages 1721–1724, Puerto Rico, 2000.
- [83] <http://www.cyberlogic.org> Cyberlogic Incorporated Website, 2001.
- [84] A.H. Harker and J.A. Ogilvy. Coherent wave propagation in inhomogeneous materials: A comparison of theoretical models. *Ultrasonics*, 29:235–244, 1991.
- [85] M. Blakemore and G.A. Georgiou, editors. *Mathematical Modelling in Non-Destructive Testing*. Clarendon Press, Oxford, 1988.
- [86] J.A. Ogilvy. An interactive ray tracing model for ultrasonic non-destructive testing. Technical Report AEA-RS-4205, Atomic Energy Authority Industrial Technology Harwell Laboratory, 1992.
- [87] D.H.F. Robb of EWOS Norway. Private correspondence, 2002.
- [88] A.S. Glassner. *An Introduction to Ray Tracing*. Academic Press Limited, London, 1989.
- [89] <http://www.ncbi.nlm.nih.gov/entrez> U.S. National Center for Biotechnology Information Database, 2002.

- [90] H. Hart and R.D. Schuetz. *Organic Chemistry: A Short Course*. Houghton Mifflin Company, Boston, fifth edition, 1978.
- [91] R.P. Wilson and C.B. Cowey. Amino acid composition of whole body tissue of rainbow trout and atlantic salmon. *Aquaculture*, 48:373–376, 1985.
- [92] M. Grossel, Senior Lecturer in Organic Chemistry at Southampton University and Teaching Lecturer at Christ Church Oxford. Private communication, 2002.
- [93] G.D. Fullerton and J.A. Zagzebski. *Medical Physics of CT and Ultrasound: Tissue Imaging and Characterization*. American Institute of Physics, USA, 1980.
- [94] S.A. Goss, L.A. Frizzell and F. Dunn. Dependence of the ultrasonic properties of biological tissue on constituent proteins. *Journal of the Acoustical Society of America*, 67(3):1041–1044, 1980.
- [95] W.D. O'Brien Jr. The relationship between collagen and ultrasonic attenuation and velocity in tissue. In *Ultrasonics International 1977*, pages 194–202. IPC Science and Technology Press, 1977.

- [96] J.A. Rooney, P.M. Gammell, J.D. Hestenes, H.P. Chin and D.H. Blankenhorn. Velocity and attenuation of sound in arterial tissues. *Journal of the Acoustical Society of America*, 71(2):462–466, 1982.
- [97] D.R. Lide, editor. *CRC Handbook of Chemistry and Physics*. CRC Press, London, 81st edition, 2001.
- [98] S.A. Goss and W.D. O'Brien Jr. Direct ultrasonic velocity measurement of mammalian collagen threads. *Journal of the Acoustical Society of America*, 65(2):507–511, 1979.
- [99] J.M. Bland and D.G. Altman. Statistical methods for assessing agreement between two methods of clinical measurement. *The Lancet*, I:307–310, February 1986.
- [100] J.M. Bland and D.G. Altman. Measuring agreement in method comparison studies. *Statistical Methods in Medical Research*, 8:135–160, 1999.
- [101] J.A. Ogilvy. *Theory of Wave Scattering from Random Rough Surfaces*. Adam Hilger, Bristol, 1991.